Wissenschaftszentrum Weihenstephan für Ernährung, Landnutzung und Umwelt
Lehrstuhl für Systemverfahrenstechnik

Investigation of Cell Rupture and Viability Loss in Different Hydrodynamic Setups

---

Dimitrios Kokkinos

Vollständiger Abdruck der von der Fakultät Wissenschaftszentrum Weihenstephan für Ernährung, Landnutzung und Umwelt der Technischen Universität München zur Erlangung des akademischen Grades eines Doktors der Naturwissenschaften genehmigten Dissertation.

Vorsitzende: Prof. Dr. Mijana Minceva

Prüfende/-r der Dissertation:

1. Prof. Dr.-Ing Heiko Briesen

---

2. Prof. Dr. Andreas Wierschem

---

3. Prof. Dr. Natalie Germann

Die Dissertation wurde am 01.03.2019 bei der Technischen Universität München eingereicht und durch die Fakultät Wissenschaftszentrum Weihenstephan für Ernährung, Landnutzung und Umwelt am 08.08.2019 angenommen.

Declaration

The work is original and my own, carried out under the supervision of Prof. Dr.-Ing. Heiko Briesen; where this is not so, credit has been duly given.
This doctorate thesis has not been previously submitted, in whole or in part, for any degree at this or any other university.

Place, date

Name

Acknowledgements

First and foremost, I would like to thank Prof. Dr.-Ing. Heiko Briesen, for giving me the opportunity to perform scientific research in one of the top scientific institutions in the world, and for his guidance and assistance throughout the time it took for the completion of my work. And for believing in me.

Second, I want to thank Prof. Dr. Natalie Germann for their valuable time, required to read and grade this dissertation, and Prof. Dr. Mirjana Minceva for chairing my thesis committee. I would like to thank Prof. Dr. Andreas Wierschem, and Dr. Haider Dakhil for the good suggestions and great collaboration. I would also like to thank Dr. Andre Braun, and Prof. Dr. Andreas Boudouvis, for their help and support during the beginning of my efforts. And I would like to thank Dr. Nikolaos Tegos for the fruitful discussions.

I want to thank everyone at the Chair of Process Systems Engineering of TUM, that were present during the time I was working on the Thesis, as their help, discussions, pleasantness, and kindheartedness, has constantly and significantly helped me in moving forward with this task. I want to especially thank Michael Kuhn and Tijana Kovacevic for their patience, as they had to bear with me complaining for 4 straight years in a row. And for their friendship, though you cannot thank anyone enough for that.

I would like to thank my family and my friends for not letting the distance affect our relationship, for always being there, despite being far away sometimes. If there are reasons that make it worth living, watching the bonds you make hold strong in time certainly is one of them.

The Bayerische Forschungsstiftung is gratefully acknowledged for the financial support of this work, carried out through grant DOK-147-12. Also, I would like to thank the Culture Collection of Algae at Goettingen University for providing the necessary microalgae strains.

Abstract

Biotechnological processes are divided into two categories, upstream processes focusing on cell cultivation and growth, and downstream processes centered on recovering the biological products of the cells. In both types of processes, hydrodynamic stresses arise, which might affect cell viability, and even lead to cell rupture and release of intracellular chemicals, which can be detrimental for upstream- and beneficial for downstream processes. Understanding the influence of different hydrodynamic stress conditions on cell populations would be beneficial for the design of new or the optimization of existing biotechnological processes involving those cells.

Dunaliella salina, one of the world's best natural sources of beta-carotene, was chosen as the model organism for this investigation. Three different hydrodynamic setups were used, a narrow-gap rheometer with transparent parallel plates, a syringe connected to a capillary tube, and a rotor-stator device submerged in a cell suspension, each providing different types of flow conditions (from laminar to turbulent) and intensities of hydrodynamic stress. The cell response to each set of conditions was measured through bright-field and fluorescence microscopy, and the Bradford spectrophotometric assay of intracellular protein release

Following these methods, the conditions of cell rupturing and viability loss of *D. salina* cells in different setups were identified, and relevant measures of sensitivity to hydrodynamic stress (such as cell death rates) were obtained, which are useful both for upstream and downstream processing of the cells. The tested methodology has a broad applicability regarding cell types and hydrodynamic stress conditions, and can provide additional insights to the cell response under these conditions, such as the observation of cell formations in flow, and the prediction of cell viability loss through intracellular protein release. Finally, the issues of comparing different hydrodynamic setups were examined, and a new population balance model was presented, connecting cell rupture and viability loss to the heterogeneity of cell populations.

Zusammenfassung

Biotechnologische Prozessen werden in zwei Kategorien unterteilt: Upstream-Prozesse, die auf Zellkultivierung und -wachstum fokussieren, und Downstream-Prozesse, die sich auf die Gewinnung der biologischen Produkte der Zellen konzentrieren. In beiden Prozesstypen treten hydrodynamische Belastungen auf, die die Viabilität der Zellen beeinflussen und sogar zu Zellbruch und Freisetzung intrazellulärer Chemikalien führen können, was für Upstream-Prozesse nachteilig und für Downstream-Prozesse von Vorteil sein kann. Das Verständnis des Einflusses verschiedener hydrodynamischer Stressbedingungen auf Zellpopulationen wäre von Vorteil sowohl für die Gestaltung neuer als auch für die Optimierung bestehender biotechnologischer Prozesse.

Dunaliella salina, eine der besten natürlichen Quellen der Welt für Beta-Carotin, wurde als Modellorganismus für diese Untersuchung ausgewählt. Es wurden drei verschiedenen hydrodynamische Aufbauten verwendet, ein Dünn-Spalt-Rheometer mit transparenten parallelen Platten, eine an ein Kapillarrohr angeschlossene Spritze und ein in eine Zellsuspension getauchte Rotor-Stator-Gerät, die jeweils unterschiedliche Arten von Strömungsbedingungen (von laminar bis turbulent) und Intensitäten der hydrodynamischen Belastung liefern konnten. Die Zellreaktion auf jede Bedingung wurde durch Hellfeld- und Fluoreszenzmikroskopie und den spektrophotometrischen Bradford-Test der intrazellulären Proteinfreisetzung gemessen.

Anschließend wurden die Bedingungen für den Zellbruch und den Viabilitätsverlust von *D. salina* Zellen in verschiedenen Einstellungen identifiziert, und es wurden relevanten Messgrößen für die Empfindlichkeit gegenüber hydrodynamischem Stress (z. B. Zelltodraten) erhalten, die sowohl für die Upstream- als auch für die Downstream-Prozesse der Zellen nützlich sind. Die getestete Methodik ist im Bezug auf Zelltypen und hydrodynamischen Stressbedingungen breit anwendbar und kann unter diesen Bedingungen zusätzliche Einblicke in die Zellreaktion bieten, wie die Beobachtung von Zellbildungen unter Fließbedingungen und die Vorhersage des Viabilitätsverlusts durch intrazelluläre Proteinfreisetzung. Schließlich wurden

die Probleme beim Vergleich verschiedener hydrodynamischer Einstellungen untersucht und ein neues Populationsbilanz-Modell vorgestellt, das den Zellbruch und den Viabilitätsverlust mit der Heterogenität von Zellpopulationen in Verbindung bringt.

Contents

Declaration iii

Acknowledgements v

Abstract vii

Zusammenfassung ix

List of figures xvi

Abbreviations xvii

Nomenclature xix

1 Introduction 1

1.1 Motivation 1

1.2 Aim 3

1.3 State of the Art 3

1.3.1 Hydrodynamics of cells in flow 3

1.3.2 Cellular response to hydrodynamic stress 10

1.3.3 Cell heterogeneity and Population Balance Modeling 14

1.4 Microalgae cells 16

1.4.1 General 16

1.4.2 Microalgal Culture 17

1.4.3 Products of microalgae 18

1.4.4 Hydrodynamics of microalgae suspensions 19

1.5 The genus *Dunaliella* 21

1.5.1 Taxonomy 21

1.5.2 Cellular morphology 21

1.5.3 Life cycle and sexual reproduction . . . 22
1.5.4 Cultivation and salt tolerance . . . 23
1.5.5 Osmotic behavior . . . 23
1.5.6 Intracellular salt and solute concentrations . . . 24
1.5.7 Commercial production . . . 25
1.5.8 Requirements for optimal growth . . . 27
1.5.9 Hydrodynamic stress studies on *Dunaliella* species . . . 28

2 Materials and Methods **31**
2.1 General . . . 31
2.1.1 Microorganism and culture medium . . . 31
2.1.2 Microscopy for cell count, morphology and viability . . . 32
2.1.3 Intracellular protein release . . . 35
2.1.4 Normalized cell density . . . 37
2.1.5 Cell death rate . . . 37
2.2 Narrow-gap rheometer experiments . . . 38
2.2.1 Aim . . . 38
2.2.2 Experimental procedure . . . 38
2.2.3 Cell count and deformation . . . 39
2.2.4 Normalized cell density . . . 39
2.2.5 Cell death rate . . . 40
2.2.6 Intracellular protein release . . . 40
2.2.7 Exposure to hydrodynamic stress . . . 40
2.2.8 Rheo-optical setup . . . 41
2.2.9 Analytical equations . . . 42
2.2.10 Critical shear stress criterion . . . 43
2.3 Capillary flow experiments . . . 43
2.3.1 Aim . . . 43
2.3.2 Experimental procedure . . . 44
2.3.3 Cell count and viability . . . 44
2.3.4 Normalized cell density . . . 45
2.3.5 Cell death rate . . . 45
2.3.6 Intracellular protein release . . . 45
2.3.7 Exposure to hydrodynamic stress . . . 45

2.3.8 Cell proliferation ability . . . 46
2.3.9 Rheological equations . . . 46
2.3.10 Critical hydrodynamic stress for the syringe-capillary system . . . 48
2.4 Rotor-stator stirring experiments . . . 49
2.4.1 Aim . . . 49
2.4.2 Experimental procedure . . . 50
2.4.3 Cell count and viability . . . 50
2.4.4 Normalized cell density . . . 50
2.4.5 Cell death rate . . . 51
2.4.6 Intracellular protein release and comparison with cell viability loss . . . 51
2.4.7 Rotor-stator and cell damaging experiments . . . 52
2.5 Population balance modeling of cell rupture under hydrodynamic stress . . . 52
2.5.1 Aim . . . 52
2.5.2 Problem formulation and model equations . . . 53
2.5.3 Numerical approach . . . 56

3 Results **59**
3.1 Narrow-gap rheometer experiments . . . 59
3.1.1 Rheological characterization . . . 59
3.1.2 Observations using the rheo-optical setup . . . 60
3.1.3 Cell morphology and viability loss . . . 61
3.1.4 Critical hydrodynamic stress and energy dissipation . . . 64
3.2 Capillary flow experiments . . . 66
3.2.1 Cell morphology . . . 66
3.2.2 Cell viability loss . . . 66
3.2.3 Intracellular protein release . . . 68
3.2.4 Cell proliferation ability . . . 70
3.2.5 Critical hydrodynamic stress and energy dissipation . . . 72
3.3 Rotor-stator stirring experiments . . . 74
3.3.1 Cell morphology . . . 74
3.3.2 Cell viability loss . . . 75
3.3.3 Intracellular protein release . . . 76
3.3.4 Energy dissipation . . . 78
3.4 Population balance modeling of cell rupture under hydrodynamic stress . . . 81

3.4.1 Cell population heterogeneity 81
3.4.2 Cell population growth rate 82

4 Discussion **85**

Bibliography **113**

Appendix A **115**

Appendix B **117**

List of Figures

1.1 Schematic: Cell in predominantly shear flow 5
1.2 Schematic: Cell in predominantly normal flow 5
1.3 Schematic: Cell in turbulent flow 7
1.4 Effect of shear rate on the maximum specific growth rate of *P. tricornutum* cells 12
1.5 Effect of shear stress on the viability of *C. muelleri* cells 13
1.6 Effect of shear stress on the viability and regrowth ability of carrot cells 14
1.7 Length distribution of *B. cereus* cells 15
1.8 Cell wall's Young's modulus distribution of a population of *A. thaliana* cells . . 16
1.9 *Dunaliella salina*: Bright field and fluorescence images 22
1.10 Aggregation and zygote formation of *D. salina* 24
1.11 β-carotene-production plant of *D. salina* cells 26

2.1 FDA staining of *D. salina* cells 34
2.2 FDA fluorescence reduction of *D. salina* cells under constant irradiation . . . 36
2.3 Intact and deformed *D. salina* cells in the narrow gap rheometer experiments 40
2.4 Sketch of the setup used for the narrow-gap rheometer experiments 42
2.5 The setup used for the syringe-capillary experiments 45
2.6 The setup used for the rotor-stator experiments 51

3.1 Viscosity and shear stress of the cell suspension as a function of shear rate in the narrow gap rheometer 60
3.2 Formations of cells in laminar flow depending on maximum shear stress in the narrow gap rheometer 61
3.3 Normalized cell density (NCD_t) as a function of shear stress in the narrow gap rheometer 62
3.4 Normalized cell density (NCD_v) as a function of shear stress in the narrow gap rheometer 63

3.5 Cell death rate as a function of shear stress in the narrow gap rheometer . . 64
3.6 Normalized cell density (NCD_v) as a function of maximum total energy dissipation in the narrow gap rheometer 65
3.7 Morphology of viable and non-viable *D. salina* cells after passing through the capillary 67
3.8 Normalized cell density per passage through the capillary 68
3.9 Change in normalized cell density as a function of residence time in the capillary ($0.18\,\mathrm{ml\,sec^{-1}}$) 69
3.10 Change in normalized cell density as a function of residence time in the capillary ($0.36\,\mathrm{ml\,sec^{-1}}$) 69
3.11 Increase in absorbance at $595\,\mathrm{nm}$ after 40 passages through the capillary . . 71
3.12 Growth rates of *D. salina* populations after 40 passages through the capillary 72
3.13 Normalized cell density as a function of maximum total energy dissipation near the capillary wall 73
3.14 Normalized cell density as a function of stirring time by the rotor-stator 75
3.15 Change in normalized cell density as a function of stirring time by the rotor-stator ($3000\,\mathrm{rpm}$) 76
3.16 Change in normalized cell density as a function of stirring time by the rotor-stator ($5000\,\mathrm{rpm}$) 77
3.17 Increase in absorbance at $595\,\mathrm{nm}$ as a function of stirring time by the rotor-stator 78
3.18 Correlation between cell viability loss and intracellular protein release 79
3.19 Normalized cell density as a function of volume average total energy dissipation in the rotor-stator 80
3.20 Simulation of a two-dimensional distribution of cells experiencing constant hydrodynamic stress 82
3.21 Simulation of the temporal evolution of the viable cell density in populations affected by constant hydrodynamic stress 83

4.1 Sample MATLAB code for counting microalgae cells in microscope images . 115

Abbreviations

Abbreviation	Meaning
CFD	Computational fluid dynamics
ED	Energy dissipation
EDR	Energy dissipation rate
FDA	Fluorescein diacetate
NCD	Normalized cell density
PBM	Population balance model
RGB	Red-Green-Blue color model

Nomenclature

Symbol	Interpretation	Units
a	Absorbance at $595\,\mathrm{nm}$	$-$
Ca	Capillary number	$-$
k_e	Cell population growth rate	h^{-1}
k_d	Cell death rate	h^{-1}
p	Pressure	Pa
Re	Reynolds number	$-$
$\dot{V}$	Volumetric flow rate	$\mathrm{m}^3 \cdot \mathrm{s}^{-1}$
R	Radius (parallel plates or capillary)	m
v	Velocity	$\mathrm{m} \cdot \mathrm{s}^{-1}$
x	Cell radius	m
Greek Letters		
$\dot{\gamma}$	Shear rate	s^{-1}
ϵ_V	Energy dissipation rate per unit volume	$\mathrm{W} \cdot \mathrm{m}^{-3}$
ϵ_M	Energy dissipation rate per unit mass	$\mathrm{W} \cdot \mathrm{kg}^{-1}$
E_V	Total energy dissipation per unit volume	$\mathrm{J} \cdot \mathrm{m}^{-3}$
E_Y	Cell membrane's Young's modulus	Pa
η	Dynamic viscosity	$\mathrm{Pa} \cdot \mathrm{s}$
θ	Kolmogorov length scale of turbulence	m
ν	Kinematic viscosity	$\mathrm{m}^2 \cdot \mathrm{sec}^{-1}$
ρ	Density	$\mathrm{kg} \cdot \mathrm{m}^{-3}$
τ	Shear stress	Pa
ω	Angular velocity	$\mathrm{rad} \cdot \mathrm{s}^{-1}$

Chapter 1

Introduction

1.1. Motivation

Biotechnology is a rapidly expanding field including numerous microorganisms with promising applications. The processing of such microorganisms is divided into two different types, upstream (e.g. cell cultivation and growth) and downstream (e.g. cell disruption and release of intracellular chemicals) (Hu et al., 2011). Hydrodynamic stresses arise in both types of processing, influencing a variety of biological processes, including cell metabolism, cell growth and even lead to cell membrane rupture and death (Joshi et al., 1996). A thorough understanding of the relevant hydrodynamic stresses and the influence they exert on various cell populations would assist in the optimization of current processes, as well as the design of new or up-scaled ones.

In recognition of the importance of the sensitivity of cells to hydrodynamic stress, numerous studies have been published in the scientific literature, as presented in the review papers of Joshi et al. (1996) and Hu et al. (2011), and references therein. One principal axis of investigation is the hydrodynamics of cells in flow, as the flow conditions, in the spectrum between laminar and turbulent flow, as well as the equipment used, e.g. rheometers, pumps, bioreactors, had varying effects on the cells, and provided different insights into their sensitivity (Joshi et al., 1996).

What the term “sensitivity” entails, i.e. what is the response of the cells to hydrodynamic stress, has also been investigated thoroughly. Diverse responses to hydrodynamic stress have been witnessed, from physical, such as cell rupture and lysis (Spiden et al., 2013), to biological, such as the loss of the cell’s proliferation ability (Dunlop et al., 1994). Some of

these responses have been found to be universal; some were specific to the cell species. There were also different approaches to this sensitivity of cells, regarding upstream and downstream processes, as the usual attempt in upstream processes is to protect the cells from the negative effect of hydrodynamic stress (Chisti, 2001), while in downstream, the sensitivity of cells is taken advantage of, to e.g. facilitate the release of intracellular chemicals (Guenerken et al., 2015).

Additionally, heterogeneity of the members of a population of cells has been investigated (Born et al., 1992), as they exhibit differences in e.g. their size (Collins and Richmond, 1962), and cell membrane elasticity (Radotic et al., 2012), that can affect their response to hydrodynamic stress, resulting for example in some cells of the population dying, while others survived and continue reproducing normally (Michels et al., 2010).

As already mentioned, not all cell types have been found equally sensitive to hydrodynamic stress, since mammalian cells are for example generally more sensitive than plant cells that are enclosed in a cell wall (Joshi et al., 1996). Microalgae cells have been found to be particularly sensitive, as is evident by the numerous investigations on the subject, presented in the review paper of Wang and Lan (2018), and references therein. The interest in microalgae has been rising in the recent years, due to the various products of high value that can be extracted from them, relevant to e.g. cosmetic and nutrition industries (García-González et al., 2005; Garcia-Chavarria and Lara-Flores, 2013). This interest has led to increased attempts of optimization of the upstream and downstream processes of these cells (Hamed, 2016; Lee et al., 2017), which include dealing with the issue of their sensitivity to hydrodynamic stress.

The microalgae genus *Dunaliella*, with its prominent species *D. salina* and *D. Bardawil*, has been particularly important (Oren, 2005), as it provides one of the best natural sources of β-carotene (Richmond and Hu, 2013), a chemical widely used in nutrition supplements. These cells are considered sensitive to hydrodynamic stress because they lack a cell wall, and are instead only enclosed in a plasma membrane. Based on this fact, *D. salina* was chosen in order to perform the investigations on cell sensitivity to hydrodynamic stress in different hydrodynamic setups.

1.2. Aim

The main goal of the current thesis was the development and testing of an experimental approach for identifying the conditions of cell death through rupturing of the cell membrane in different hydrodynamic setups (narrow-gap rheometer, syringe connected to a capillary tube and rotor-stator submerged in a cell suspension). We compared between those setups — and others from the literature — with regards to the hydrodynamic stresses experienced by the cells and the resulting cell death rates.

The tested methodology comprised a combination of two direct methods (bright-field and fluorescence microscopy) and one indirect method (measurement of intracellular protein release in the cell suspension using the Bradford assay).

The microalgae species *D. Salina*, a widely researched species considered to be one of the best natural sources of carotenoids, was chosen as a model organism, in an effort to investigate its response to hydrodynamic stress and clarify the optimization levels of the proposed methodology.

Finally, a mathematical model was introduced, in an attempt to obtain a more in-depth understanding of the death of a cell population by hydrodynamic stress. The model was based on the physics of capsule rupturing in flow, and is applicable for a wide range of cell populations (e.g. microalgae) and hydrodynamic stress conditions.

1.3. State of the Art

1.3.1. Hydrodynamics of cells in flow

The investigation of the effect of hydrodynamic stress on cells consists of two primary components: determination of the hydrodynamic forces affecting the cells and determination of the cell response to these forces, which may be mechanical, biological, or both, depending upon the respective conditions. The importance of this investigation for the field of biotechnology has been continually discussed and underlined by scientific publications throughout the years (Joshi et al., 1996; Chisti, 2001; Chan et al., 2011).

To begin with, the definition of hydrodynamic stress will be provided, as well as the way it can exert influence upon a cell placed in flow (for laminar or turbulent conditions), and how to

measure that influence. In laminar flow, the fluid comprises streams of different velocities, and the gradient between those velocities can impose shear or normal strain upon the cells. Strain is the deformation of an object (here: a biological cell) through the application of an external force, where shear strain is caused by forces acting parallel to the surface of the cell, and normal strain is caused by forces acting perpendicular to the cell surface. In Newtonian fluids, multiplying the strain rate with the viscosity of a given fluid gives the normal or shear stress accordingly, and the combination of normal and shear stress generated by the fluid flow is called hydrodynamic stress.

A simplified example of a cell experiencing predominantly shear stress in flow is a cell placed in a water solution flowing between two parallel plates, where the upper plate is moving with a velocity $v = v_{max}$ ($\mathrm{m} \cdot \mathrm{s}^{-1}$), while the lower plate is immobile ($v = 0$), as presented in figure 1.1. The initially spherical cell will start to stretch and deform, as the upper part of it (the part closer to the upper plate), will move at a higher speed than the lower part of it. Then, depending on the elasticity of the cell membrane, the cell will either burst due to the deformation, or tumble, with the upper part of the cell moving towards the lower part of the plate, allowing the cell to return to its original shape. This process is bound to repeat itself in this order, as long as the velocity difference between the two plates remains.

A simplified example of a cell experiencing predominantly normal stress in flow is a cell placed in a water solution flowing through the narrowing of a pipe, as presented in figure 1.2. If the water flowing through the wider part of the pipe has velocity $v = v_1$, then the water flowing through the narrower part of the piper will have a higher velocity, $v = v_2 > v_1$. As the cell passes through the center of the narrowing, the upper part of the cell will be pushed downward and forward by the fluid forces, while the lower part will be pushed upward and forward. Also, the anterior part of the cell (with regard to flow direction), will be moving at a speed v much closer to v_2, while the posterior part of the cell will be moving at a speed much closer to v_1. The result of the combination of these forces will be the stretching and deformation of the cell in the flow direction. Then, depending on the elasticity of the cell membrane, the cell will either burst due to the deformation, or return to its original shape after passing through the narrowing.

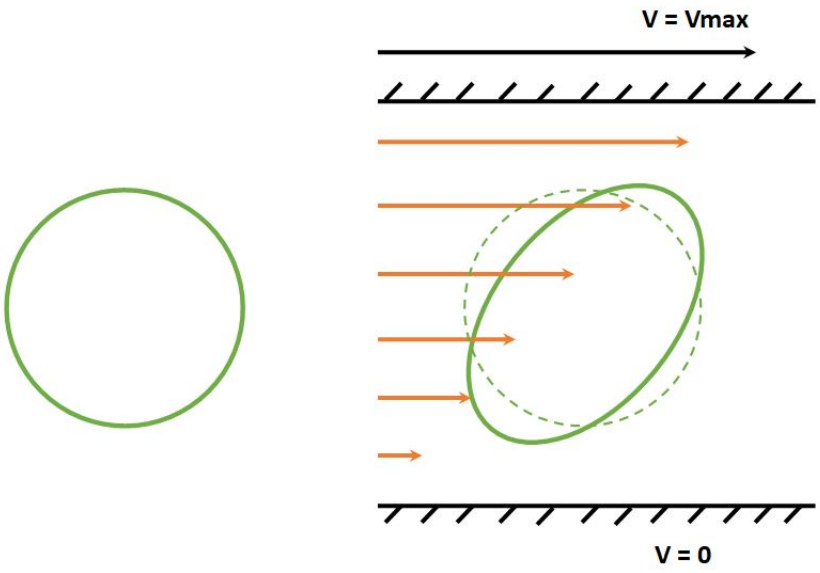

Figure 1.1: *Schematic representation of an originally spherical cell (a) deformed in predominantly shear flow between two parallel plates (b). The black arrow represents the velocity of the moving plate (upper plate), the orange arrows represent the corresponding form of the velocity inside the fluid.*

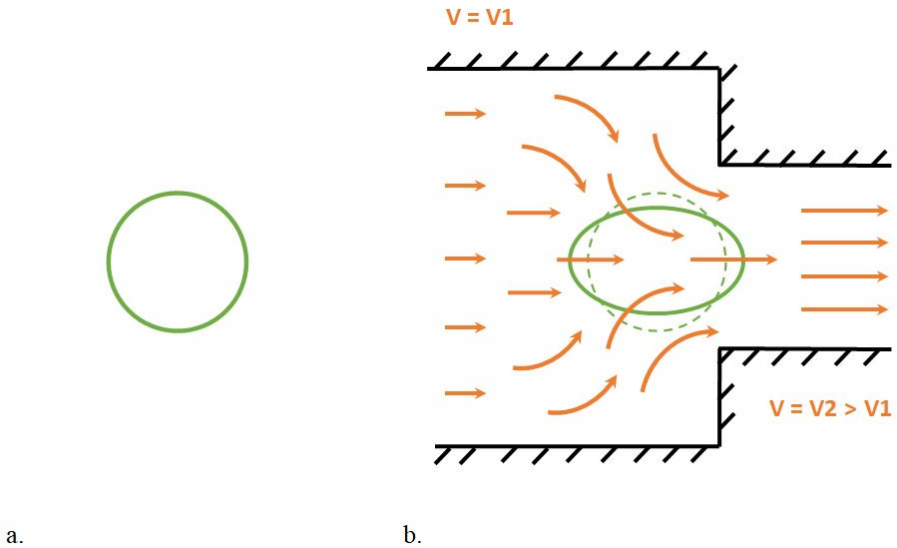

Figure 1.2: *Schematic representation of an originally spherical cell (a) deformed in predominantly normal flow through the narrowing of a pipe (b). The orange arrows represent the corresponding form of the velocity inside the fluid.*

Hydrodynamic stress is usually described in tensor form as summarized below:

$$\boldsymbol{\tau} = \eta \cdot \begin{bmatrix} 2\frac{\partial u_x}{\partial x} & \left(\frac{\partial u_x}{\partial y} + \frac{\partial u_y}{\partial x}\right) & \left(\frac{\partial u_x}{\partial z} + \frac{\partial u_z}{\partial x}\right) \\ \left(\frac{\partial u_y}{\partial x} + \frac{\partial u_x}{\partial y}\right) & 2\frac{\partial u_y}{\partial y} & \left(\frac{\partial u_y}{\partial z} + \frac{\partial u_z}{\partial y}\right) \\ \left(\frac{\partial u_z}{\partial x} + \frac{\partial u_x}{\partial z}\right) & \left(\frac{\partial u_z}{\partial y} + \frac{\partial u_y}{\partial z}\right) & 2\frac{\partial u_z}{\partial z} \end{bmatrix} \tag{1.1}$$

where the elements in the principal diagonal of the tensor represent the strain rates and the rest represent the shear rates in each of the three spatial dimensions. There are different ways on how to use this tensor to describe the maximum stress exerted on the cells. One way, usually applicable in well-defined flow conditions, is to extract specific elements of the tensor to represent shear or normal stress (Acosta-Martinez et al., 2010). Alternatively, the entire tensor can be used to determine a value for hydrodynamic stress, in order to take into account that, especially in non-ideal cases, all elements of the tensor would participate in fluid deformation and thus the deformation of a cell in flow (Apel et al., 2001; Shadden and Arzani, 2015). This is achieved by using the following mathematical formula:

$$\tau_{total} = \frac{1}{\sqrt{3}}\sqrt{\sum \tau_{ii}^2 - \sum \tau_{ii} \cdot \tau_{jj} + 3\sum \tau_{ij}^2} \tag{1.2}$$

where, τ_{ii}^2 represents the elements of the diagonal of equation 1.1, and τ_{ij}^2 represents the rest of the elements.

In turbulent conditions, as they arise e.g. in a stirred tank or a pump, instead of streams of velocities, there appear continuous fluctuations in flow in the form of swirls called eddies. They emerge in different sizes in the flow, and their relative size to the size of the cells determines the impact they exert on them. More specifically, if an eddy is significantly larger than a cell, then the eddy will surround the cell completely, and the latter will remain unaffected. On the other hand, when an eddy is significantly smaller than a cell, it will flow over its surface without affecting it. The main interest appears when the eddy is of comparable size to the cell, in which case it can inflict hydrodynamic stress on the cell's surface. A schematic representation of the possible relation between eddy size and cell size is presented in figure 1.3.

There is a way of estimating the relevant scale of the eddies in turbulent conditions, which is based on Kolmogorov's theory of isotropic turbulence, and is defined as (Hinze, 1975):

$$\theta = \left(\frac{\nu^3}{\epsilon_M}\right)^{1/4} \tag{1.3}$$

where θ (m) the Kolmogorov length scale of turbulence, ν ($\mathrm{m}^2 \cdot \mathrm{sec}^{-1}$) the kinematic viscosity of the fluid, and ϵ_M ($\mathrm{W} \cdot \mathrm{kg}^{-1}$) the energy dissipation rate per unit mass. Above this measure, inertial forces dominate, while below this measure, viscous dissipation forces dominate. It has been a long time assumption that, if the length scale calculated for specific conditions is smaller or of similar order of magnitude to the cell size, the cells will be damaged by the eddies in the turbulent field, while if it is larger, the cells will be engulfed by the much-larger eddies and thus remain unaffected (Cherry and Papoutsakis, 1986). This assumption has been supported by several publications (McQueen et al., 1987; Croughan et al., 1989; Joebses et al., 1991; Contreras et al., 1998).

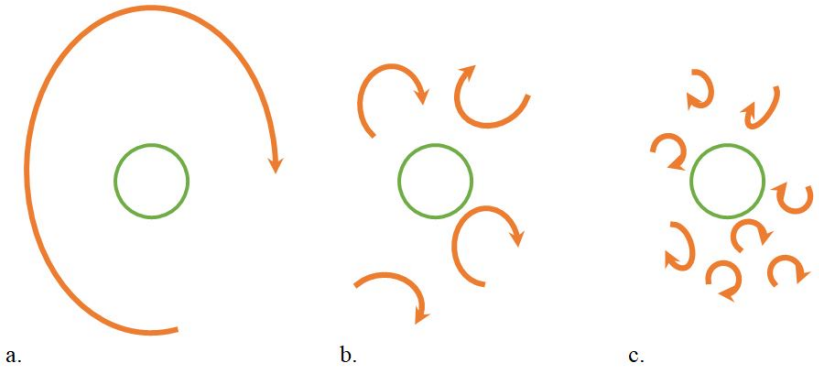

Figure 1.3: *Schematic representation of a cell (colored green) interacting with eddies of various sizes (colored orange) in turbulent flow: (a) eddies significantly larger than the cell; (b) eddies of similar size to the cell; (c) eddies significantly smaller than the cell.*

It is evident that laminar and turbulent conditions differ in the way they influence a cell in flow. When considering cell rupture in flow, there should still be a way to compare between the two conditions, as well as among different hydrodynamic systems in general. A solution is offered by measuring and comparing the energy dissipation rate (EDR) and total energy dissipation that is released in the cell suspension (Dunlop et al., 1994). The energy dissipation rate ϵ (Hu et al., 2011) is calculated by the following formula:

$$\epsilon = \eta \cdot \dot{\gamma}^2 \tag{1.4}$$

which describes the energy introduced into the system per unit volume of liquid. This parameter is easily obtainable for well-defined flows but can also be easily determined as an average value for complex flows, for example by dividing the energy required by a stirrer to mix a suspension in a bioreactor by the total volume of the suspension (Hu et al., 2011).

When the energy dissipation rate is multiplied by the duration of the process, it gives the total energy dissipation E. This is another measure considered relevant for process design and comparison (Dunlop et al., 1994), as different processes could reach the same levels of total energy dissipation either by adjusting the energy dissipation rate or the time the cells are subjected to hydrodynamic stress. The measurement of the energy dissipation was first introduced to describe hemolysis (Bluestein and Mockros, 1969), i.e. the rupture of erythrocytes and the consequent release of hemoglobin, and has been widely used ever since (Kresta, 1998; Hu et al., 2011). Literature findings offer equations connecting both the laminar shear stress and the turbulent eddies to energy dissipation, thus allowing for a direct comparison among different conditions (Dunlop et al., 1994; Shadden and Arzani, 2015). Therefore, both the energy dissipation rate and the total energy dissipation are relevant when designing a cultivation system or a downstream process for biological cells.

To summarize, the main environmental parameters relevant to the subject of cell sensitivity to hydrodynamic stress are the type of flow, i.e. laminar or turbulent, and the type of hydrodynamic stress, as well as its corresponding energy dissipation. Having determined the necessary parameters, the next most important issue becomes how to properly measure those parameters. First of all, the experiments need to be set-up and performed under well-defined hydrodynamic conditions, since information acquired from a “black box” is unlikely to be applicable to other systems. Various devices can generate well-defined hydrodynamic fields, and have been implemented in the literature by researchers, depending upon the type of flow that needs to be tested and the relevant equipment being used by the respective research group.

Considering laminar flow, the standard measurement device is a rheometer, with different configuration types [e.g. parallel plates (Levesque and Nerem, 1985; Stathopoulos and Hellums, 1985), cone and plate (Brooks, 1984; Sutera et al., 1988), or concentric cylinders (Dunlop et al., 1994; Michels et al., 2010)], each type bearing its own advantages. When the cells are placed inside such a setup, in the parallel plates case for example, the ones

near the center of rotation experience almost no hydrodynamic stress. This is due to the fact that the velocity gradient and the corresponding hydrodynamic stress near the center are almost zero. On the other hand, the cells near the edge experience the highest amount of hydrodynamic stress, as this is where the velocity gradient is maximized. Depending on the configuration and speed of rotation of the moving part, the shear rate is measured, and additional useful data can be determined, such as the viscosity of the cell suspension, or the relevant shear stress that the cells experienced. Such systems have the advantage of being easy to operate and having their arising flow conditions fully characterized and described by analytical rheological equations (Joshi et al., 1996), even though some support by computational fluid dynamics (CFD) simulations might be necessary in some complex cases (Marchesini et al., 2015; Lac and Parry, 2017). In many publications using such systems, the cells are either immobilized, or placed in a modified medium that includes chemical thickeners to increase the hydrodynamic stress exerted upon the cells. Thus, in such cases, the cells are not experiencing hydrodynamic stress in their natural state, as they would e.g. experience it while suspended in a bioreactor. This fact leaves an open window for investigation in terms of the measured critical stresses during cell rupture.

Another viable option is laminar flow through a capillary (Lange et al., 2001; Tanzeglock et al., 2009), which is usually obtained by connecting a pump to a capillary tube, thus generating a flow field inside the capillary through pressure difference. The cells flowing in this setup experience initially a combination of shear and normal stress when entering the contraction between the tube exit and the capillary entrance, and then experience predominantly shear stress while flowing inside the capillary (the cells nearest to the capillary wall experience higher intensities of hydrodynamic stress than the cells flowing near its center). To determine the exact hydrodynamic stress inflicted in capillary flow, both analytical equations and CFD simulations are required, since the flow in syringe-capillary systems is not as well characterized as the respective flow in rheometers. Such analyses from the literature have led to the expectation that the highest amount of hydrodynamic stress in this setup is experienced by the cells as they enter the capillary, an observation supported both by experimental data, and computational fluid dynamics simulations (Tanzeglock et al., 2009; Down et al., 2011).

Considering turbulent flow, there is a substantial body of experiments on cell rupture, since turbulence is the most widely used source of mixing in the bioreactor (Zhang et al., 1993;

Cherry, 1993). In some cases, capillaries have also been used to generate the turbulent flow affecting the cells (McQueen et al., 1987; Zhang et al., 1993; Tanzeglock et al., 2009). Another commonly used approach is the mixing of a cell suspension by some standard impeller (Oh et al., 1989; Kunas and Papoutsakis, 1990; Li et al., 2006). In such cases, the cells are flowing freely inside a vessel, and either experience hydrodynamic stress when in the proximity of the impeller, or might be affected by the size of the generated turbulent eddies, as mentioned previously. An additional source of damaging to the cells in turbulent flow might be the repeated relaxation and stressing that the cells undergo in such conditions, which could conceivably wear down their membrane after repeated exposure (Dunlop et al., 1994). The flow regime in those setups has some well-known characteristics, such as the energy input from the impeller and the mixing conditions, which are considered as containing adequate information to determine the stresses that the cells experience, even though the flow is not perfectly characterized. In such cases, CFD simulations have been proven essential to gain an understanding of what the cells really experience in flow (Hutmacher and Singh, 2008). Finally, there are also cases where non-standard equipment has been used, due to the equipment's scientific or industrial relevance at that particular time period (Contreras et al., 1998; Barbosa et al., 2004; Garcia-Camacho et al., 2007).

To summarize, hydrodynamic stress consists of shear and normal stress and, in turbulent conditions, is mostly expressed in the form of swirling eddies. Both the hydrodynamic stress and the energy dissipation can be used as measures of cellular stressing in flow, with the latter having the added benefit that it can be used to compare between laminar and turbulent conditions. Finally, different types of equipment for measuring and inflicting hydrodynamic stress upon cell suspensions were mentioned, along with the corresponding information regarding the flow conditions that are obtainable by them.

1.3.2. Cellular response to hydrodynamic stress

The response of cells to hydrodynamic stress is extremely diverse, regarding the strain of the affected cells and the levels of stress that are relevant for that specific strain. Despite the various experiments performed in the literature to measure cell response to hydrodynamic stress, it is still relatively unclear how to distinguish between purely physical and biological responses. In terms of the pure physical part, hydrodynamic stress can cause cell membrane rupturing and eventual cell disruption, which is regarded as a form of non-programmed cell death (i.e. cell lysis). However, upon damaging of the cell membrane, the biological response

kicks in, since the cellular mechanisms of membrane repair are activated, always bearing the same mode of action across different cellular types (Hernandez-Onate and Herrera-Estrella, 2015). This particular mechanism involves especially eukaryotic cells, gradually reversing the damage on the cell membrane, by using the cell's resources to repair it. It can provide a possible explanation for decreasing growth rates in bioreactors after increasing shear stress (Cherry, 1993), as the cells have to divide their resources to both repair and proliferation. A second biological response of relevance is the possible activation of programmed cell death (i.e. apoptosis) due to hydrodynamic stress. It can occur either due to the activation of the caspase pathways (Hsieh and Nguyen, 2005), or due to mechanostasis (i.e. the cell's attempt to balance the hydrodynamic forces affecting it) (Chan et al., 2011), and would obviously also result in decreased cell proliferation rates.

For upstream processes, the rate of cell growth and proliferation under conditions of hydrodynamic stress must be optimized (Hosaka et al., 1995; Garcia-Camacho et al., 2007). There is an expected optimum range when balancing out the need for efficient mixing by increasing, e.g. the stirring rate and hence the hydrodynamic stress in the system. On the other hand, the need to avoid cell death is maintained by lowering, e.g. the stirring rate, and hence the hydrodynamic stress in the system. Few studies have directly searched for that optimum range for a given microorganism, and always under very specific setup conditions (Contreras et al., 1998; Garcia-Ochoa et al., 2013). One example is the study of Contreras et al. (1998), presented in figure 1.4, where they could determine an optimum between the tested shear rates (corresponding to an optimal shear stress) for *P. tricornutum* cells growing in an airlift photobioreactor. This also indicated the existence of an optimum shear rate value for this species in this setup, which would require additional measurements to be determined.

Another approach regarding the issue of cell sensitivity to hydrodynamic stress in upstream processes is to perform experiments of increasing hydrodynamic stress in order to determine the critical threshold of hydrodynamic stress, below which the cells remain unaffected. The system is subsequently designed to operate in hydrodynamic stresses much lower than critical, therefore ensuring the safety of the upstream process, while at the same time retaining adequate mixing conditions for the cell culture. For example, Michels et al. (2010) performed rheometer experiments on *C. muelleri* cells, and were able to determine a critical threshold value of about $1 - 1.3\,\mathrm{Pa}$, as presented in figure 1.5. Having determined thresholds for other microalgae species as well, Michels et al. (2016) attempted to grow those species

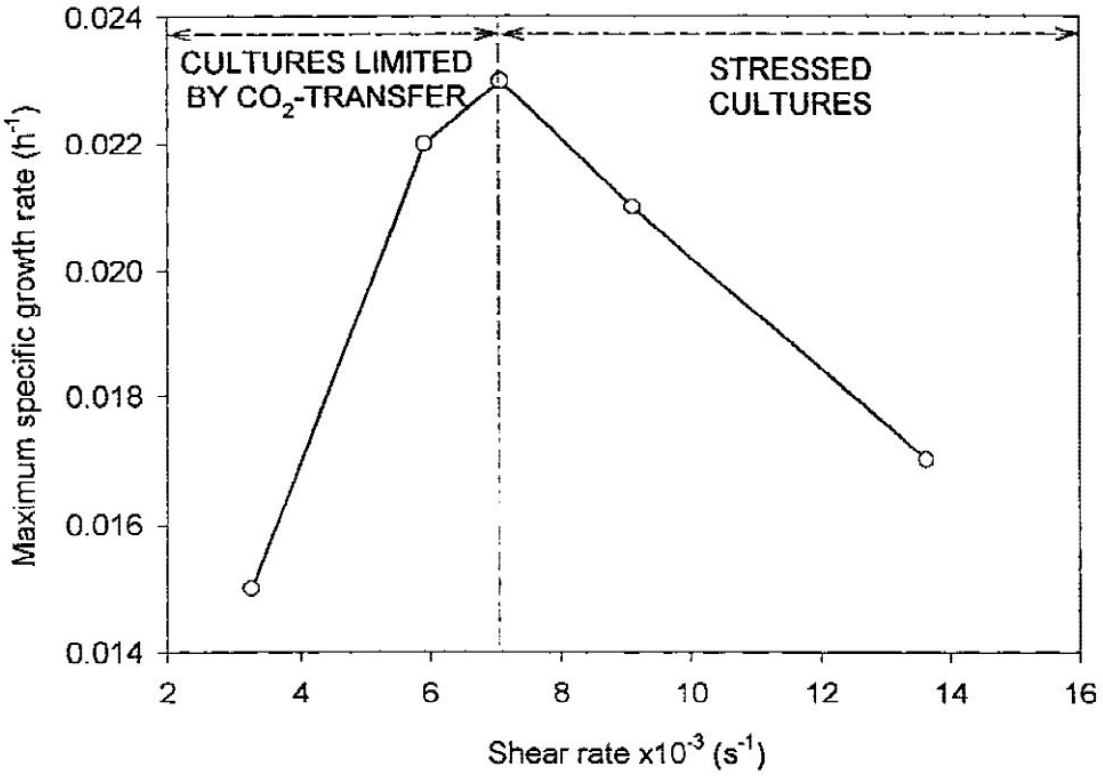

Figure 1.4: *Effect of shear rate on the maximum specific growth rate of P. tricornutum cells. Based on the experimental data, the optimal shear rate (corresponding to an optimal shear stress) for P. tricornutum cells in their setup was determined to be about* $7000\,\mathrm{sec}^{-1}$ *(Contreras et al., 1998).*

in a tubular photobioreactor, inflicting levels of shear stress of about $0.57 - 1.82\,\mathrm{Pa}$ on the cells through pumping. As expected, *C. muelleri* cells could not grow in the bioreactor, as the experienced shear stress levels were near the critical threshold, while *T. suecica* cells, that were shown in the rheometer measurements to be more resistant to hydrodynamic stress, were successfully cultivated. It is also important to mention that the critical hydrodynamic threshold causing cell death might be measured at much higher levels than the ones required for the cell population to lose the ability to proliferate. Dunlop et al. (1994) found that carrot cells would lose their ability to proliferate after experiencing significantly lower levels of total energy dissipation, than the ones required to compromise the membrane integrity and cause cell lysis, as presented in figure 1.6. This shows that not only viability measurements, but also testing cell proliferation ability after treatment, might be necessary to determine the real sensitivity of cells to hydrodynamic stress.

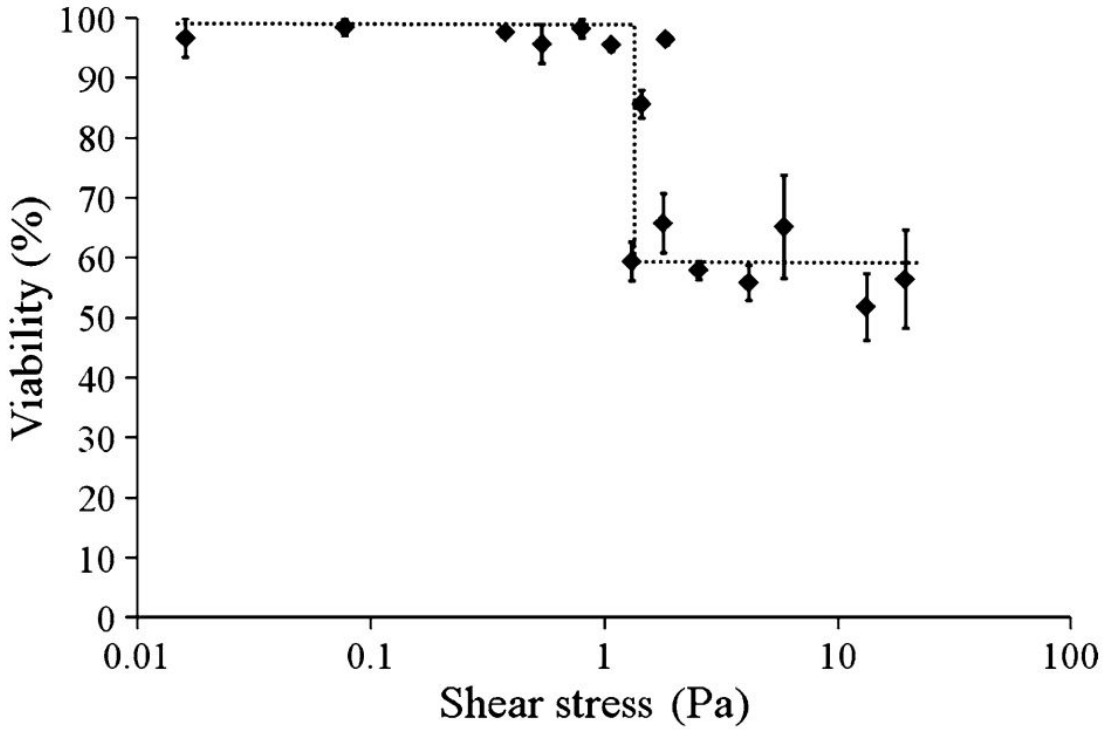

Figure 1.5: *Effect of shear stress on the viability of C. muelleri cells. Based on the experimental data, the critical hydrodynamic stress threshold for C. muelleri was determined to be between* $1 - 1.3\,\mathrm{Pa}$ *(Michels et al., 2010).*

As biotechnology is becoming increasingly more relevant, with the corresponding bioreactor productivity being pushed to the limit, the need for good mixing increases accordingly, thus increasing the hydrodynamic stress inflicted upon the cells, through such processes as pumping (Barbosa et al., 2003, 2004; Miron et al., 2003; Suzuki et al., 1995), stirring or gas sparging (Jaouen et al., 1999; Vandanjon et al., 1999; Brindley et al., 2004). Therefore, the more accurate the determination of critical hydrodynamic stress, the better the mixing that can be obtained by designing new and up-scaled systems operating as near to the critical boundary as possible (Hu et al., 2011).

On the other hand, for downstream processes, the rate of intracellular material release by hydrodynamic stress must be optimized. Cell rupture by liquid shear has already several applications, with the most common being high pressure or high shear homogenization, where the focus lies more on the minimum hydrodynamic stress required to cause disruption of the cell membrane and release of the intracellular materials, as well as the maximum stress required to ruptured all cells in a given sample. The parameter of hydrodynamic stress

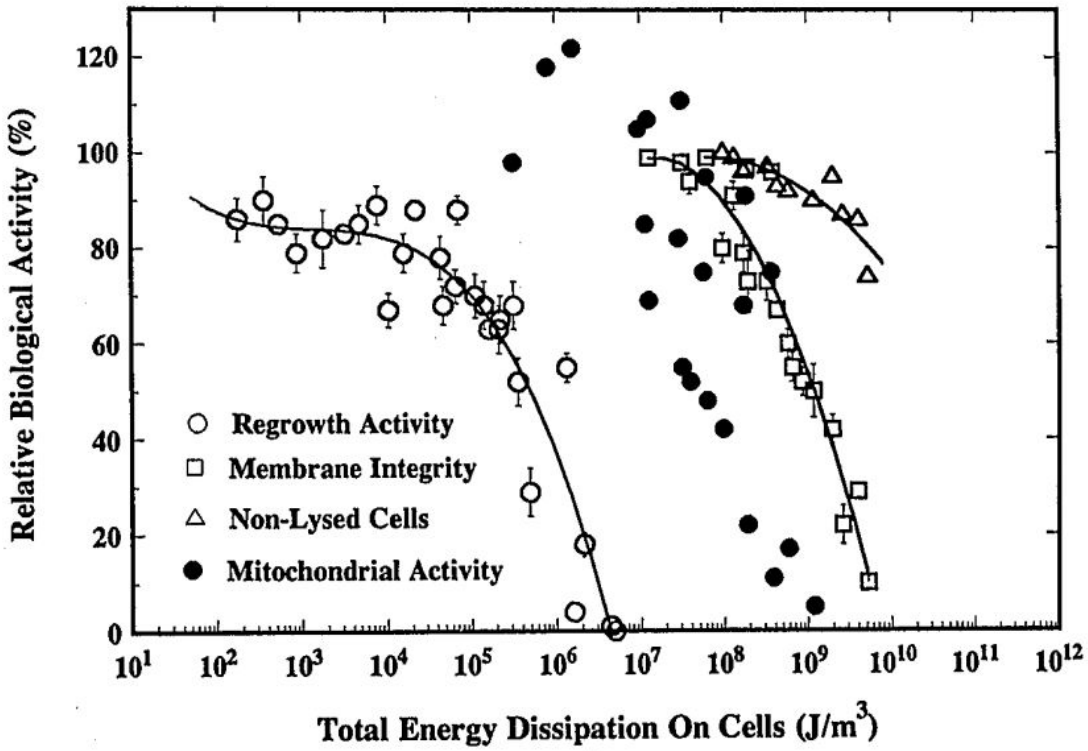

Figure 1.6: *Effect of shear stress on the viability and regrowth ability of carrot cells. Based on the experimental data, at total energy dissipation levels up to three orders of magnitude lower than the ones required to cause decrease in cell membrane integrity and cell lysis (Dunlop et al., 1994).*

corresponds to the minimum energy input and thus the minimum cost for the process, or alternatively to the maximum stress required to rupture all cells and the maximum possible release of the intracellular materials (Guenerken et al., 2015). In this respect, it is evident that hydrodynamic stress is not a problem, but a tool, when regarding downstream processing of cells. Downstream processes that use hydrodynamic stress as a method of cell disruption, have been widely applied for a long period of time (Middelberg, 1995; Guenerken et al., 2015). Finally, as with the upstream processes, it would be useful to be able to transfer the knowledge from one downstream process to another, when trying to design a new or an up-scaled version of the same equipment.

1.3.3. Cell heterogeneity and Population Balance Modeling

It is a well-known fact that all individual cells are different and even perfect clones start differentiating from each other after the first few minutes of existence (Elowitz et al., 2002). Given the versatility of cell heterogeneity, the question arises, whether cell heterogeneity

can significantly influence the sensitivity of cells to hydrodynamic stress. There are findings, indicative of a varying degree of cellular response to hydrodynamic stress between individual cells of the same population, leading to membrane rupturing or not (Born et al., 1992; Michels et al., 2010). They have been attributed to heterogeneity of the cell population, i.e. some cells of the population were more resistant to hydrodynamic stress than others. There have been measured variations of the cell population, regarding parameters that could influence cell rupture in flow, e.g. in the case of the cell size distribution during proliferation (Collins and Richmond, 1962) (presented in figure 1.7), or the cell membrane's Young's modulus (Radotic et al., 2012) (presented in figure 1.8), which is a measure of the strength of the cell membrane. Therefore, cell heterogeneity needs to be taken into account when determining the critical hydrodynamic stress, as there is a possibility of large deviations between members of the same cell culture, influencing optimal upstream and downstream process design.

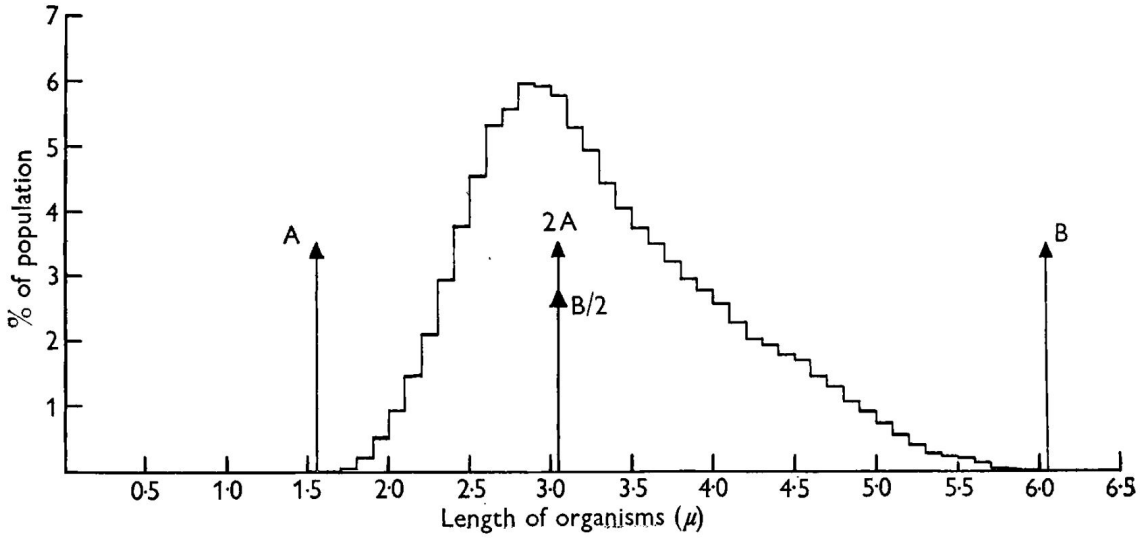

Figure 1.7: *Length distribution of B. cereus cells in a sample taken from an exponentially growing culture (Collins and Richmond, 1962).*

The simplest way to include heterogeneity in the modeling of shear sensitivity is by including normal distributions of the property values instead of constants, as was performed e.g. in the investigation of shear sensitivity of murine hybridomas (Born et al., 1992). However, if heterogeneity evolves in time, as is e.g. the case for the cell size distribution (Collins and Richmond, 1962), then equations that can describe this temporal evolution need to be included in the original study design. These equations are termed population balance equations and are becoming increasingly popular for applications with different cell types (Fernandes et al., 2011; Bertucco et al., 2015).

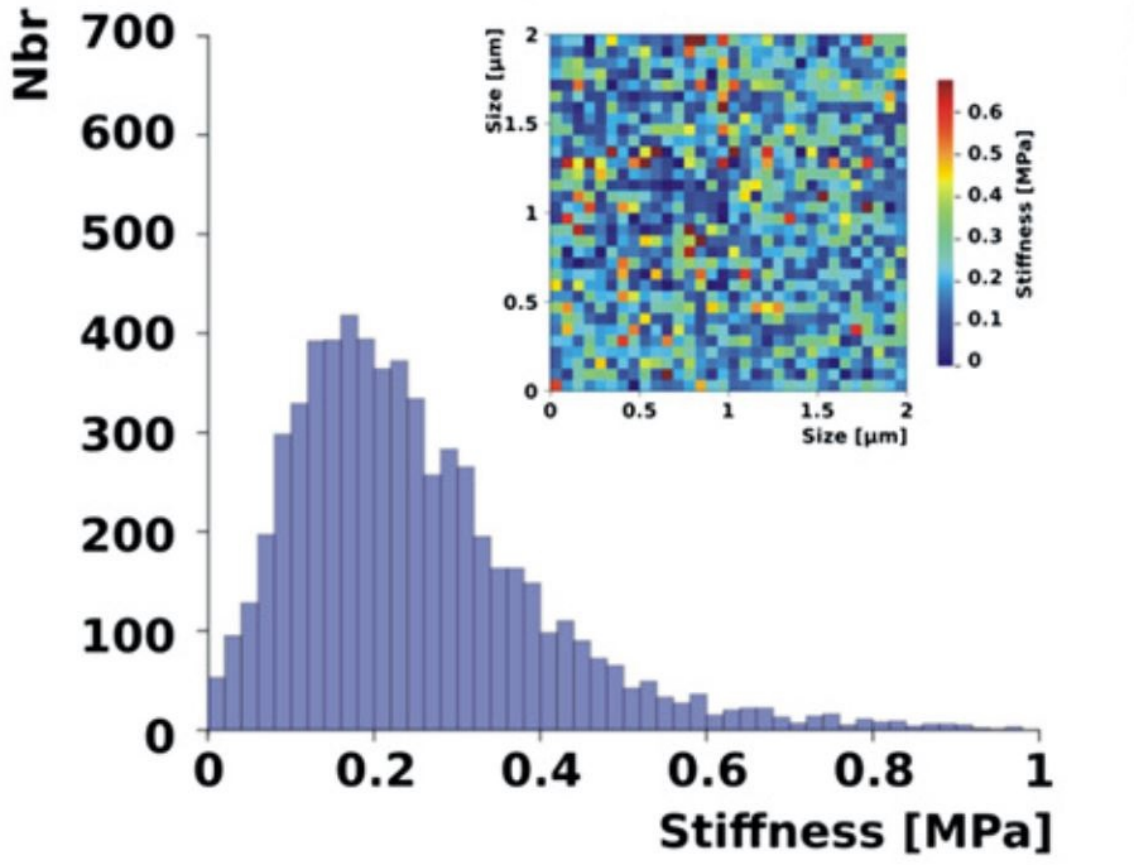

Figure 1.8: *Cell wall's Young's modulus distribution of a population of A. thaliana cells (Radotic et al., 2012).*

1.4. Microalgae cells

1.4.1. General

Microalgae are ubiquitous organisms and they can be found in fresh water (e.g. ponds, canals, lakes), in marine and hyper-saline environments (Williams and Laurens, 2010). They comprise two groups of prokaryotic microorganisms (Cyanophyta and Prochlorophyta) and various eukaryotic microorganisms (Chlorophyta, Rhodophyta, Phaeophyta, Bacillariophyta and Chrysophyta) (Mutanda, 2013). The term "microalgae" lacks a solid intensional definition, because the scientific knowledge on the species is still increasing rapidly, providing new reasons for altering the exact meaning of the term (Barsanti and Gualtieri, 2014). An extensional definition of the term would include eukaryotic, aquatic, oxygen-releasing photosynthetic organisms that lack complex multicellular structures and also a species of prokaryotic cells called cyanobacteria (Richmond and Hu, 2013). The metabolic mode can be either autotrophic or heterotrophic. The former group of microalgae cells require only

inorganic components in order to grow (e.g. salts, CO_2, light), whereas the latter group of microalgae cells are non photosynthetic organisms. There are also mixotrophic algae which, depending upon their needs, perform either photosynthesis or obtain exogenous organic nutrients (Behera et al., 2015).

They comprise one of the most prominent categories of microorganisms currently investigated in the field of biotechnology (Priyadarshani and Rath, 2012), having numerous applications, are easy to cultivate, do not cover land that could be used for traditional agriculture, allow the capture of carbon and the production of biomass, can survive in extreme environments, produce industrially relevant products of high quality [i.e. carotenoids (Del Campo et al., 2007) and omega-3/6 fatty acids (Ward and Singh, 2005)], and even have possible applications in terms of energy and biomass production in space (Lehto et al., 2006).

1.4.2. Microalgal Culture

Microalgal culture, on a large scale, can be classified into (i) open systems where the culture is directly exposed to the environment [e.g. natural ponds, artificial ponds (circular ponds, raceway ponds)], (ii) closed systems (e.g. tubular photobioreactors, vertical column photobioreactors, flat-plate photobioreactors) where the culture is entirely enclosed within the culture container, (iii) hybrid systems (e.g. hybrid photobioreactor) and (iv) newer technologies (e.g. internally illuminated photobioreactors, spectral shifting, membrane photobioreactors, offshore membrane enclosures for growing algae) (Dormido et al., 2014).

The vast range of research applications of microalgae generated a need for optimization, both in upstream and downstream processes involving those cells. More specifically, for upstream processes, there are current attempts of reducing energy consumption, by e.g. introducing baffles in photobioreactors and raceway ponds, which would improve mixing with the same energy input (Lam and Lee, 2012). On the other hand, for downstream processes, the main issue appears in the extraction of the lipids and intracellular chemicals, which is highly dependent upon the particular microalgae type and sometimes requires too much energy input, essentially creating the same issue as for the upstream processes (Lam and Lee, 2012). One significant optimization parameter for both upstream and downstream processes is hydrodynamic stress, as it needs to be below critical levels in upstream processes, since it can have negative effects on growth rates (Joshi et al., 1996), but is necessary for cell disruption in several downstream processes, such as high shear or high pressure homogenization

(Guenerken et al., 2015).

1.4.3. Products of microalgae

The main products of microalgae are the photosynthetic pigments they produce and store intra-cellularly, which are classified in three main categories: carotenoids, phycobilins, and chlorophylls. Carotenoids are natural pigments that are widely distributed in nature, comprising more than 600 known structures with a known antioxidant protective role (Krinsky, 1989). From the known carotenoids, mainly β-carotene and astaxanthin are used commercially (Rajesh et al., 2017). B-carotene, extracted from *Dunaliella salina*, is mainly used in the food industry as a natural food colorant and as provitamin A. This particular carotenoid form has further applications in cancer prevention (Stahl and Sies, 2003), as well as cosmetic and nutraceutical industries (García-González et al., 2005; Garcia-Chavarria and Lara-Flores, 2013). Another important carotenoid is astaxanthin which is found in the green microalga Haematococcus pluvialis. It is mainly used in aquaculture as a natural red colorant for farmed salmon flesh (Sastre, 2012). Additional uses include protection against cancer, inflammation and strengthening of the immune system (Guerin et al., 2003). Other carotenoids such as lutein, zeaxanthin, and canthaxanthin, produced in less important quantities, are used in animal feed and for pharmaceutical purposes (Rasmussen and Morrissey, 2007; Sastre, 2012).

Phycobiliproteins are protein-pigment complexes and can either be phycocyanobilin (blue pigment) or phycoerythrobilin (red pigment). They are produced on a large scale from *Spirulina* (cyanobacterium) and *Porphyridium* (red microalga). Their role is mainly hepatoprotective and anti inflammatory against various diseases (e.g. gastric ulcers, neurodegenerative diseases, cancer) (Ge et al., 2006). They have also antioxidant properties and they can be used as natural colorants in cosmetology (e.g. eye liner, lipstick), and in the food industry (eg chewing gum, ice sorbets, popsicles, candy, and milk products) (Elias et al., 2008; Lordan et al., 2011).

Chlorophylls are green pigments that are found in photoautotrophic organisms (plants, algae, and cyanobacteria). This pigment is primarily used in the food industry as a natural colorant in foods and beverages. Additionally, chlorophylls and their derivatives exhibit anticancer activity (Hosikian et al., 2010). During the past years, there is an ongoing interest in developing the biotechnological tools necessary for the production of chlorophylls from

microalgae (Rasmussen and Morrissey, 2007).

Finally, there are additional attempts to obtain valuable products from microalgae, such as using the lipids, proteins, and carbohydrates they contain for human or animal nutrition (Chew et al., 2017), since they have strong advantages over terrestrial crops, such as e.g. *Dunaliella* can produce up to a hundred times more protein than normal crops at an industrial scale (Hamed, 2016).

1.4.4. Hydrodynamics of microalgae suspensions

Research on the hydrodynamics of microalgae suspensions have been focusing on the issue of mixing, as it is considered a key issue for the cultivation process of many microalgae (Gudin and Chaumont, 1991). Mixing in a bioreactor is achieved by agitation, pumping or gas sparging, which introduce shear stress into the cell suspension. Low agitation rates induced oxidative stress to *P. reticulatum* cells (Gallardo Rodriguez et al., 2009), and high agitation rates generated bubbles that ruptured at the surface of the culture, damaging nearby cells, where the damage threshold for stirring speed was different for *P. tricornutum* and *P. cruentum* cells (Sobczuk et al., 2006). Bronnenmeier and Maerkl (1982) have shown for *C. reinhardii* and *S. platensis*, that the damaging levels of agitation rates could be predicted from the rate of energy dissipation from the stirrer to the cell suspension. It has also been shown that cell death in a bioreactor could affect the proliferation rates of the remaining viable cells, as e.g. was the case for *C. reinhardii*, where the release of intracellular chemicals resulting from non-programmed cell death led to a significant reduction in cell proliferation (Durand et al., 2011). Pumping led to loss of motility for *T. suecica* (Jaouen et al., 1999), chain breaking for *S. costatum* and damaging of *H. ostrearia* cells (Vandanjon et al., 1999), depending mainly on the pump type and frequency of loops. Gas sparging increased the death rate of microalgae *D. salina* (Barbosa et al., 2004), *P. tricornutum* (Miron et al., 2003) and *P. reticulatum* (Garcia-Camacho et al., 2007), primarily through an increase in superficial gas velocity.

Some researchers did not just investigate the effects of shear stress but also attempted to determine a critical, strain-dependent threshold. Contreras et al. (1998) found that for shear rates higher than $7 \cdot 10^3\,\mathrm{s}^{-1}$ (corresponding to an energy dissipation rate of about $5 \cdot 10^4\,\mathrm{W \cdot m}^{-3}$), there would be a decrease in the maximum specific growth rate of *P. tricornutum*. The calculated Kolmogorov length scale at the critical threshold was about $45\,\mu\mathrm{m}$, where

higher shear rates that generated smaller eddies caused cell damage. Garcia-Camacho et al. (2007) have shown that a critical shear stress as low as $0.16 \cdot 10^{-3}\,\mathrm{Pa}$ (corresponding to an EDR of about $8 \cdot 10^{-3}\,\mathrm{W \cdot m^{-3}}$) led to growth inhibition of *P. reticulatum*, and a further increase of shear stress led to cell death. Michels et al. (2010) determined a critical shear stress of about $1.3\,\mathrm{Pa}$ (corresponding to an EDR of about $20\,\mathrm{W \cdot m^{-3}}$) for *C. muelleri*. However, the cells in these experiments lost viability without any visible signs of deformation. Continuing their work, Michels et al. (2016) investigated the shear sensitivity of three more microalgae species using shear cylinders, finding that *I. galbana* and *S. costatum* are damaged by shear stresses of about $1 - 5\,\mathrm{Pa}$ (corresponding to an EDR of about $10^1 - 10^3\,\mathrm{W \cdot m^{-3}}$), while *T. suecica* remained unaffected for shear stresses up to $88\,\mathrm{Pa}$ (corresponding to an EDR of about $10^5\,\mathrm{W \cdot m^{-3}}$). Additionally, they investigated growing these strains in a tubular bioreactor using a centrifugal pump, where only *T. suecica* was successfully cultivated in the end, a fact the authors attribute to the shear tolerance exhibited by that specific microalgae species in their shear cylinder experiments.

Additionally, there were investigations on several types of photobioreactors, mainly for the characterization of their hydrodynamics of flow, such as plate (Perner et al., 2003), jet loop (Szafran and Kmiec, 2004), or torus bioreactors (Pramparo et al., 2008). There were even some attempts at modeling the influence of irradiation on the microalgae growth rates in the bioreactors (Merchuk and Wu, 2003). Finally, there have been several computational fluid dynamics (CFD) simulations focusing on optimization of the cultivation process of microalgae cells, as presented in the review paper of Bitog et al. (2011), and references therein. In particular, it seems that the main interest in CFD of microalgae is around bubble column bioreactors, with many researchers focusing on the mixing and the hydrodynamics of bubble rising in these reactors (Ranade and Tayalia, 2001; Ekambara et al., 2005; dos Santos et al., 2007).

To summarize, the investigation of the hydrodynamics of microalgae suspensions and their effect on the cells is a highly relevant and active scientific field, and has presented very diverse results regarding different microalgae species, setups of cultivation, and levels of hydrodynamic stress.

1.5. The genus *Dunaliella*

1.5.1. Taxonomy

The current status in the taxonomy of the genus *Dunaliella* is not very clear, since many rare species have been described and classified, whereas the implementation of molecular biology techniques has not resulted in a definite taxonomic scheme (Polle et al., 2009). They are unicellular algae and belong to the family *Polyblepharidaceae*. A number of different morphological studies have recognized a total number of 28 different species and classified 14 of them as halophilic (Massyuk, 1973; Preisig, 1992). This type of classification recognizes and accepts the *Dunaliella* section, which comprises the species *D. parva*, *D. salina* and *D. pseudosalina* and the *Viridis* section, which comprises the species *D. ruineniana*, *D. gracilis*, *D. bioculata*, *D. carpatica*, *D. granulata*, *D. baasbeckingii*, *D. minuta*, *D. media*, *D. minutissima*, *D. terricola* and *D. viridis*. Evaluations of the genus *Dunaliella* have been described in the literature, including the addition of further halophilic species (*D. asymmetrica*, *D. peircei*, *D. turcomanica*).

The field of molecular taxonomy of the genus *Dunaliella* is valid for the past 15 years, with the majority of the studies being using the 18S rRNA sequences and targeted intron sequences and additionally the ITS1-5.8S-ITS2 gene cluster sequences, as target regions for the implementation of a specific molecular technique (Olmos-Soto et al., 2000, 2009, 2012; Hejazi et al., 2010). Sequencing analysis of the species *D. viridis* and *D. salina* have confirmed the presence of at least four clades in the former species and three clades in the latter species (Assuncao et al., 2013). Furthermore, there are isolated findings of selected studies, highlighting the size of a particular intron as a suitable marker for the differentiation of different species of the genus *Dunaliella* (Olmos-Soto et al., 2012; Zamani et al., 2011).

1.5.2. Cellular morphology

Dunaliella cells present a variety of different shapes (eg oval, spherical, ovoid, pyriform, ellipsoidal, cylindrical), with round anterior and posterior ends (in the majority of the cases symmetrical). However, under extreme weather conditions (e.g. low temperature), the relative cellular morphology may change towards a bilateral, dorsiventral or asymmetrical shape. The length ranges from $5 - 29\,\mu m$ (mean length range between $10.9 - 16.9\,\mu m$ and the width ranges from $3.8 - 20.3\,\mu m$ (mean width range between $7.9 - 13.2\,\mu m$) (Richmond and Hu,

2013). The majority of the cells lack a cell wall, although there are cases where a glycocalyx layer is formed outside the plasma membrane. There is a single chloroplast, in the shape of a cup, and depending upon the carotenoid concentration levels, a change in the coloring of the cells is achieved (green to orange to red, as shown in figure 1.9 (Kleinegris et al., 2010)). The accumulation of the carotenoids is taking place in the intrathylakoid spaces of the chloroplast.

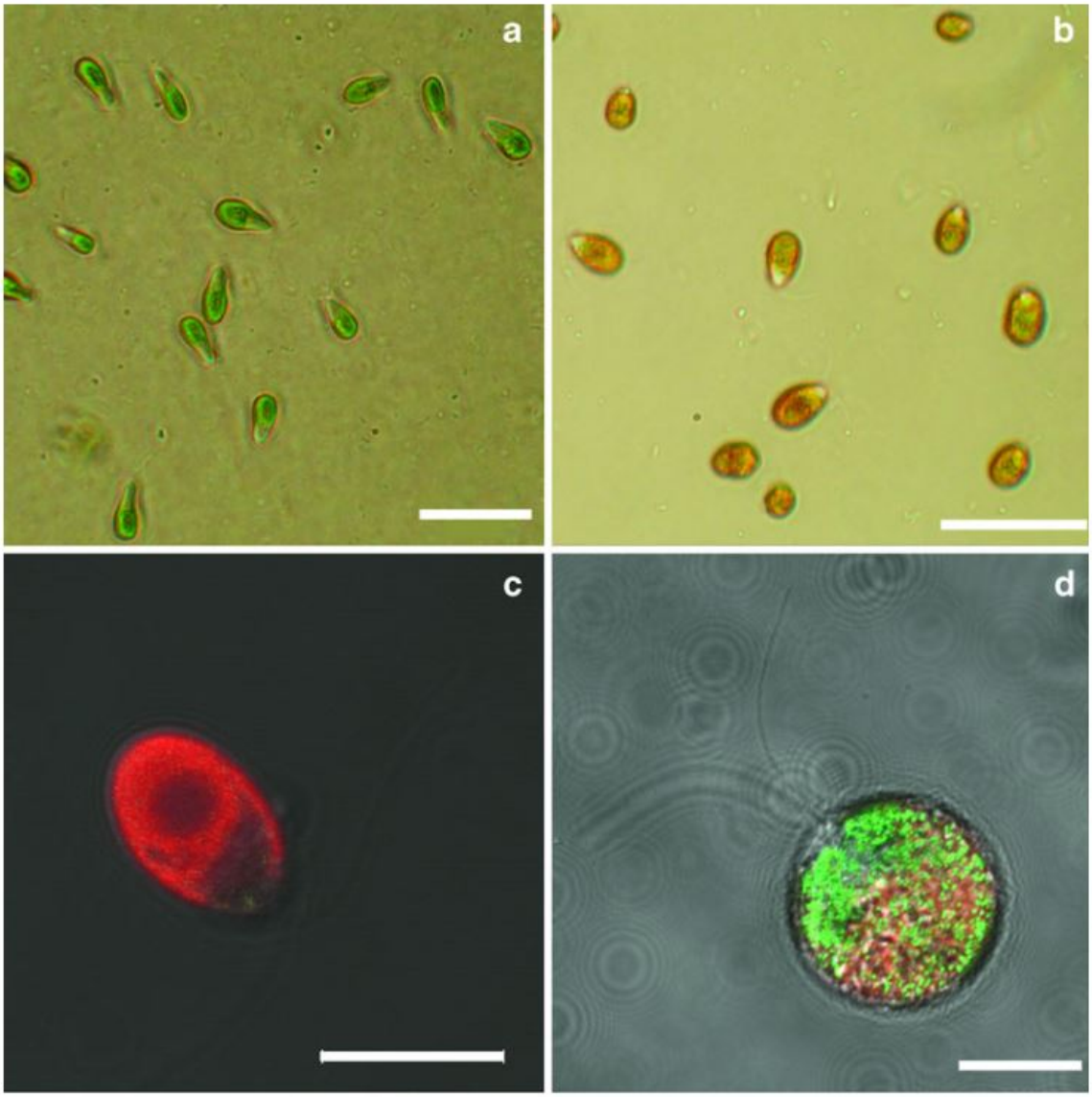

Figure 1.9: *Microscopy images of Dunaliella salina cells: bright field with low (a) and high (b) carotenoid concentration; fluorescence with low (c) and high (d) carotenoid concentration. Scales represent* 10 µm *(Kleinegris et al., 2010).*

1.5.3. Life cycle and sexual reproduction

The life cycle of *D. salina* along with other species of the genus *Dunaliella* can be characterized as complex and includes two possible scenarios, namely the division of motile

vegetative cells and sexual reproduction. The pioneering work of Lerche (1937), according to which sexual zygote formation was recorded in five different species of the genus *Dunaliella* (namely *D. salina*, *D. parva*, *D. peircei*, *D. euchlora* and *D. minuta*), verified findings of previous studies (Hamburger, 1905; Teodoresco, 1906; Hamel, 1931). The formation of the zygote was correlated with a reduction in the salt concentration from 10% to 3%, resulting in the release of 32 haploid daughter cells (Lerche, 1937). Figure 1.10 presents schematically the aggregation of red and green cells towards the formation of a zygote, a finding that was later confirmed by Oren et al. (1995).

There are also additional findings in the literature about formation of asexual cysts of *D. salina* in environments of reduced salinity (Hamburger, 1905; Loeblich, 1969), as well as the formation of a vegetative palmelloid stage of non-motile cells (Lerche, 1937; Brock, 1975).

1.5.4. Cultivation and salt tolerance

Initial experiments for assessing the effect of salt tolerance upon growth of different *Dunaliella* species were performed in the 1930s. *Dunaliella viridis* strains grew in the range of 1-4 M NaCl and a pH range of 6-9 (Baas-Becking, 1931). Furthermore, a high calcium and magnesium concentration was associated with a decreased rate of growth. Lerche (1937) recorded an optimal growth for the majority of tested *Dunaliella* isolates between 2-8% NaCl concentration and a mean daily number of 0.47-1.22 divisions. Following these studies, nutritional requirements for different *Dunaliella* species were recorded, namely around 6% NaCl for *D. viridis* and 12% for *D. salina*, respectively (Borowitzka, 1981). An interesting conclusion being deduced was that the salinity of the natural environment of detection of a particular isolate was much higher than the respective value in the laboratory setting. This assumption clearly highlights the fact that growth of a particular isolate in a specific environment does not necessarily mean that this environment is the optimal one for that particular isolate.

1.5.5. Osmotic behavior

Dunaliella cells are devoid of a cell wall and therefore are prone to intense osmotic changes, a finding being highlighted by Lerche (1937) experiments, according to which addition of distilled water in an environment of salt concentration of 20% results in cell rupture for the majority of *D. salina* cells. Nevertheless, there is a small cell fraction that survives this particular handling.

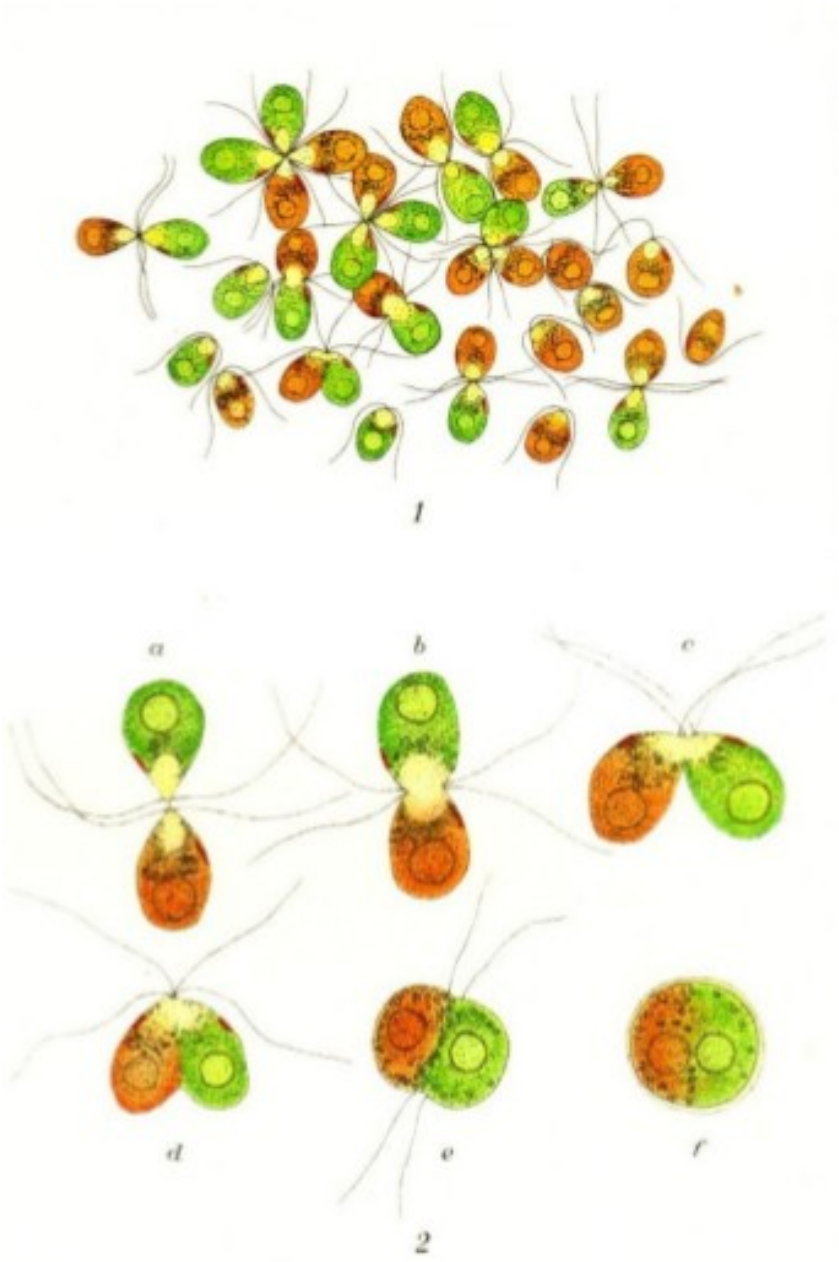

Figure 1.10: *Aggregation of the red and the green form of D. salina (upper part) and zygote formation of D. salina (green and red form) (lower part) (Oren, 2005).*

1.5.6. Intracellular salt and solute concentrations

The first information regarding the intracellular salt concentration of *D. salina* cells in 1959 estimated a concentration value of $>$ 3.9 M, as the necessary prerequisite for cell growth (Marre and Servettaz, 1959). The above notion was rejected by Johnson et al. (1968), who showed that some of the key enzymatic players participating in the algal metabolism are inhibited by NaCl. It is today a well known fact that the intracellular ionic concentration of

Dunaliella is very low, namely it does not exceed 100 mM (Katz and Avron, 1985). Furthermore, the need for osmotic equilibrium in the cell contents of *D. salina* is achieved through the accumulation of glycerol, which acts as a compatible solute. This mechanism was first referred by Teodoresco, whose work stated that when *D. salina* cells are suspended in a 75% glycerol medium, they temporarily lose their mobility which is rapidly restored once the cells enter an environment with high levels of humidity (Teodoresco, 1906). Suspension in glycerol medium of 75% resulted in the death of the majority of the cells, although the same principle - in terms of mobility restorement - remained the same. On the other hand, there have been reports about *D. salina* cells which grew in a 4 M NaCl environment and were found to contain intracellularly 7.8 M glycerol (Brown, 1990). This situation is indicative of the fact that the *Dunaliella* membrane has the capacity for extremely low permeability for glycerol, enabling for its intracellular accumulation (Brown et al., 1982; Gimmler and Hartung, 1988). The exact mechanism that the membrane of *Dunaliella* exhibits is still not clarified in the literature.

The high degree of *Dunaliella* adaptation to environments with varying degrees of salt concentration, has led to its use as a model organism in studying protein formation in response to changes in medium salinity. Proteomic studies have purified and characterized two specific membrane proteins, whose expression is induced by changes in salt concentration, resulting in assisting roles in terms of carbon dioxide absorbance and iron transport in the cell interior (Fisher et al., 1996, 1997). The study of Liska et al. (2004) compared the protein patterns of cells grown in a high and low-salt concentration environment and identified 76 proteins, which are involved in basic cellular pathways (e.g. Calvin cycle, redox energy production, protein biosynthesis, protein degradation). These findings provide evidence in favor of a mechanism of intensified carbon dioxide assimilation and conversion of carbon and energy resources in favor of glycerol synthesis.

1.5.7. Commercial production

Commercial production of *D. salina* was first attempted in Australia, Israel and the United States. Two different approaches are being used nowadays, namely the ‘extensive’ production in shallow open ponds and the ‘intensive’ production in raceway-type ponds. The former approach requires areas with warm climate, low levels of rainfall and a high annual irradiance. The largest production sites in the world are in Australia and they are shown in figure 1.11. These ponds have an average depth of about $0.3\,\mathrm{m}$ and use seawater as the main water source. Results from experiments have shown that maximum carotenoid production is

achieved in an environment of about 25% NaCl (Borowitzka et al., 1984). High levels of salinity act in a protective manner for *D. salina* against different protozoan predators and other algal species (Post et al., 1983). On the other hand, levels of NaCl below 15% result in cyst formation of crustaceans and a decline in the production rate of *Dunaliella* species. The annual production of *Dunaliella* is maintained due to high levels of salinity in the winter months. Nitrate or urea are the preferable nitrogen sources for optimal β-carotene production (Borowitzka and Borowitzka, 1989).

Figure 1.11: *Cognis Dunaliella salina β-carotene plant at Whyalla, Australia (Milledge, 2011).*

The latter approach is being used in $20 - 30\,\mathrm{cm}$ raceway ponds in Israel, India and China. Compared to Australia, the weather conditions are completely different and hence productivity cannot be maintained throughout the year (Tseng, 2001). The production cost is significantly increased in this case, since *Dunaliella* harvesting requires centrifugation. A two-stage cultivation for *D. salina* β-carotene production is possible in raceway ponds (Ben-Amotz, 1995).

Dunaliella salina harvesting presents certain obstacles, compared to other microalgae, due to the small size of the cells and oxidation resulting in losses of β-carotene. Therefore, meth-

ods such as flocculation and flotation and/or centrifugation have been applied for commercial production of *Dunaliella* (Sammy, 1987; Guelcher and Kanel, 1999).

1.5.8. Requirements for optimal growth

1.5.8.1. Light

Dunaliella uses only light for its metabolism, since it is an obligate photoautotroph (Borowitzka and Borowitzka, 1989). Open ponds use sunlight, whereas photobioreactors use either sunlight or fluorescent lamps. Light intensity plays an important role in carotenoid production and different wavelengths (eg UV-A radiation) lead to more pronounce carotenoid accumulation in certain *Dunaliella* species (e.g. D. bardawil) (Jahnke, 1999).

1.5.8.2. Temperature

Dunaliella can be adaptable within a wide range of temperatures (from below $0^{\circ}\mathrm{C}$ up to $45^{\circ}\mathrm{C}$). The optimal temperature in the laboratory setting is about $32^{\circ}\mathrm{C}$ and experiments in open ponds showed that low temperatures in night decrease *Dunaliella* growth (Borowitzka and Borowitzka, 1987). On the other hand, temperatures around $40^{\circ}\mathrm{C}$ slow the growth rate and enhance β-carotene production (Borowitzka and Borowitzka, 1989). Finally, temperatures $> 40^{\circ}\mathrm{C}$ lead to glycerol leaking, a medium playing the role of solvent for *Dunaliella* species (Wegmann et al., 1980).

1.5.8.3. pH control

Dunaliella species are extremely tolerant to pH changes (range between $0 - 11$), whereas the respective range for *D. salina* is $9 - 11$. High Ca^{+2} is associated with a decline in the rate of production and therefore a pH value > 8 must be prohibited (Ben-Amotz and Avron, 1989). Maintenance of pH < 8 is accomplished in open ponds through control of CO_2 and HCl (Ben-Amotz, 1995).

1.5.8.4. Nutrient requirements

The photoautotrophic nature of *Dunaliella* is requiring the presence of an inorganic carbon source (CO_2 or bicarbonate) and hence absence of that source inevitably leads to reduced growth rate (Borowitzka and Borowitzka, 1989). Optimal growth for *D. salina* is achieved by adding $NaNO_3$ or KNO_3 to a defined medium. Nitrate limitation leads to induced carotenoid production, yet prolonged limitation may lead to cell death and significant carotenoid reduction.

The element phosphorus, in the form of KH_2PO_4 or NaH_3PO_4, constitutes the valid choice for optimized results. However, high concentrations in open ponds may eventually lead to algal flocculation (Sukenik and Shelef, 1984).

1.5.8.5. Control of predators

Dunaliella cells are at an extreme danger at temperatures $> 38^{\circ}\mathrm{C}$ by amoeba and zooplankton ciliates (Ben-Amotz and Avron, 1989). These predators are characterized by an increased growth and injestion rate for *Dunaliella* (Moreno-Garrido and Canavate, 2001). As a result, different non-toxic for the algae chemicals need to be implemented, in order to kill the above mentioned predators. One promising option was treating algal mass cultures with quinine sulfate, after which all ciliates were killed and the algal-cell growth rate continued normally.

1.5.9. Hydrodynamic stress studies on *Dunaliella* species

While the *Dunaliella* species are highly relevant for biotechnology, investigation was focused on optimizing their proliferation rates and carotenoid production in bioreactors, while ignoring the problem of hydrodynamic stress (Zhu and Jiang, 2008; Kleinegris et al., 2011). The two main exceptions were the research of Silva et al. (1987) and Barbosa et al. (2004), both of which investigated the effect of hydrodynamic stress caused by bubble rupture on the cells, both concluding that higher gas flow rates would lead to higher death rates for the cells. Therefore, there is still room for investigation with regard to the effect of hydrodynamic stress on the *Dunaliella* species.

Dunaliella salina, which comprises one of the world's richest natural sources of β-carotene, was chosen as the model organism for this particular thesis. It is enclosed in a plasma membrane with no cell wall (Oren, 2005), an important parameter since microalgae without cell wall are considered to be more susceptible to hydrodynamic stress effects (Barbosa et al., 2003), which is already assumed to be true for *D. salina* (Silva et al., 1987). The cells are mostly grown in large open-ponds, where hydrodynamic stress is avoided (Borowitzka, 1999), or raceway ponds where shear stress is minimal (Richmond and Hu, 2013). As the effort on optimizing growth and carotenoid production of *D. salina* is still ongoing (Hejazi et al., 2003; Kleinegris et al., 2011), determining the critical levels of hydrodynamic stress for this cell species would allow ensuring good mixing rates, while avoiding any lethal effects on the cellular level for upstream processes. On the other hand, it would allow designing more

efficient downstream processes that ensure the release of intracellular material of *D. salina* through mechanical cell disruption by liquid shear stress (Guenerken et al., 2015).

Chapter 2

Materials and Methods

2.1. General

The combination of the relevant materials and methods, for each individual investigation, which were used for the duration of this PhD thesis, are presented in this chapter. Different subheadings are used, in order to fully describe the depth of each performed investigation.

2.1.1. Microorganism and culture medium

Dunaliella salina, strain no. 184.80, was provided by the Culture Collection of Algae at Goettingen University (SAG). It was cultivated in a modified Johnson's medium (Johnson et al., 1968), with the following composition (all quantities in $\mathrm{g\,L^{-1}}$): Na_2EDTA ($189 \cdot 10^{-6}$), $FeCl_3 \cdot 6H_2O$ ($244 \cdot 10^{-6}$), H_3BO_3 ($61 \cdot 10^{-6}$), $(NH_4)_6Mo_7O_{24} \cdot 4H_2O$ ($38 \cdot 10^{-6}$), $CuSO_4 \cdot 5H_2O$ ($6 \cdot 10^{-6}$), $CoCl_2 \cdot 6H_2O$ ($5.1 \cdot 10^{-6}$), $ZnCl_2$ ($4.1 \cdot 10^{-6}$), $MnCl_2 \cdot 4H_2O$ ($4.1 \cdot 10^{-6}$), $MgCl_2 \cdot 6H_2O$ (1.5), $MgSO_4 \cdot 7H_2O$ (0.5), KCl (0.2), $CaCl_2 \cdot 2H_2O$ (0.2), KNO_3 (1), $NaCl$ (65), $NaHCO_3$ (0.04), KH_2PO4 (0.04) (Carl Roth, Germany). Cells were grown in $1\,\mathrm{L}$ flasks (Carl Roth, Germany) placed $30\,\mathrm{cm}$ away from a warm light source (Osram, T8 L 18W/827 LUMILUX INTERNA G13, color temperature $2700\,^\circ\mathrm{K}$, Germany), with an alternating day/night cycle ($12\,\mathrm{h}$, $12\,\mathrm{h}$). Subcultures were created every two weeks, placing $500\,\mathrm{ml}$ of the culture and $500\,\mathrm{ml}$ fresh medium in a $1\,\mathrm{L}$ flask.

We made sure the cells were always cultivated at the same conditions and the cells used in the experiments were always between two and three weeks old, which should increase the comparability of the experimental results in all setups used.

2.1.2. Microscopy for cell count, morphology and viability

2.1.2.1. Cell count

A Thoma cell-counting chamber (Carl Roth, Germany), in combination with microscope pictures, was used for the determination of the concentration of suspended cells for all the tested samples. All samples were thoroughly mixed with a micropipette (Carl Roth, Germany), before the estimation of their cellular concentration. The counting chamber has a known depth of $0.1\,\mathrm{mm}$, allowing for the determination of the corresponding volume of the cell suspension captured in each microscope image, given that the microscope contains the µm/pixel information for each magnification of a given image. This is achieved by translating the area in pixel from the microscope image to area in µm, multiplying by the depth, and finally multiplying by the number of cells visible in the image to obtain the final cell concentration. Microscope images were taken at 10-50x magnification, depending upon the case of the tested samples.

In the experiments, there was an attempt for minimizing the duration of the procedure of cell concentration determination, specifically in terms of two different aspects: the first was gathering the information, i.e. capturing high-quality microscope images as fast as possible, and the second was counting the cells in each image as fast as possible (a process lasting up to several hours for a single experiment, given a high initial cell concentration number and obtained microscope images). Regarding the first aspect, finding the etched area takes time, and confining the pictures only to the etched area requires additional re-sampling and refilling of the chamber in order to obtain cell counts of adequate accuracy. Therefore, microscope pictures from the entire chamber were taken, making sure never taking pictures of the same cell/area of the chamber twice. In terms of the second aspect, i.e. fast counting of the cells in a microscope image, a program was written in MATLAB (version R2014a) by a former student of the Chair of Process Systems Engineering of the Technical University of Munich, Nicholas Sager, as a follow-up work to his Bachelor thesis (Sager, 2014).

This code uses a simple technique, more specifically, splitting the RGB microscope image information to three images, one for each of the three color channels, i.e. red, green, and blue, and then performing a subtraction by using the following formula:

$$image_1 = green(image_0) - red(image_0) \tag{2.1}$$

where $image_0$ is the original microscope image, and $image_1$ is the modified image to be used for cell counting. This process generates an empty image, except for the green colored objects of the original image, which in this case are the microalgae cells. Then the code tried to fit ellipses to the modified image and counted one object per each successful fit, providing the total object count as an output. The counted objects were subsequently colored and exported into new images, which allowed the user to check for errors in the cell count, making the necessary corrections. Thus, both the speed and the accuracy of the cell counting was increased (automatic counting of large batches of images; low level for human interventions). The essential parts of the used code are included as supplementary material in Appendix A.

2.1.2.2. Cell morphology

The cells were examined for any visible differences in cell morphology resulting from hydrodynamic damage, by using bright-field microscopy (Olympus, BX51, Germany) and a magnification of 10-50x. Additionally, differences in the visibility of the cell's flagellas were investigated in the microscope images, in cases where tearing of the flagellas was observed.

2.1.2.3. Cell viability

Fluorescence microscopy was used for the assessment of cell viability, a procedure based on illuminating a sample with light of a specific wavelength, so as to cause the fluorophores in the sample (fluorescing chemical compounds) to emit light of a longer wavelength. A mercury lamp (Olympus, Germany) was used, emitting light that passed through a dichroic mirror, allowing only blue light reaching the sample and activating the respective fluorophores.

The selected viability assay was based on fluorescein diacetate (FDA), a non-polar, non-fluorescent chemical substance that can easily penetrate the cells, and while inside, nonspecific esterases can break its molecule into two acetates and one fluorescein which brightly fluoresces, emitting in the green part of the visible light spectrum (about $530\,\mathrm{nm}$). As fluorescein is highly polar, it becomes entrapped in the cells, thus making the living cells easily distinguishable from the dead ones, due to their distinct bright-green fluorescence. Specifically, for microalgae (and other plant cells), there is an additional visual advantage to this method, as chlorophyll fluoresces in the red part of the visible light spectrum (about $650\,\mathrm{nm}$), making microalgae appear red in the fluorescence microscopy images. However, given a high FDA concentration, FDA fluorescence becomes stronger than the chlorophyll fluorescence of viable cells, and therefore all the viable cells in a microscope image appear green, while all

the non-viable cells appear red. This is especially useful for determining the percentage of viable cells in the tested sample (figure 2.1).

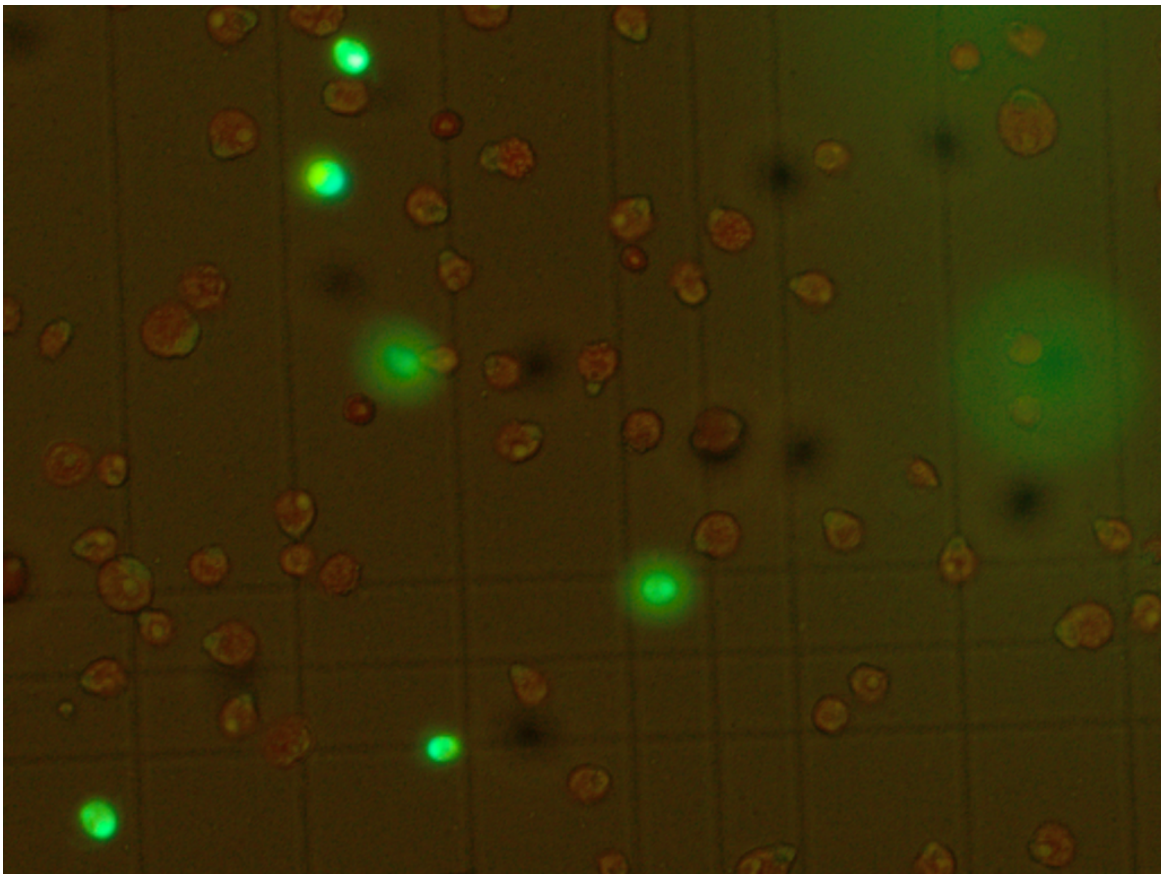

Figure 2.1: *Fluorescence microscopy picture of cells stained with FDA: (green) fully viable cells; (red) dead or apoptotic cells.*

We followed the method developed by Hejazi et al. (2003) for *D. salina* cells, based on the original work by Ross et al. (1989) on mammalian cell cultures and Gilbert et al. (1992) on microalgae. The method was subsequently optimized for fluorescence intensity as a function of time by Jochem (1999). Additionally, the FDA staining method has been shown by Altman et al. (1993) to be more accurate than the standard trypan blue method for determining cell viability, as with the former method only fully viable cells will fluoresce, while with the latter one cannot distinguish between fully viable and apoptotic cells. It is worth noting that the standard trypan blue solution did not mix with the cell growth medium used, forming blue clumps instead that stuck together, making determination of the cell membrane rupture using trypan blue for *D. salina* cells grown in a medium with the defined specifications an impossible task.

An FDA solution was prepared by dissolving $1\,\mathrm{mg}$ FDA powder (Sigma-Aldrich, Germany) in $1\,\mathrm{ml}$ acetone (Carl Roth, Germany). After each experiment, $50\mu\mathrm{l}$ of the solution were added to $1\,\mathrm{ml}$ of suspended cells, mixed by lightly shaking the tube with the sample, and then given a five minute incubation time. Following the incubation step, the sample was placed under a fluorescence microscope to obtain images of the cells for assessment of cell viability.

The preliminary experiments to test this method were performed by Quitt for his Bachelor thesis in the Chair of Process Systems Engineering of the Technical University of Munich (Quitt, 2015). Supervision of the thesis, along with the biological cells required for the experiments were provided by the current author. In those experiments it was noticed that the cells with the added FDA solution would cease fluorescing, when under a constant direct irradiance for periods of time longer than about $20 - 25\,\mathrm{sec}$, as presented in figure 2.2. This effect could reduce the accuracy of the derived data, therefore the measurement was redesigned in such a way as to overcome it. This effect was overcome by opening the shutter for the blue light to pass after all parameters were already at an optimal state, i.e. the camera was placed correctly, the lens focus was verified to be correct using normal light, the experimenters were trained to capture the microscope images as fast as possible, and the shutter was closed again immediately after taking each picture.

2.1.3. Intracellular protein release

Cell membrane damage often leads to rupture and as a result intracellular proteins are released in the cell suspension. Hence, measurement of the released intracellular proteins in the cell suspension can provide an indication of cell membrane rupture. The Bradford assay, introduced by Bradford (1976), is a quick and accurate method of measuring low levels of protein concentration in a solution (in the area of $\mu\mathrm{g} \cdot \mu\mathrm{l}^{-1}$) and is still commonly used in scientific publications (Spiden et al., 2013). Its principle is based on the binding of Coomassie Brilliant Blue G-250 to proteins that generates a peak at $595\,\mathrm{nm}$, which can be detected by any standard spectrometer that measures in the visible light spectrum. In general, the more cells ruptured in a process, the higher the peak at $595\,\mathrm{nm}$ should be, when the Bradford assay is used on a given sample of the cell suspension.

A sample of the cell suspension was first taken and centrifuged at $3000\,\mathrm{rpm}$ for $5\,\mathrm{min}$ to remove the cells and cell debris. Thereafter, $1600\,\mu\mathrm{l}$ of the supernatant were mixed with $400\,\mu\mathrm{l}$ Bradford reagent (Sigma Aldrich, Germany) and incubated for $5\,\mathrm{min}$ before measuring its

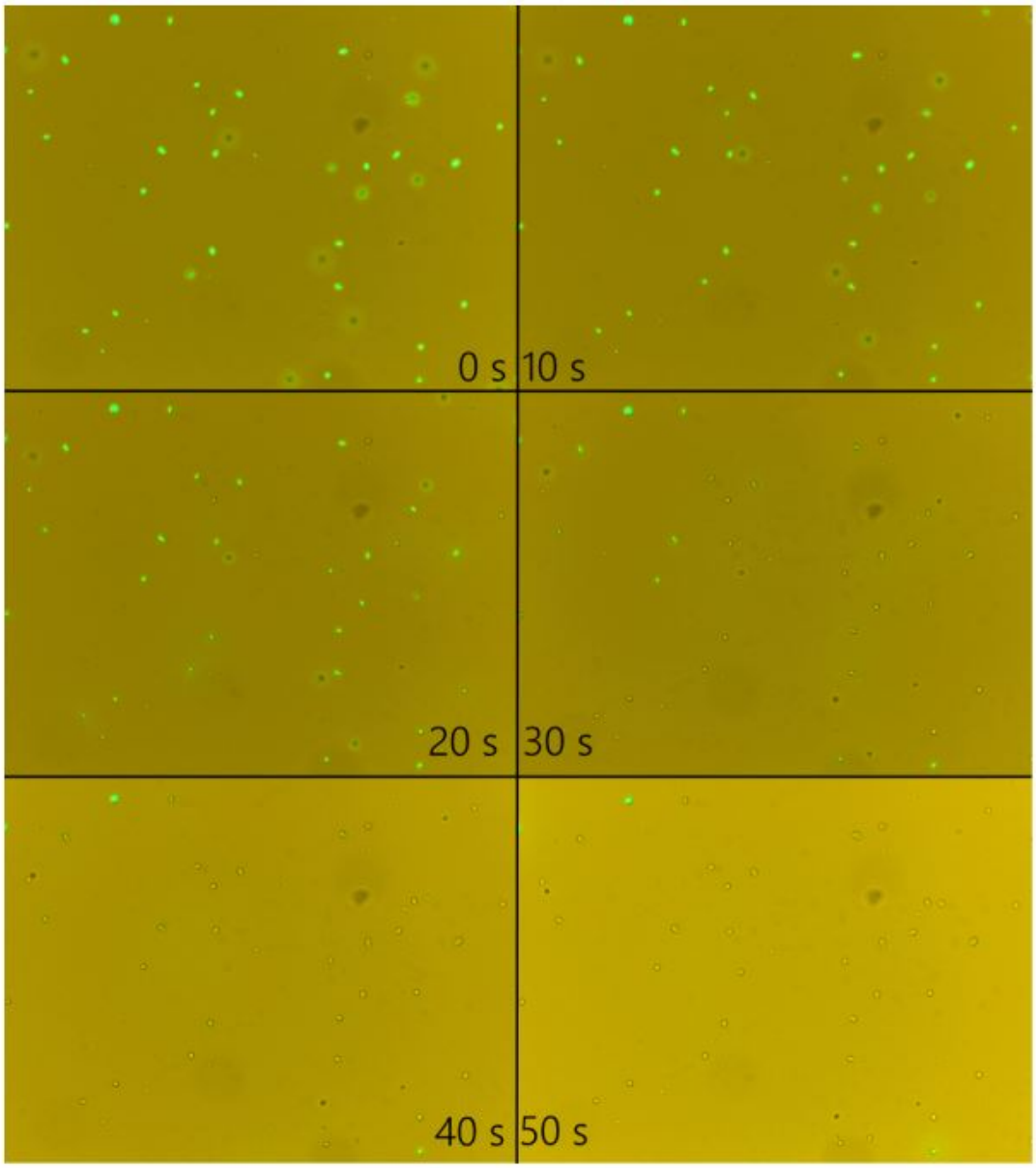

Figure 2.2: *FDA fluorescence reduction of D. salina cells under constant irradiation. The same image is presented at different time intervals, each marked by the total duration of exposure in* sec *(Quitt, 2015).*

absorbance a using a UV-VIS spectrometer (Spekord 50 Plus, Jena Analytic, Germany). The difference in absorbance:

$$\Delta a(t) = a(t) - a(0) \tag{2.2}$$

where $a(t)$ the absorbance of a sample at time t, and $a(0)$ the absorbance the supernatant of the untreated sample, was used as a measure of comparison in the experiments.

2.1.4. Normalized cell density

One standard way to quantify the effect of hydrodynamic stress on cells is to count the number of viable cells after being subjected in flow, which is usually termed normalized cell density NCD. There are currently two used formulas, both of which are presented in scientific publications (Vickroy et al., 2007). The first formula is summarized below:

$$NCD_t(t) = \frac{C_v(t)}{C_{total}(t)} \tag{2.3}$$

where C_v is the viable cell count at time t, and C_{total} is the total cell count at time t, including the dead cells. The second formula is summarized below:

$$NCD_v(t) = \frac{C_v(t)}{C_v(0)} \tag{2.4}$$

where $C_v(0)$ is the viable cell count at time $t = 0$, i.e. the viable cell count in the untreated sample.

Both formulas have advantages and disadvantages, depending upon the type of system they are being used. Both formulas were used to determine NCD in the experiments using the narrow-gap rheometer. A strong aggregation was exhibited by the non-viable *D. salina* cells (contrary to the viable ones), which tended to form clusters and attach to parts of the experimental equipment, e.g. pipette tips. This phenomenon posed many difficulties in proper sampling of the non-viable cells, moreover coming across a cluster of non-viable cells and capturing it in an image, and especially difficult to accurately count the number of non-viable cells comprising a cluster when one cell was captured, introducing a substantial error in the first described formula, which was mentioned above. Therefore, for the rest of the experiments only the second described formula was used, and hence any comparison between the experiments was also based on equation 2.4 solely.

2.1.5. Cell death rate

Determining cell death rates in a process is a common way used to compare among different hydrodynamic setups. When considering cell proliferation rates negligible for the timescale involved in the process, cell death rate can be described by the equation (Barbosa et al., 2004):

$$\ln\left(\frac{C_v(t)}{C_v(0)}\right) = \ln(NCD(t)) = -k_d \cdot t \tag{2.5}$$

where $C_v(t)$ is the viable cell count at time t, $C_v(0)$ is the viable cell count at time $t = 0$, whose fraction corresponds to the $NCD(t)$, as described by equation 2.4, and k_d (h^{-1}) is the cell death rate constant.

2.2. Narrow-gap rheometer experiments

2.2.1. Aim

The findings in the introductory section 1.3.1 were taken into consideration and supported the idea of using free-flowing cells in the experiments, as the respective conditions would most closely relate to the natural state of the *D. salina* cells (i.e. free flowing inside a suspension). We also chose to use an improvement to the standard rheometer, the narrow-gap rheometer (Dakhil and Wierschem, 2014), whose advantages are two-fold: one can obtain high shear stress without the use of thickeners, and the cells can be observed in flow through the transparent plates of the rheometer and the use of a high-speed camera. The parallel-plate configuration of a rheometer has already been used for inflicting shear stress upon cells, and referred to in some publications (Stathopoulos and Hellums, 1985; Levesque and Nerem, 1985), mainly due to the ease of operating such a system, as well as the fact that its arising flow conditions are fully characterized and described by analytical rheological equations (Joshi et al., 1996).

The goal of the narrow-gap rheometer experiments was the application of a novel rheo-optical setup for the observation of cells in laminar shear flow and the determination of the critical shear stress that leads to their deformation, without the addition of thickeners in the culture medium. It has been shown for droplet rupture, which could be considered a mechanically similar system to cell rupture, that shear and normal stress have different effects on the droplets, specifically droplets that rupture more easily under normal stress (Grace, 1982). Therefore, it was important to perform experiments determining the effect of pure shear stress on the cells, before moving on to the more complex systems.

2.2.2. Experimental procedure

Cell count, motility and deformation were evaluated through off-line microscope images, prior to shearing in the narrow-gap rheometer. Next, a sample of the cell culture was placed in the rheometer and shearing was initiated. During shearing, a high-speed camera video of the cells in shear flow was captured, with the camera positioned near the edge of the plates,

where the cells would experience maximum shear stress. Subsequently, the upper plate was raised, causing a droplet of the entire cell suspension to form in the center of the plate, making it impossible to take samples from specific radial positions. Thus, a homogenized sample was taken and used to obtain off-line microscope images of the cells after the completion of the shearing process.

2.2.3. Cell count and deformation

Dunaliella salina cells are highly motile biflagellate cells that use their flagellas for movement. The cells move constantly and relatively fast when observed in the microscope under normal conditions, so that their motility cannot be mixed up with random fluid movement, and can therefore be considered as a measure of cell viability. However, this constant cell movement results in the cells continuously shifting in and out of focus, an issue that could affect the accuracy of the cell count. This particular obstacle can be overcome by the addition of a 5% Lugol Potassium-Iodine solution to samples containing moving cells, before taking the off-line microscope images. Hence, immediate loss of cell motility and sedimentation is observed, which allows obtaining well-focused images and therefore accurate cell counts. For the cell counts, a sample from the cell suspension was placed in a Thoma cell-counting chamber (Carl Roth, Germany) with a depth of $0.1\,\mathrm{mm}$. The cell concentration of each measurement was in the order of 10^6 cells per ml. The volumetric proportion of the suspended cells was up to about 1%, which suggests that no significant cell-cell interaction should be expected during the measurements.

Regarding cell deformation, cells were differentiated between intact (i.e. the cells that retained the original ellipsoidal shape of *D. salina*) and deformed (i.e. the cells that visibly deviated from this shape). This particular distinction is presented in figure 2.3.

2.2.4. Normalized cell density

Regarding the parameter of normalized cell density, both equations 2.3 and 2.4 were used, which were mentioned in section 2.1.4. These equations refer to viable cells, however cell viability was not directly measured in the narrow-gap rheometer experiments. The only directly measured parameter was cell intactness, i.e. the ability of the cells to retain or not their original ellipsoidal shape.

[1] Reprinted from Biorheology, Vol 53, Kokkinos, D., Dakhil, H., Wierschem, A., Briesen, H., and Braun, A., Deformation and rupture of *Dunaliella salina* at high shear rates without the use of thickeners, Pages

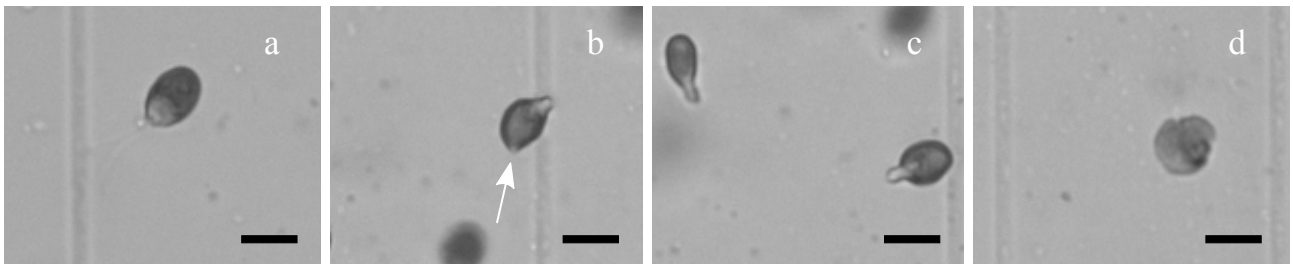

Figure 2.3: *Four (4) types of cells visible in the off-line microscope images after shearing.* ***a:*** *intact;* ***b:*** *deformed with a visible rupture of the cell membrane;* ***c:*** *deformed and elongated where the flagellas are usually attached;* ***d:*** *deformed with a collapsed membrane structure. Scales represent* $10\,\mu\mathrm{m}$ *(Kokkinos et al., 2016).*[1]

2.2.5. Cell death rate

Cell death rates were determined as described in section 2.1.5, and applied to the measured data about intact cells.

2.2.6. Intracellular protein release

We did not test for intracellular protein release in the cell suspension in the rheometer experiments, contrary to the rest of the experiments. This was mainly due to the fact that the $200\,\mu\mathrm{l}$ volume of cell suspension, placed in the narrow-gap rheometer, was difficult to retrieve after each experiment, allowing for only a few µl sample volume to be obtained for the necessary microscope measurements and hence not enough for a reliable Bradford assay measurement with the available equipment.

2.2.7. Exposure to hydrodynamic stress

The experiments were performed with a narrow-gap rheometer working in the parallel-plate configuration, where the upper plate had a $50\,\mathrm{mm}$ diameter and the lower plate $75\,\mathrm{mm}$. The narrow-gap rheometer is based on a rotational rheometer (Physica, UDS 200, Germany) that was modified to gain a gap-width precision of $\pm\,0.7\,\mu\mathrm{m}$. To obtain this precision, optical windows (Melles Griot, Netherlands) were used as plates and aligned them parallel to each other and perpendicular to the rotational axis, employing a confocal interferometric sensor which allows determination of the gap width independently from the rheometer reading. The

1-11, Copyright (2016), with permission from IOS Press. The publication is available at IOS Press through http://dx.doi.org/10.3233/BIR-15057.

rheometer was re-calibrated on a daily basis, following a previously published procedure (Dakhil and Wierschem, 2014).

The cells were sheared after two weeks of growth, at which point they were in the stationary phase. Two hundred (200) µl samples were placed between the parallel plates and sheared in constant maximum shear stresses between 0 and 90 Pa, for a duration of $1000\,\mathrm{sec}$. A $30\,\mu\mathrm{m}$ gap was selected, which allowed free cell flow, since *D. salina* cells have an average major axis length of $10\,\mu\mathrm{m}$. After each experiment, the upper plate was raised and a homogenized sample was taken for the microscope measurements. The experiments were performed at ambient temperature, which fluctuated between $24-26\,^{\circ}\mathrm{C}$, which is well within the fully viable range of temperatures for *D. salina* (which is between $0\,^{\circ}\mathrm{C}$ and $40\,^{\circ}\mathrm{C}$, as discussed in section 1.5.8.2 of the introductory chapter). Viscous heating was considered negligible for these experiments, as previously shown (Dakhil and Wierschem, 2014).

2.2.8. Rheo-optical setup

The transparent glass plates of the parallel-plate geometry allowed for witnessing cells in shear flow with the use of a high-speed camera (Mikrotron, Phantom Miro M310, Germany) connected to a 20x-lens, as shown in figure 2.4. The camera was placed under the bottom plate of the geometry and the lens was pointed to the outer rim of the plate, where the cells experience the maximum shear stress for a given shear rate. Additionally, a white LED-lamp (Volpi, VLP IntraLED 2020/W, Germany) connected to a light guide (Lumatec, 3716, Germany) was used to shed light directly from above at an angle of 45° with respect to the camera axis. The lamp was placed about $3\,\mathrm{cm}$ away from that area, and was turned off immediately after each experiment, to avoid continuous heating of the area and heat-shock-induced cell death. A sample frame rate of $10000\,\mathrm{fps}$ with an exposure time of $10\,\mu\mathrm{s}$ were adequate to observe cells in flow for a maximum shear stress up to $70\,\mathrm{Pa}$. For the cases of 80 and $90\,\mathrm{Pa}$, frame rates of $16000\,\mathrm{fps}$ and $18000\,\mathrm{fps}$, and exposure times of $10\,\mu\mathrm{s}$ and $20\,\mu\mathrm{s}$ were used, respectively. The exposure time was increased in the case of $90\,\mathrm{Pa}$ to provide adequate lighting conditions for the video.

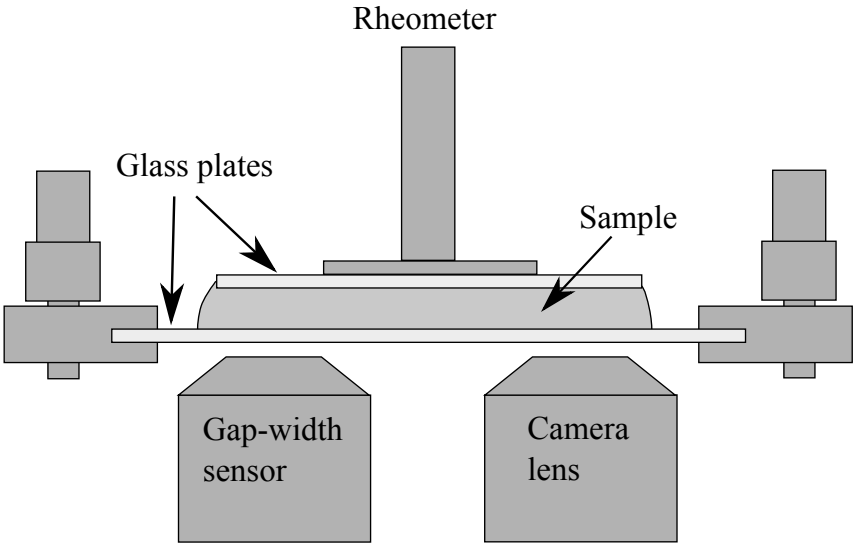

Figure 2.4: *Sketch of the setup used for the narrow-gap rheometer experiments. The top plate rotates and is connected to the rheometer. The bottom plate is stationary, and the position of the camera lens can be adjusted along the radius of the bottom plate (Kokkinos et al., 2016).*[2]

2.2.9. Analytical equations

The narrow-gap rheometer measurements were performed, using a parallel-plate geometry, for which the shear rate $\dot{\gamma}$, is defined by the equation (Malkin and Isayev, 2006):

$$\dot{\gamma} = \frac{r \cdot \omega}{H} \tag{2.6}$$

where r (m) is the position relative to the center of the plate, ω (rad $\cdot$ sec^{-1}) is the angular velocity and H (m) is the gap between the plates. The dimensionless Reynolds number Re for the parallel-plate system is calculated by (Malkin and Isayev, 2006):

$$Re = \frac{\rho \cdot \dot{\gamma} \cdot H^2}{\eta} \tag{2.7}$$

where ρ (kg $\cdot$ m^{-3}) is the density and η (Pa $\cdot$ sec) the dynamic viscosity of the cell suspension. As the cell suspension was similar to water, the Reynolds number for water (25°C) was calculated.

[2]Reprinted from Biorheology, Vol 53, Kokkinos, D., Dakhil, H., Wierschem, A., Briesen, H., and Braun, A., Deformation and rupture of *Dunaliella salina* at high shear rates without the use of thickeners, Pages 1-11, Copyright (2016), with permission from IOS Press. The publication is available at IOS Press through http://dx.doi.org/10.3233/BIR-15057.

The distribution of shear stresses is not homogeneous in the gap between the two plates, since it depends on the position r on the plate. The radial distribution is characterized by:

$$\tau(r) = \frac{r}{R} \cdot \tau_{max} \tag{2.8}$$

where R (m) is the radius of the upper plate and τ_{max} (Pa) the maximum shear stress at the edge of the plate. As indicated by equation 2.8, cells placed in the center of the plate experience no shear stress, while the cells near the boundary experience the maximum for a given stirring speed.

2.2.10. Critical shear stress criterion

To determine the safe operational levels of shear stress, it is assumed that there is a critical value of shear stress τ_{crit}, below which cells remain intact and are unaffected by shear. Also, cells are considered to be uniformly distributed in the bulk of the suspension during the shearing experiment. Based on the hydrodynamics of the parallel-plate geometry presented in equation 2.8, the critical shear stress corresponds to a specific distance from the center of the plate r_{crit}. As long as the maximum shear stress is lower than the critical, all cells should remain intact. If the maximum shear stress exceeds the critical value, only cells at a position $r < r_{crit}$ remain intact, since only these cells experience shear stress lower than critical. The relationship between the area of the plate for $r < r_{crit}$ and the percentage of cells which remain intact can be expressed as:

$$\%\,\text{intact cells} = 100 \cdot \left(\frac{r_{crit}}{R}\right)^2 = 100 \cdot \left(\frac{\tau_{crit}}{\tau_{max}}\right)^2 \text{ for } R \geq r_{crit},\ \tau_{max} \geq \tau_{crit} \tag{2.9}$$

Fitting equation 2.9 to the experimental data for each maximum shear stress where cell deformation occurred, i.e. in cases where at least 20% of the cells were deformed, determines the critical shear stress. The least-square fitting of the equation was performed using the curve-fitting toolbox in MATLAB (version R2015a), and provided the best fit along with 95% confidence intervals for the coefficient.

2.3. Capillary flow experiments

2.3.1. Aim

The findings in the introductory section 1.3.1 were once more taken into consideration and supported the idea of using free-flowing cells in the experiments, as the respective conditions

would most closely relate to the natural state of the *D. salina* cells (i.e. free flowing inside a suspension). We used a syringe-capillary system which had two main advantages, that is very easy to operate, and can generate high levels of hydrodynamic stress without the use of thickeners, which have made it one of the most widely used setups for experiments on hydrodynamic stress in the literature (Lange et al., 2001; Acosta-Martinez et al., 2010).

The goal of the capillary flow experiments was the application of a syringe-capillary system to generate high intensities of hydrodynamic stress that would lead to loss of viability for *D. salina* cells. Building on the knowledge from the previous experiments, cell deformation after exposure to hydrodynamic stress and intracellular protein release were tested as indicators of cell viability loss, using fluorescence microscopy as a standard for comparison. Additionally, a critical shear stress value for the flow inside the capillary was determined, in order to compare with the previous experiment. Finally, it was checked whether the surviving cells from the experiment had lost their ability to proliferate, and cell death rates for different flow rates inside the capillary were determined, which would allow the comparison with other hydrodynamic setups.

2.3.2. Experimental procedure

A glass syringe ($10\,\mathrm{ml}$, with metal cone and Luer-Lock-fitting, Carl Roth, Germany) with exchangeable metallic capillary tips (Disposable needles Sterican ©, blunt edge, outer diameter $0.4\,\mathrm{mm}$, gauge 27, Carl Roth, Germany) was filled with cell suspension and placed in a syringe pump (Syringe pump Elite 2.1, Harvard Apparatus, USA) with defined volumetric flow rates. During the syringe pumping, a plastic tube was placed at the end of the capillary to collect the pumped-out cell suspension, which was then used to refill the syringe from the back. Every ten repetitions, the capillary tip was changed and the syringe was cleaned with deionized water, 70% ethanol, and again deionized water, in order to avoid clogging due to cell debris. After completion of the repetitions, the final sample was used to determine viable cell count, intracellular protein release, and cell proliferation ability after shearing. The pump-syringe-capillary setup used for the experiments is presented in figure 2.5.

2.3.3. Cell count and viability

Cell count was measured using a Thoma cell-counting chamber, as described in section 2.1.2.1. Cell viability was determined using fluorescence microscopy and the FDA staining

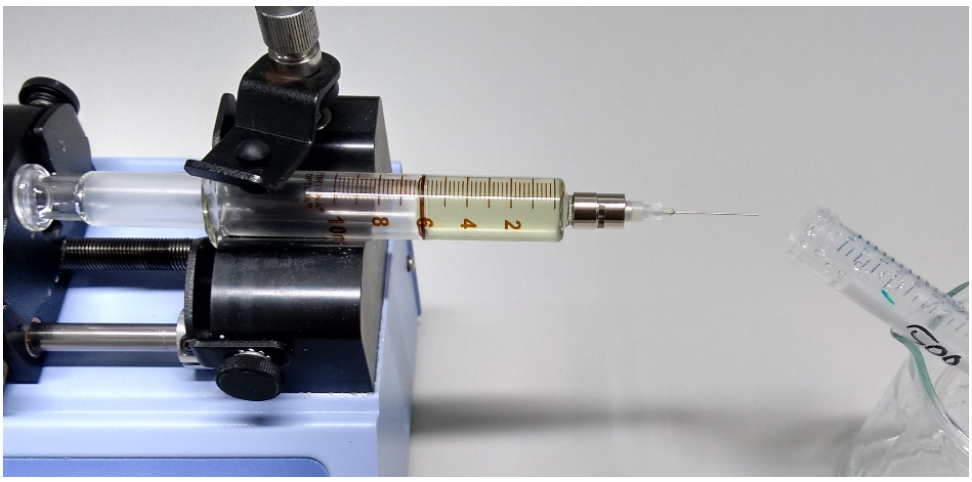

Figure 2.5: *The setup used for the syringe-capillary experiments. The glass syringe is connected to a capillary tip, and is pumped at a constant, defined rate. The cell suspension is collected at the exit to re-fill the syringe.*

method, as described in the same subsection. The concentration of cells in all experiments was in the order of 10^6 cells $\cdot$ ml^{-1}.

2.3.4. Normalized cell density

Regarding the parameter of normalized cell density, equation 2.4 was used, as described in section 2.1.4.

2.3.5. Cell death rate

Cell death rates were determined as described in section 2.1.5, for the data regarding volumetric flow rates where cell death occurred. The linear least-square fitting of the data was performed using MATLAB (version R2015a), with a fixed intercept at point (0,0).

2.3.6. Intracellular protein release

Intracellular protein release was measured in the supernatant of the cell samples, as described in section 2.1.3. The results were normalized in reference to the absorbance value of the untreated sample at 595 nm for each measurement.

2.3.7. Exposure to hydrodynamic stress

The exposure of the cells to hydrodynamic stress occurred during their repeated passage through the capillary and specifically during their passage from the narrowing between the

syringe tip and the capillary, where the highest normal and shear stresses are expected to occur (Sonntag and Russel, 1987; Blaser, 2000). The syringe used had a length of $58.9 \cdot 10^{-3}$ m and diameter of $14.7 \cdot 10^{-3}$ m with a narrower tip of length $18 \cdot 10^{-3}$ m and diameter $20 \cdot 10^{-4}$ m, and was connected through Luer-lock fitting to a capillary of length $25 \cdot 10^{-3}$ m and diameter $21 \cdot 10^{-5}$ m. All the experiments were performed at room temperature of about $24 - 26°$C. The volumetric flow rates $\dot{V}\ (\mathrm{m^3 s^{-1}})$ used in the experiments, along with other relevant flow characteristics, such as the mean velocity through the capillary $u\ (\mathrm{ms^{-1}})$, the residence time per passage through the capillary $t_r\ (\mathrm{s})$, the dimensionless Reynolds number Re_c, the shear stress at the capillary wall $\tau_{cw}\ (\mathrm{Pa})$ and its corresponding energy dissipation rate $EDR_w\ (\mathrm{Wm^{-3}})$, and the pressure drop inside the capillary $\Delta p\ (\mathrm{Pa})$ are presented in table 2.1.

$\dot{V}\ (\mathrm{m^3 s^{-1}})$	$u\ (\mathrm{ms^{-1}})$	$t_r\ (\mathrm{s})$	Re_c	$\tau_{cw}\ (\mathrm{Pa})$	$EDR_w\ (\mathrm{Wm^{-3}})$	$\Delta p\ (\mathrm{Pa})$
$4.50 \cdot 10^{-8}$	1.30	$2.02 \cdot 10^{-5}$	$2.38 \cdot 10^{2}$	56	$2.79 \cdot 10^{6}$	$2.67 \cdot 10^{4}$
$1.80 \cdot 10^{-7}$	5.20	$5.05 \cdot 10^{-6}$	$9.54 \cdot 10^{2}$	225	$4.46 \cdot 10^{7}$	$1.11 \cdot 10^{5}$
$3.60 \cdot 10^{-7}$	10.4	$2.52 \cdot 10^{-6}$	$1.91 \cdot 10^{3}$	451	$1.78 \cdot 10^{8}$	$2.34 \cdot 10^{5}$

Table 2.1: *Fluid flow characteristics of the syringe-capillary system provided by analytical equations*

2.3.8. Cell proliferation ability

After the completion of each experiment on hydrodynamic stress exposure, a 1 ml sample of the cell suspension was inoculated in 49 ml of fresh cell medium. One (1) ml samples of the resulting cell suspension were taken in varying time points in the five weeks following inoculation and the count of viable cells was determined through fluorescence microscopy. The exponential least-square fit of the experimental data using MATLAB (version R2015a), allowed for the determination of the cell population growth rates k_e for each sample.

2.3.9. Rheological equations

The cell suspension behaves as a Newtonian fluid for the cell concentrations used in the current work, therefore shear stress τ (Pa) is a linear function of shear rate $\dot{\gamma}\ (\mathrm{sec^{-1}})$ and the dynamic viscosity $\eta\ (\mathrm{Pa \cdot sec})$ (Bird et al., 2002):

$$\tau = \dot{\gamma} \cdot \eta \tag{2.10}$$

When flowing in the capillary, the shear stress τ_c (Pa) is considered analogous to the radial distance from the center of the capillary r (m), as described by the equation (Bird et al., 2002):

$$\tau_c(r) = \frac{\Delta p \cdot r}{2l} \tag{2.11}$$

where Δp (Pa) is the pressure drop inside the capillary and l (m) is the capillary length. The maximum (or wall) shear stress τ_{cw} (Pa) arises at the capillary wall, i.e. when r is equal to the capillary radius R (m).

The pressure drop inside the capillary can be described by the Hagen-Poiseuille equation, when following the assumptions of steady, permanent, incompressible, and fully developed flow in a horizontal pipe of a Newtonian fluid acting as a continuum, and is usually written with reference to the volumetric flow rate as (Bird et al., 2002):

$$\dot{V} = \left(\frac{\Delta p}{l}\right) \cdot \frac{\pi R^2}{8\eta} \tag{2.12}$$

where $\dot{V}$ ($\mathrm{m}^3 \cdot \mathrm{sec}^{-1}$) is the volumetric flow rate inside the capillary. Solving this equation for Δp and replacing the result in equation 2.11, the wall shear stress in the capillary as a function of the volumetric flow rate is obtained, i.e.:

$$\tau_{cw}(r) = \frac{4\dot{V}\eta}{\pi r^3} \tag{2.13}$$

However, equation 2.12 is not enough to describe the full pressure drop inside the syringe-capillary system, where there are additional factors that influence it, such as the narrowing of the flow when moving from the larger syringe tube to the capillary. An approximation for the expected pressure drop is provided by Bernoulli's equation, if viscous (not frictionless) flow of a fluid through a pipe is assumed (Papaioannou, 2002). In that case, there will be a kinetic energy loss due to friction w_l ($\mathrm{m}^2 \cdot \mathrm{sec}^{-2}$), which, when divided by the gravitational acceleration g ($\mathrm{m} \cdot \ \mathrm{sec}^{-2}$), provides a measure termed friction height h_t (m), depending on such factors as the capillary length, and the existence of narrowings in flow. For the case of constant, incompressible, fully developed flow of a fluid through a pipe of length l (m) from point 1 to point 2:

$$w_l = \left(gz_1 + \frac{p_1^*}{\rho}\right) - \left(gz_2 + \frac{p_2^*}{\rho}\right) \tag{2.14}$$

where z (m) is the height of each point, p^* (Pa) is the special pressure at each point (i.e. the pressure minus the atmospheric pressure), and ρ ($\mathrm{kg} \cdot \mathrm{m}^{-3}$) is the fluid density. For a horizontal pipe, $z_1 = z_2$, and solving for pressure difference it results to:

$$\Delta p = \rho w_l = \rho g h_t \tag{2.15}$$

The full derivation of equation 2.15 is presented in the Appendix B.

The distinction between laminar and turbulent flow conditions in the capillary is determined by the dimensionless Reynolds number for pipe flow Re_c, following the equation (Bird et al., 2002):

$$Re_c = \frac{\rho v_m d}{\eta} \tag{2.16}$$

where v_m ($\mathrm{m} \cdot \mathrm{sec}^{-1}$) is the mean velocity of the fluid, and d (m) is the diameter of the capillary (twice the capillary radius R). A Re_c value < 2100 corresponds to a laminar flow, whereas for a Re_c value > 2100 the flow enters the meta-stable region, and for a Re_c value > 4000, the flow is expected to be fully turbulent. We only reached up to the boundaries of the meta-stable region during the experiments, as it is shown in table 2.1. All relevant measures for the experiments, provided by the analytical equations, are presented in the same table.

2.3.10. Critical hydrodynamic stress for the syringe-capillary system

We can assume that there is a specific critical area of high hydrodynamic stress inside the syringe-capillary system which would cause rupturing of the cell membrane and cell death. A sample of the cell suspension would show a reduction in the percentage of viable cells after passing through the capillary, that is analogous to the size of the critical area, i.e. if the critical area is large, a high percentage of cells will die per passage. If, furthermore, it is assumed that the critical area is inside the capillary, then it would be near the capillary wall, and since the shear stress inside the capillary is symmetrical with regard to the center, the ratio x of the safe area (where the cells pass through unharmed) to the total area would be:

$$x = \frac{\pi \cdot r^2 \cdot l}{\pi \cdot R^2 \cdot l} = \left(\frac{r}{R}\right)^2 \tag{2.17}$$

which, for a well-mixed sample, should be equal to the ratio of cells surviving per passage. After one passage through the capillary, the equation takes the form:

$$C_{v,1} = C_{v,0} \cdot \left(\frac{r}{R}\right)^2 \tag{2.18}$$

where $C_{v,1}$ is the viable cell count after one passage, $C_{v,0}$ is the viable cell count of the untreated sample. After two passages the equation takes the form:

$$C_{v,2} = C_{v,1} \cdot \left(\frac{r}{R}\right)^2 = C_{v,0} \cdot \left(\frac{r}{R}\right)^4 \tag{2.19}$$

and thus, after n passages, the equation takes the form:

$$\frac{C_{v,n}}{C_{v,0}} = \left(\frac{r}{R}\right)^{2n} \tag{2.20}$$

or, equivalently:

$$\ln\left(\frac{C_{v,n}}{C_{v,0}}\right) = \ln\left(\frac{r}{R}\right)^{2n} = 2n \cdot \ln\left(\frac{r}{R}\right) \tag{2.21}$$

which is similar to the definition of the cell death rate, mentioned in section 2.1.5.

Death rate per passage can be defined in a similar way to equation 2.5:

$$\ln\left(\frac{C_{v,n}}{C_{v,0}}\right) = -k_{dp} \cdot n \tag{2.22}$$

and can be determined through a least-square fit of the experimental data. Substituting in equation 2.21 and solving for r, the radius corresponding to the safe area for the cells as a function of the measured cell death rate per passage is obtained:

$$r = R \cdot e^{-k_{dp}/2} \tag{2.23}$$

or, since $r/R = \tau/\tau_{cw}$ for the capillary:

$$\tau = \tau_{cw} \cdot e^{-k_{dp}/2} \tag{2.24}$$

which allows for the determination of the critical hydrodynamic stress, based on the cell death rate per passage at each volumetric flow rate.

2.4. Rotor-stator stirring experiments

2.4.1. Aim

The findings in the introductory section 1.3.1 were once more taken into consideration and supported the idea of using free-flowing cells in the experiments, as the respective conditions would most closely relate to the natural state of the *D. salina* cells (i.e. free flowing inside a suspension). There have been various stirrers used in the literature to inflict turbulent hydrodynamic stress upon the cells, such as paddle (Abureesh and Kargi, 1991), or two-disc turbine (Garcia-Ochoa et al., 2013). We chose a rotor-stator device, named thus because it consists of a moving and a non-moving part, the rotor and the stator respectively, which could obtain high stirring speeds (up to 5000 rpm), generating a strongly turbulent flow field. Stirring speeds higher than 5000 rpm were specifically avoided, as further increase in the stirring speed introduced bubbles in the cell suspension, and cell-bubble interaction is considered a possibly lethal phenomenon (Yang and Wang, 1992; Cherry, 1993; Barbosa et al., 2003; Ma et al., 2004) which was essential to prevent, so as to not have multiple cell-viability reducing phenomena acting simultaneously.

The goal of the rotor-stator stirring experiments was the application of a rotor-stator device to generate high intensities of turbulent hydrodynamic stress that would lead to loss of viability for *D. salina* cells. Building on the knowledge from the previous experiments, intracellular protein release was compared to fluorescence microscopy as a method of determining cell viability loss in systems of occurring cell rupture due to hydrodynamic stress. Additionally, cell death rates for different stirring speeds of the rotor-stator were determined, which would allow the comparison with other hydrodynamic setups.

2.4.2. Experimental procedure

The rotating head of a rotor-stator device (IKA, ULTRA-TURRAX T 25 D with the S 25 N 18 G dispersing element, Germany) was placed in the middle of a cylindrical glass vessel filled with cell suspension, $1\,\mathrm{cm}$ above the bottom of the vessel, as shown in figure 2.6. The vessel was also placed $30\,\mathrm{cm}$ away from a constant warm light source (Osram T8 L 18W/827 LUMILUX INTERNA G13, color temperature $2700\,^{\circ}\,\mathrm{K}$, Germany) throughout the duration of the experiments. The rotation speed of the rotor was changed accordingly and samples were taken at specific time intervals. They were then used to determine viable cell count through fluorescence microscopy measurements and intracellular protein release through the Bradford assay. The correlation between cell viability loss and intracellular protein release was also investigated. Finally, a measurement of the energy dissipation rate per volume fluid was used to place the cell viability loss in perspective regarding previous experiments in different hydrodynamic conditions.

2.4.3. Cell count and viability

Cell count was measured using a Thoma cell-counting chamber, as described in section 2.1.2.1. Cell viability was determined using fluorescence microscopy and the FDA staining method, as described in the same subsection. The concentration of cells in all experiments was in the order of 10^6 cells $\cdot\,\mathrm{ml}^{-1}$.

2.4.4. Normalized cell density

Regarding the parameter of normalized cell density, equation 2.4 was used, as described in section 2.1.4.

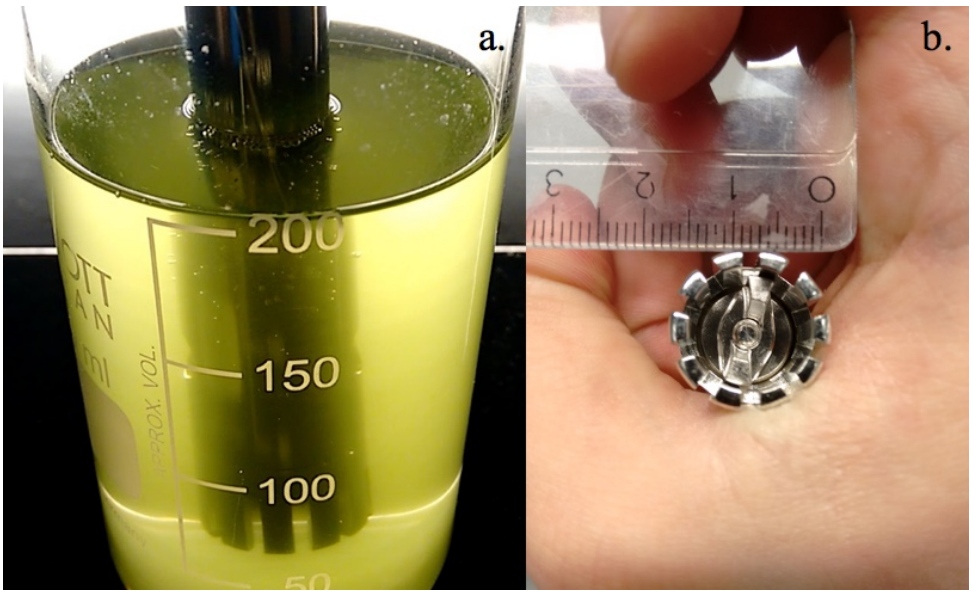

Figure 2.6: *The setup used for the rotor-stator experiments:* ***a:*** *the rotor-stator submerged in the cell suspension;* ***b:*** *close-up of the rotor-stator tip. The inside of the tip rotates at high stirring speeds (rotor), while the outside remains stationary (stator).*

2.4.5. Cell death rate

Cell death rates were determined as described in section 2.1.5, for both stirring speeds used in the rotor-stator experiments. The linear least-square fitting of the data was performed using MATLAB (version R2015a), with a fixed intercept at point (0,0).

2.4.6. Intracellular protein release and comparison with cell viability loss

Intracellular protein release was measured in the supernatant of the cell samples, as described in section 2.1.3. The results were normalized in reference to the absorbance value of the untreated sample at $595\,\mathrm{nm}$ for each measurement.

To compare intracellular protein release with cell viability loss, one must assume that they are both predictors of the same phenomenon, in this case the rupturing of the cell under hydrodynamic stress. Also, the data from the intracellular protein release measurements needed to be re-normalized over the maximum amount of protein that was released when (nearly) all cells ruptured, in order to be relevant for comparison with the data on cell viability, ranging from nearly zero to 100 %. Then, the data is plotted in a graph where each of the two axes corresponds to each predictor. The better the plotted data resembles the line $y = x$, the better the correlation between the two predictors. The linear least-square fitting of the data

was performed using the curve-fitting toolbox in MATLAB (version R2015a).

2.4.7. Rotor-stator and cell damaging experiments

The $200\,\mathrm{ml}$ cell suspension was mixed using the rotor-stator device, at a constant stirring speed of 3000 rpm or 5000 rpm for a total duration of $4\,\mathrm{h}$, at room temperature of about $25^{\circ}\mathrm{C}$. Samples were taken every $0.5\,\mathrm{h}$, including an initial pre-mixing sample. The samples taken on each occasion were a $1\,\mathrm{ml}$ sample for the cell count and viability measurement and a $1\,\mathrm{ml}$ sample for the Bradford assay measurement, for a total loss of $18\,\mathrm{ml}$ of cell suspension during an experiment (or 9% volume), which is considered negligible regarding the hydrodynamics of the system. Both measurements at 3000 rpm and 5000 rpm were performed in triplicates.

We also measured the temperature change due to stirring, as it could have affected cell viability and falsify the obtained data. Using a thermo-element device (Greisinger, Digital Thermometer GMH 3230, Germany), a change of up to $+2\,^{\circ}\mathrm{C}$ was measured when placing the thermo-element very near the stirrer, while the average temperature change was up to $+1\,^{\circ}\mathrm{C}$ for the entire cell suspension, at the conditions of maximum energy input from the stirrer, i.e. at 5000 rpm stirring speed. As a temperature of $27\,^{\circ}\mathrm{C}$ is still well within the fully viable range of temperatures for *D. salina* (which is between $0\,^{\circ}\mathrm{C}$ and $40\,^{\circ}\mathrm{C}$, as discussed in section 1.5.8.2 of the introductory chapter), the temperature change is considered negligible regarding its effects on cell viability.

2.5. Population balance modeling of cell rupture under hydrodynamic stress

2.5.1. Aim

Microalgae populations display heterogeneous characteristics, e.g. cell size and lipid content, and improving the accuracy in predicting their growth and death patterns could greatly assist in the optimization of the related upstream and downstream processes (Priyadarshani and Rath, 2012). One way of making such predictions that has received increasing attention in the last few years is population balance modeling (Bertucco et al., 2015; Pahija et al., 2017). The main advantage of the models, except for the increased accuracy in prediction, is that once the model parameters are fitted to a microbial population growing under specific conditions, then the need of costly experimental procedures for keeping track of the population, e.g. fluorescence microscopy, is greatly reduced. In the case of a cell population growing under conditions that inflict hydrodynamic stress upon it, the threshold of hydrodynamic stress

intensity that can lead to cell death (due to mechanical rupturing of the cell membrane) should also be taken into account and added in the model parameters.

The goal of the design of the population balance model was to include the phenomena of cell growth, proliferation and death by hydrodynamic stress into one complete model, based on existing knowledge of the relevant factors by the scientific literature. Then, using reasonable values for the model parameters, it was attempted to obtain results that qualitatively resemble the already existing observations from the literature.

2.5.2. Problem formulation and model equations

An agitation system is usually employed in order to ensure the efficiency of a process performed in a batch bioreactor. Agitation achieves fluid homogenization and thus, better cell growth conditions, but also inflicts hydrodynamic stress upon the cells, which may ultimately lead to cell lysis in the form of rupturing of the cell membrane. We will refer to shear stress specifically for the development of this model, as it is more frequently referenced in the literature, but there are many ways of generalizing from shear stress to hydrodynamic stress and energy dissipation rates, and compare among different conditions, as already discussed in the introduction.

To create a population balance model for cell rupture under hydrodynamic stress, a well-established model in the literature proposed by Mantzaris et al. (1999) was used as a starting point. The original model describes the life cycle of microbial cells, specifically taking into account the growth and reproduction of cells, and operates under specific biological assumptions. Cells are considered to grow exponentially with time, and to reproduce asexually. The model recognizes cells as distinguishable from each other in terms of their radius x, which is a measure of a cell's maturity. Since the maturity of a cell is assumed to correlate directly to it's radius, cells with greater radius have a higher probability to reproduce. During reproduction the mother cell divides into two daughter cells of unequal radius (a standard assumption, proven experimentally for various cell types, e.g. (Kutalik et al., 2005)). Following these assumptions, the original model was based on the population balance equation (Mantzaris et al., 1999):

$$\frac{\partial(n(x,t))}{\partial t} = -\frac{\partial(h(x)n(x,t))}{\partial x} - \gamma(x)h(x)n(x,t) + 2\int_x^\infty \gamma(x')h(x')P(x,x')n(x',t)dx' \quad (2.25)$$

where $n(x,t)$ (m^{-1}) is the number density function representing the number density of cells with radius x (m) at time t (h), $h(x)$ ($\mathrm{m}\cdot\mathrm{sec}^{-1}$) is the cell growth rate, $\gamma(x)$ is the cell division

rate kernel, and $P(x, x')$ is the cell partitioning function, accounting for the unequal division of a mother cell of radius x'.

Equation 2.25 is subject to the initial condition:

$$n(x, 0) = n_0(x) \tag{2.26}$$

where $n_0(x)$ is the initial cell distribution, and the boundary condition:

$$n(0, t) = 0 \tag{2.27}$$

which simply states that no cells with zero radius can exist.

The cell growth rate is defined as

$$h(x) = g \cdot x \tag{2.28}$$

where $g = \ln(2)/T_d$ (h^{-1}) is the growth rate constant for exponential cell growth, defined so that the average division time for the population is T_d (h).

The cell division rate function is defined as:

$$\gamma(x) = \frac{f(x)}{1 - \int_0^x f(x')dx'} \tag{2.29}$$

where $f(x)$ is the division probability density function, which is a normal distribution, depending only on cell radius. Cells with greater radius have a higher value of γ, which indicates that they are more probable to divide.

Each mother cell is considered to give birth to two unequal daughter cells, a phenomenon that is assumed to be successfully described by the partitioning function:

$$P(x, x') = \frac{1}{B(q, q)} \frac{1}{x'} \left(\frac{x}{x'}\right)^{q-1} \left(1 - \frac{x}{x'}\right)^{q-1} \tag{2.30}$$

where x is the radius of the daughter cell, x' the radius of the mother cell, q is a parameter of the distribution, which is referred to as the partitioning constant and $B(q, q)$ is the Beta function, which is defined by the equation:

$$B(a, b) = \frac{(a-1)!(b-1)!}{(a+b-1)!} \tag{2.31}$$

whose value at point (q, q) is used as a normalization constant, ensuring that the integral of the partitioning function amounts to 1.

To include the effect of cell death by shear stress to the original model, cells will be considered spherical in shape and mechanically analogous to capsules. An established measure for the effect of shear stress on the rupture of capsules is the dimensionless capillary number Ca, defined as (Barthés-Biesel, 1998; Clausen and Aidun, 2010):

$$Ca(x, E_Y) = \frac{\dot{\gamma}\mu x}{E_Y d_w} \tag{2.32}$$

where $\dot{\gamma}$ (sec^{-1}) is the shear rate, μ ($\mathrm{Pa} \cdot \mathrm{sec}$) the viscosity of the fluid, E_Y (Pa) is the cell membrane's Young's modulus, and d_w (m) the cell wall thickness. An increase in the value of the capillary number represents an increase in the shear stress affecting the cells. The model considers that cell death occurs when the capillary number reaches or surpasses a certain critical threshold Ca_{cr} that would lead to the rupture of a capsule with the same mechanical properties.

From the variables related to the capillary number, two have been shown to be significant for the life cycle of cells and to be distinguishable among the members of a cell population, namely cell radius (Collins and Richmond, 1962), and cell membrane's Young's modulus (Radotic et al., 2012). These have also been shown to be uncorrelated with each other (Stenson et al., 2011; Radotic et al., 2012). Therefore, the new model considers a two-dimensional distribution of cells, of both cell radius and cell membrane's Young's modulus, instead of just the original one dimension of cell radius. During cell reproduction, the mother cell is assumed to divide into two daughter cells of unequal radius (as in the original model), but equal membrane's Young's modulus (as there was no available indication from the literature to assume otherwise). Finally, the model assumes that the only external influence on the population of cells is the shear stress, causing cell death when a critical threshold is reached.

The resulting population balance equation is:

$$\begin{aligned} \frac{\partial(n(x, E_Y, t))}{\partial t} &= -\frac{\partial(h(x)n(x, E_Y, t))}{\partial x} - \gamma(x)h(x)n(x, E_Y, t) \\ +2\int_x^\infty \gamma(x')h(x')P(x, x')n(x', E_Y, t)dx' &- d(x, E_Y)n(x, E_Y, t) \end{aligned} \tag{2.33}$$

where $n(x, E_Y, t)$ ($\mathrm{m}^{-1} \cdot \mathrm{Pa}^{-1}$) is the number density function representing the number density of cells with radius x and cell membrane's Young's Modulus E_Y (Pa) at time t, and $d(x, E_Y)$ (h^{-1}) the cell death rate kernel.

Equation 2.33 is subject to the initial condition:

$$n(x, E_Y, 0) = n_0(x, E_Y) \tag{2.34}$$

where $n_0(x, E_Y)$ is the initial cell distribution, and the boundary conditions:

$$n(0, E_Y, t) = 0,\ n(x, 0, t) = 0 \tag{2.35}$$

which state that no cells with zero radius or zero membrane's Young's Modulus can exist.

The cell death rate is defined as:

$$d(x, E_Y) = \begin{cases} 0 & \text{if } Ca(x, E_Y) < Ca_{cr} \\ k_d & \text{if } Ca(x, E_Y) \geq Ca_{cr} \end{cases} \tag{2.36}$$

which simply states that for $Ca(x, E_Y) < Ca_{cr}$, no cell lysis occurs, while $Ca(x, E_Y) \geq Ca_{cr}$ cells die at a constant death rate k_d (h^{-1}).

2.5.3. Numerical approach

For the solution of the PBM, an already published numerical approach was followed (Mantzaris et al., 1999), as it has been used for a similar problem with sufficient accuracy. The approach is based on a combination of two schemes, the leapfrog and the Lax-Friedrichs scheme (Strikwerda, 1989; Press et al., 1992), using a two step discretization for time and five points discretization for each of the two properties, i.e. the cell radius and the cell Young's modulus. More details on the approach can be found in the corresponding publication (Mantzaris et al., 1999). The model was solved using code written by the author and compiled in MATLAB (version R2014a).

For the purpose of demonstrating the capabilities of the model, the values for the model parameters were either chosen through suggestions in the publication by Mantzaris et al. (1999), or were reasonable for *D. salina* in particular, as this was the microorganism the authors were most familiar with. In order to use the model's full capabilities, these values must instead be obtained through experimental data, e.g. on the Young's modulus distribution of the cells. However, no access to such data was obtainable at the time. Regarding the simulation parameters, the end of the simulation was decided to correspond to a simulated time of $10\,\mathrm{h}$, with a time-step size of $10^{-4}\,\mathrm{h}$. We used 400 integration points in the cell radius dimension, and 60 in the cell membrane's Young's modulus dimension, with the upper boundaries of the solution grid being at four times the mean of the initial cell radius distribution and two times the mean of the initial cell membrane's Young's modulus. The initial, two-dimensional, normal distribution had a mean cell radius of $10\,\mu\mathrm{m}$, with a standard deviation of $2\,\mu\mathrm{m}$, and a mean cell membrane's Young's modulus of $10^3\,\mathrm{Pa}$, with a standard deviation of $200\,\mathrm{Pa}$. The

cell growth rate g was $0.1386\,\mathrm{h}^{-1}$. The division probability density function $f(x)$ had a mean of $12\,\mu\mathrm{m}$, a standard deviation of $2.4\,\mu\mathrm{m}$, and the related partitioning constant q is 40. The cell death rate k_d was $2\,\mathrm{h}^{-1}$, for a critical capillary number of 0.05. Finally, the cell wall thickness d_w was $0.5\,\mu\mathrm{m}$ and the range of shear stresses tested was between $0 - 600\,\mathrm{Pa}$.

Chapter 3

Results

3.1. Narrow-gap rheometer experiments

The narrow-gap rheometer experiments were performed in collaboration with Prof. Dr. Andreas Wierschem and Dr. Haider Dakhil, from the Institute of Fluid Mechanics of the University of Erlangen, and their results were subsequently published by the Journal of Biorheology (Kokkinos et al., 2016).

3.1.1. Rheological characterization

The measured maximum shear stress increased linearly with an increase in maximum shear rate, while the apparent viscosity remained relatively constant for maximum shear rates in the range of $2 \cdot 10^3 - 10^5\,\mathrm{s}^{-1}$ (less than 5% difference from average viscosity), which indicates the cell suspension acted as a Newtonian fluid. The average dynamic viscosity η measured in that range was estimated to be $1.14 \pm 0.01\,\mathrm{mPa \cdot s}$ (at $25\,^{\circ}\mathrm{C}$, with 95% confidence), similar to that of water at room temperature ($25\,^{\circ}\mathrm{C}$), which is $0.8891\,\mathrm{mPa \cdot s}$, yet closer to the viscosity of water at $15\,^{\circ}\mathrm{C}$, which is $1.1373\,\mathrm{mPa \cdot s}$. At lower shear rates than the chosen range, the torque resolution of the narrow gap rheometer was too low for an accurate measurement of the viscosity. On the other hand, at higher shear rates inertial forces were too strong, pushing the suspension out of the gap between the parallel plates. The measured rheological trends are presented in figure 3.1.

Given that the measured cell suspension presented a reasonable rheological behavior (not too concentrated so as to act as a non-newtonian fluid), while at the same time the cellular concentration was high enough for obtaining accurate cell counts, this concentration of cells (in the order of 10^6 cells per ml) was maintained throughout the experiments. Since all the

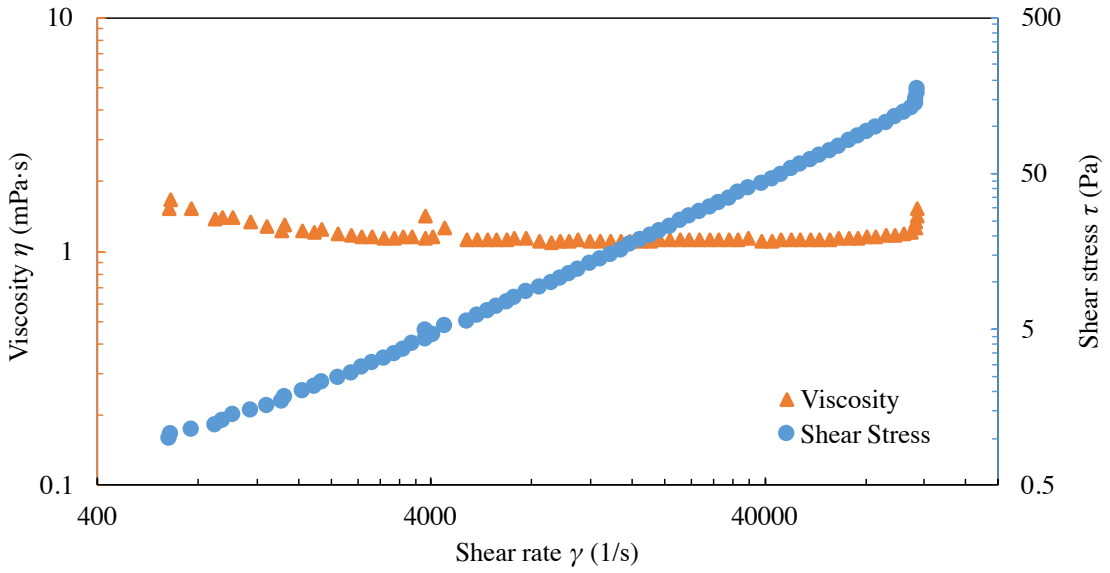

Figure 3.1: *Viscosity (orange triangles) and shear stress (blue circles) of the cell suspension as a function of shear rate. Irregularities appear at low shear rates, due to the torque resolution of the rheometer and at high shear rates due to inertia. Each datapoint represents a single measurement.*

experiments were performed at room temperature, the value for the dynamic viscosity could be used for calculations regarding the rest of the experiments as well.

3.1.2. Observations using the rheo-optical setup

After placing the cell suspension in the gap between the parallel plates, and before the rotation of the plates was initiated, the cells appeared able to move unobstructed, without any visible signs of immobilization or attachment to the plates. During shearing, single cells could be observed in flow, moving in the direction of rotation. For a maximum shear stress of $10\,\mathrm{Pa}$, cells started forming strings, while for maximum shear stresses higher than $15\,\mathrm{Pa}$, most cells arranged in string formations, as shown in the *in situ* high-speed camera frames presented in figure 3.2. Additionally, clusters of cells appeared for all shear stresses investigated, forward-tumbling in the flow direction without visibly breaking up into smaller clusters. The clusters consisted of about $5-10$ cells, and were generally stretched in the vortex direction.

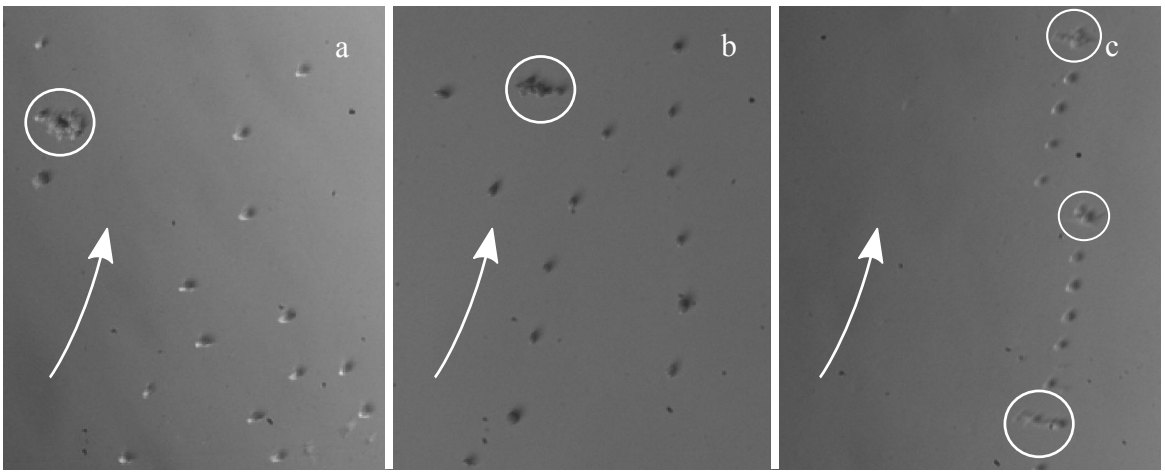

Figure 3.2: *Formations of cells in laminar flow depending on maximum shear stress:* ***a:*** $5\,\mathrm{Pa}$*;* ***b:*** $15\,\mathrm{Pa}$*;* ***c:*** $70\,\mathrm{Pa}$*. Arrows indicate direction of flow, circles indicate clusters of cells. The in situ high-speed camera frames show cells experiencing maximum shear stress, since the frame location was positioned near the edge of the plates (Kokkinos et al., 2016).*[1]

3.1.3. Cell morphology and viability loss

We considered cell motility loss and cell deformation as indicators of cell damage. However, the first was assumed as a weaker indicator, due to the observations by Jaouen et al. (1999) when shearing the flagellate microalgae *T. suecica*, where they determined that 40% of the population of intact cells would regain motility after a $5\,\mathrm{h}$ resting time. This finding suggested that the loss of the cell's flagellas, and therefore the loss of cell motility in the case of *D. salina*, might not be a permanent issue for the cell, as another microalgae had clearly demonstrated the ability to regrow them. As there were no similar findings available for the *Dunaliella* species, it is important to note that this finding only serves as indication. On the other hand, deformation of the cells as they appear in the microscope pictures after being subjected to hydrodynamic stress is more generally accepted as an indicator of cell damage, and cell death (Tanzeglock et al., 2009).

The normalized cell density NCD_t of intact cells after each experiment, as calculated by equation 2.3, is presented in figure 3.3. Increasing the stirring rate of the upper plate of the setup, and therefore increasing the maximum shear stress that the cells could experience

[1] Reprinted from Biorheology, Vol 53, Kokkinos, D., Dakhil, H., Wierschem, A., Briesen, H., and Braun, A., Deformation and rupture of *Dunaliella salina* at high shear rates without the use of thickeners, Pages 1-11, Copyright (2016), with permission from IOS Press. The publication is available at IOS Press through http://dx.doi.org/10.3233/BIR-15057.

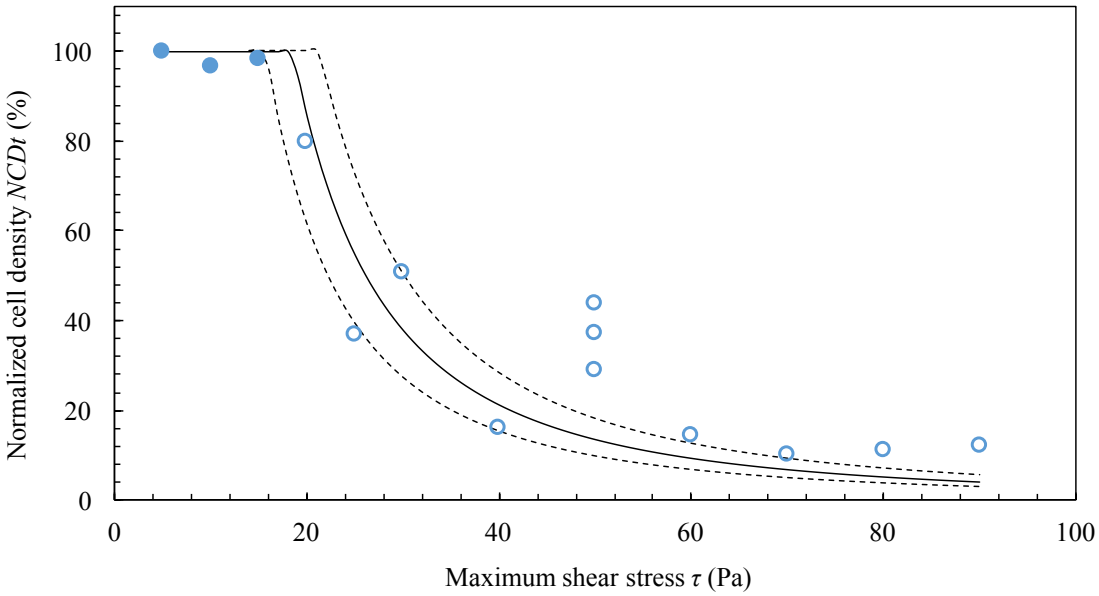

Figure 3.3: *Effect of shear stress on the percentage of intact cells when calculated with equation 2.3: (filled circles) experimental data of intact and motile cells; (empty circles) experimental data of intact but non-motile cells; (solid line) best least-square fit of equation 2.9; (dashed lines)* 95% *confidence interval. Maximum shear stress denotes the shear stress at the edge of the plate. Each datapoint represents a single measurement (Kokkinos et al., 2016).*

led to a decrease in the visible intact cells. Up to a maximum shear stress of $15\,\mathrm{Pa}$, the majority of the cells remained fully motile, appearing intact and symmetrical after treatment, with their flagellas visible in the off-line microscope images (after immobilization with Lugol Potassium-Iodine solution). These results are presented in figure 2.3 a.

For a maximum shear stress of $20\,\mathrm{Pa}$ and higher, there was a strong difference in behavior, with all cells losing motility after treatment, and no flagellas visible in the off-line microscope images. Also, deformed asymmetrical cells, some with visible points of rupture in their membrane, were noticeable in the microscope images, as shown in figure 2.3 b, c, and d. We consider this strong difference in cell behavior as an indication that hydrodynamic damage only occurred for a maximum shear stress of $20\,\mathrm{Pa}$ and higher. Finally, for a maximum shear stress of $60\,\mathrm{Pa}$ or higher, more than 80% of the cells appeared deformed in the off-line microscope images.

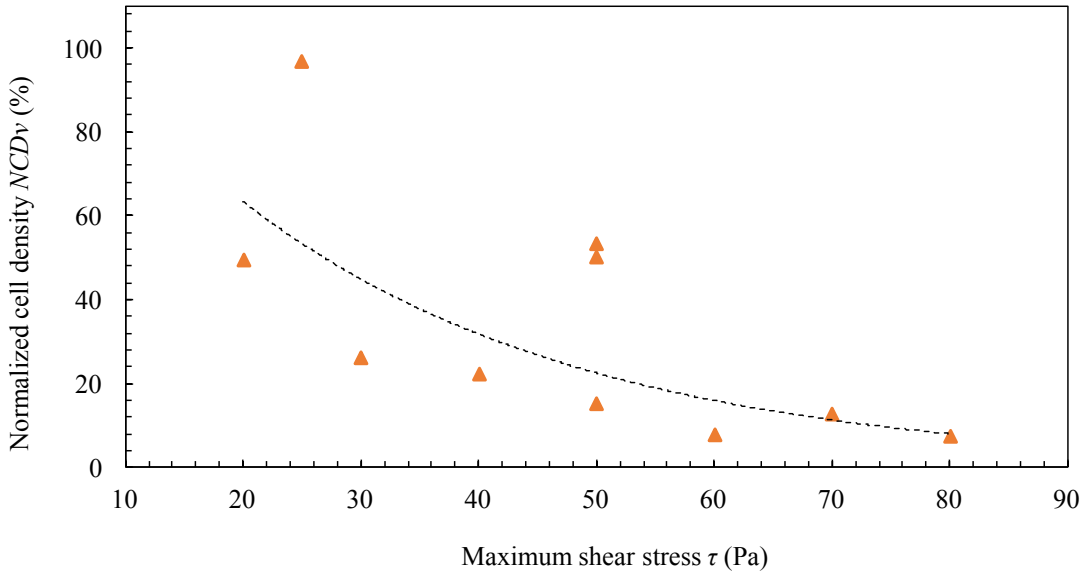

Figure 3.4: *Effect of shear stress on the percentage of intact cells when calculated with equation 2.4: (triangles) experimental data of intact but non-motile cells; (dashed line) exponential fit showing the general trend of the experimental data. Maximum shear stress denotes the shear stress at the edge of the plate. Each datapoint represents a single measurement.*

As described in section 2.1.4, the information required to calculate NCD_t using equation 2.3, i.e. both intact/viable and deformed/dead cell counts after treatment, was not as readily available for the rest of the experiments, where the dead cells would strongly aggregate into clusters that were hard to find and hard to count the number of cells forming them. Therefore, to be able to compare among different setups, equation 2.4 was used to describe the same data. The results are presented in figure 3.4 for the cases where hydrodynamic damage occurred, i.e. for a maximum shear stress of $20\,\mathrm{Pa}$ and higher. It is clear that the trend of the data is very similar to the one resulting from the previous equation, i.e. exposure to higher maximum shear stress leads to a lower percentage of intact cells. However, there are still inconsistencies to be found, as is the case for $25\,\mathrm{Pa}$, where nearly no difference in the viable cell count was found when comparing with the control sample. We attribute such inconsistencies to the existence of large cell aggregates that would form during flow for low shear stresses, while for higher shear stresses it is assumed they would break down to smaller ones, leading to less inconsistency in the off-line microscope pictures. This underlines the importance of making triplicate measurements for each hydrodynamic stress intensity, in order to obtain more consistent data, as was the case for the rest of the experiments.

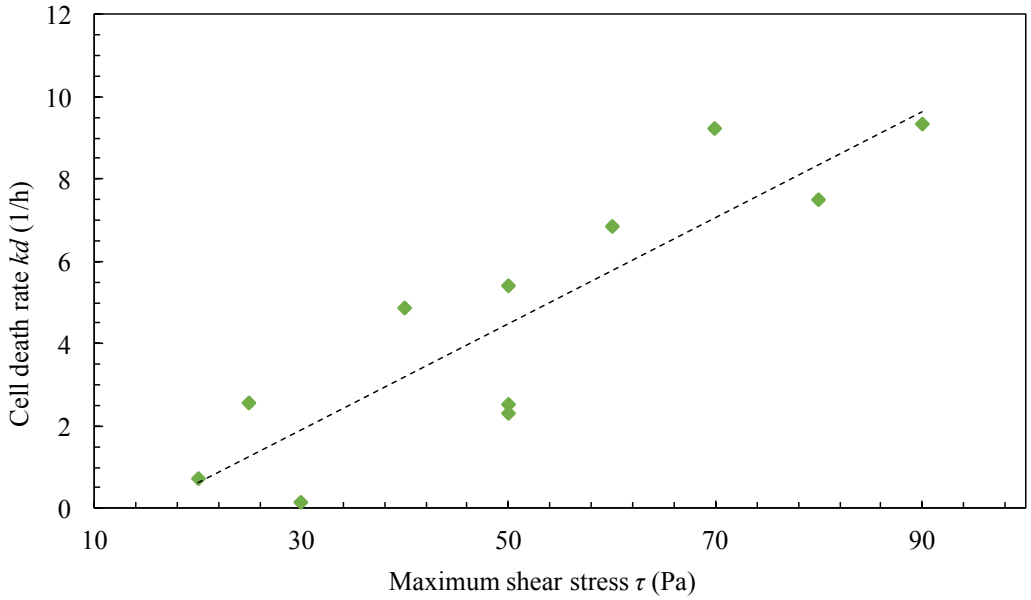

Figure 3.5: *Cell death rate as a function of maximum shear stress experienced by the cells in the narrow gap rheometer, for a shearing duration of* $1000\,\text{sec}$*: (diamonds) experimental data of intact but non-motile cells; (dashed line) linear fit showing the general trend of the experimental data. Maximum shear stress denotes the shear stress at the edge of the plate. Each datapoint represents a single measurement.*

The measured cell death rates k_d as a function of maximum shear stress are presented in figure 3.5, (for the cases where cell damage is considered to have occurred, i.e. for a maximum shear stress of $20\,\text{Pa}$ and higher). The trend of the data is clear, higher maximum shear stress leads to higher death rates for the cells, and a simple linear fit seems to successfully describe the experimental data. These death rates should serve only as an indication of the order of magnitude of the death rates in the narrow-gap rheometer setup, and not taken too literally. The proper way to accurately measure death rates is to maintain a constant maximum shear stress, at $50\,\text{Pa}$ for example, take measurements for varying shearing intervals, at 10, 50, 100, and 500sec for example, and then determine the cell death rate for a given maximum shear stress from the least-square fit of those data, as was done in the rest of the experiments. Nevertheless, even an indication of the order of magnitude of the death rates is sufficient for a comparison between different hydrodynamic setups.

3.1.4. Critical hydrodynamic stress and energy dissipation

Using the critical shear stress criterion, as described in equation 2.9, a critical shear stress τ_{crit} of $18 \pm 3\,\text{Pa}$ (with 95% confidence) was determined. The fit of the equation to

the experimental data of the NCD_t is presented in figure 3.3. As the critical shear stress criterion refers to cases where cell death occurred, at least 20% deformed cells were observed after shearing, the non-linear regression curve was fitted to the data for a maximum shear stresses of $20\,\mathrm{Pa}$ or higher. The fitting included some outliers, such as the measurements for a maximum shear stress of $50\,\mathrm{Pa}$. However, these outliers were impossible to connect to some systematic error. The measured critical shear stress corresponds to a critical shear rate γ_{crit} of $1.6 \cdot 10^4\,\mathrm{s}^{-1}$, and a Reynolds number Re of 12. The duration of shearing was not necessary for the critical shear stress criterion to adequately fit the experimental data. This indicates that $1000\,\mathrm{s}$ of shearing were suitable for damaging most *D. salina* cells. The duration of shearing is negligible when compared to the usual cultivation time of *D. salina*, which lasts several days (Hejazi et al., 2003). Therefore, reaching a damaging level of shear stress in the bioreactor would immediately impact the specific growth rate of the culture, which underlines the significance of determining a critical hydrodynamic stress for this cell species.

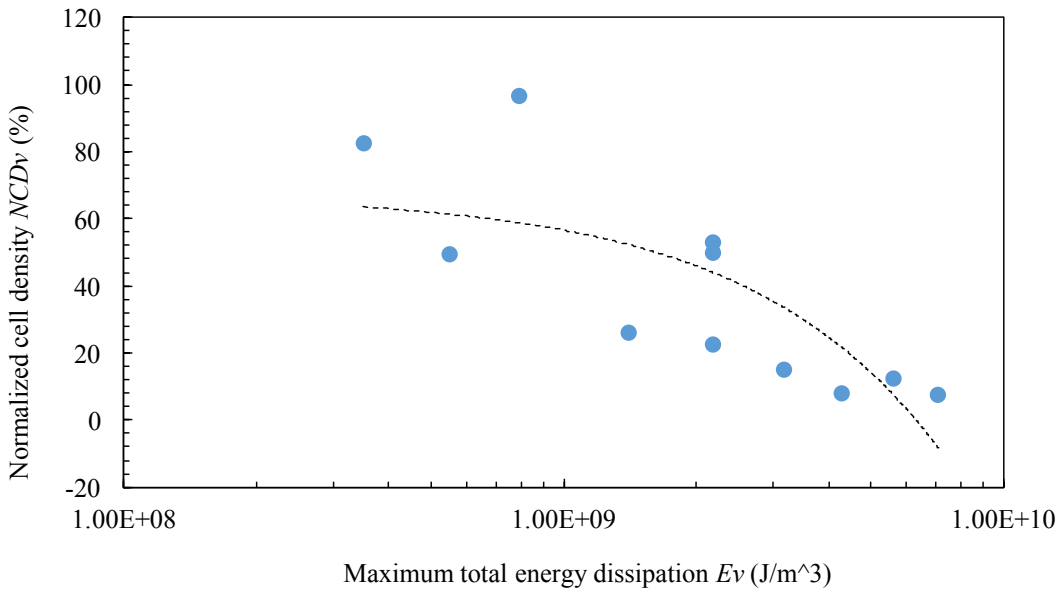

Figure 3.6: *Effect of maximum total energy dissipation on the percentage of intact cells: (dots) experimental data; (dashed line) linear fit showing the general trend of the experimental data. Maximum total energy dissipation denotes the total energy dissipation at the edge of the plate. Each datapoint represents a single measurement.*

The range of energy dissipation rates ϵ_V in the narrow-gap rheometer setup was $2.19 \cdot 10^4 - 7.23 \cdot 10^6\,\mathrm{W \cdot m^{-3}}$, while for total energy dissipation E_V, it was $2.19 \cdot 10^7 - 7.23 \cdot 10^9\,\mathrm{J \cdot m^{-3}}$, based on the maximum hydrodynamic stress the cells could experience at the edge of

the parallel-plate geometry. The energy dissipation rate corresponding to the critical shear stress is $2.84 \cdot 10^5\,\mathrm{W\,m^{-3}}$, and the total energy dissipation for the critical shear stress is $2.84 \cdot 10^8\,\mathrm{J\,m^{-3}}$. The correlation between the NCD_v and the maximum total energy dissipation experienced is presented in figure 3.6, along with a linear fit of the experimental data to serve as an indicator of their general trend, i.e. to show that higher total energy dissipation corresponds to a lower percentage of viable cells.

3.2. Capillary flow experiments

The capillary flow experiments were performed in collaboration with Jiekui Zou, as part of his Master thesis in the Chair of Process Systems Engineering of the Technical University of Munich (Zou, 2016). Supervision of the thesis, along with the biological cells required for the experiments were provided by the current author.

3.2.1. Cell morphology

We used fluorescence microscopy with the FDA staining method to assess cell viability before and after the cells were subjected to hydrodynamic stress. We also wanted to match viable and dead cells with their respective morphological characteristics. It became apparent that dead *D. salina* cells, had distinct morphological differences from viable cells for these experiments. More specifically, while viable cells maintained a perfect spherical or ellipsoidal shape after treatment, dead cells had visible imperfections on their membrane, such as discernible points of rupture or strong deviations from the spherical/ellipsoidal shape, as can be seen in figure 3.7. Also, viable cells appeared less "flat" than their dead counterparts, i.e. they seemed to have an internal shading, while the dead cells did not. Generally, one could distinguish whether the cells were non-viable just from their morphology. This supports the notion from the previous experiments in the narrow-gap rheometer setup, discussed in section 3.1, that the cells appearing intact in the microscope pictures were viable, while the visibly deformed cells were dead.

3.2.2. Cell viability loss

The measured NCD_v is presented in figure 3.8. For a flow rate of $0.045\,\mathrm{ml \cdot sec^{-1}}$, even after 40 passages through the capillary, no significant decrease in the NCD_v was noticed. This suggests that there is no particular issue with the syringe-capillary setup, that could have caused cell death that is uncorrelated to hydrodynamic stress, e.g. if the capillary was too

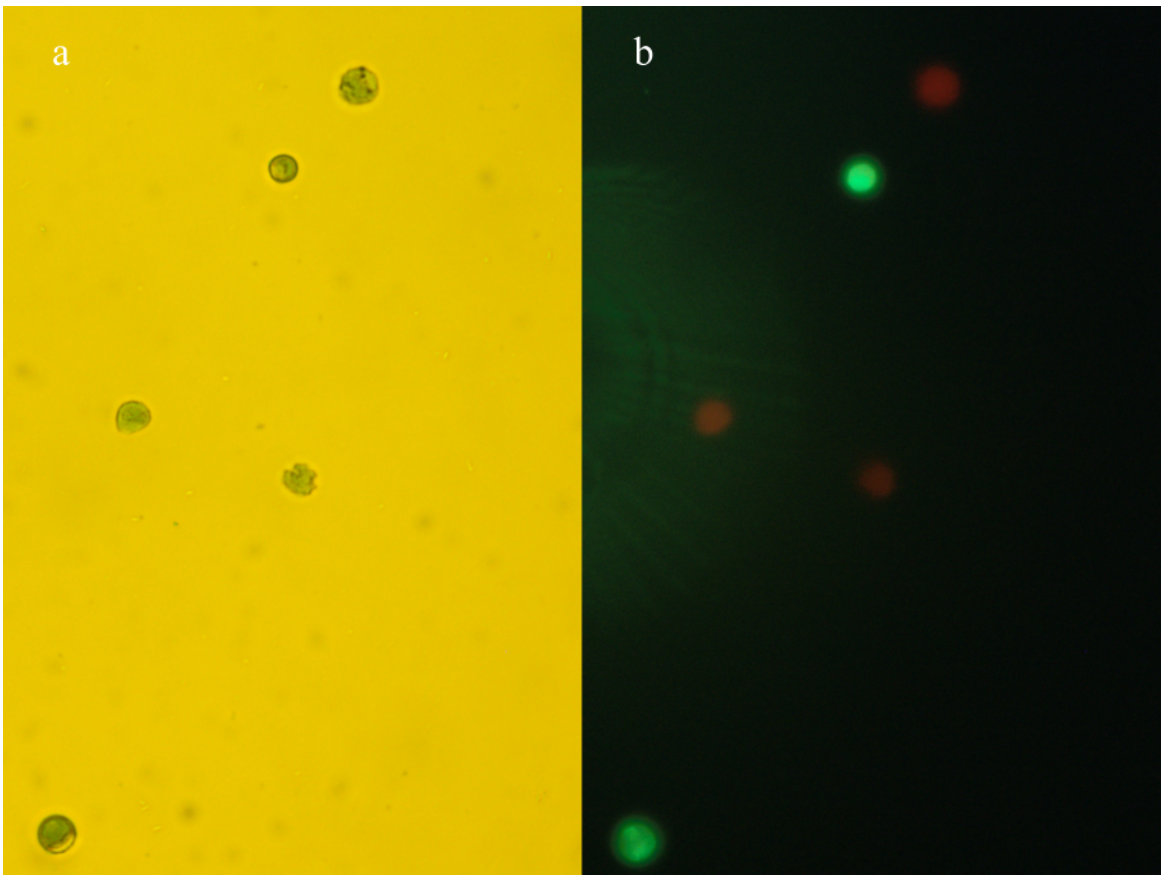

Figure 3.7: *Morphology of viable and non-viable D. salina cells after passing through the capillary: (a) bright-field microscopy image of the cells at 50x zoom; (b) FDA-fluorescence image of the same cells.*

narrow for the cells to pass through unharmed. This also suggests that the hydrodynamic stresses arising in the syringe-capillary system for that case were below critical. For a flow rate of $0.18\,\mathrm{ml}\cdot\mathrm{sec}^{-1}$, NCD_v decreased with increasing number of passages, reaching a viable cell density of about 60% after 40 passages. For a flow rate of $0.36\,\mathrm{ml}\cdot\mathrm{sec}^{-1}$, NCD_v decreased much more sharply with the number of passages, leading to a viable cell density of about 18% after only 20 passages, after which, no further reduction in the viable cell density was noticed. Also, after 20 passages for the case of $0.36\,\mathrm{ml}\cdot\mathrm{sec}^{-1}$, a limited number of cells were witnessed in the microscope pictures. This allows for the assumption that the limits of accuracy of the method have been reached.

We also determined cell death rates for the syringe-capillary system, which would allow easier comparison with other hydrodynamic setups. There was no point in determining a cell death rate for the case of $0.045\,\mathrm{ml}\cdot\mathrm{sec}^{-1}$, as there was no consistent decrease in the NCD_v. For $0.18\,\mathrm{ml}\cdot\mathrm{sec}^{-1}$, a cell death rate k_d of $8.85 \pm 2.87 \cdot 10^6\,\mathrm{h}^{-1}$ (with 95% confidence and an

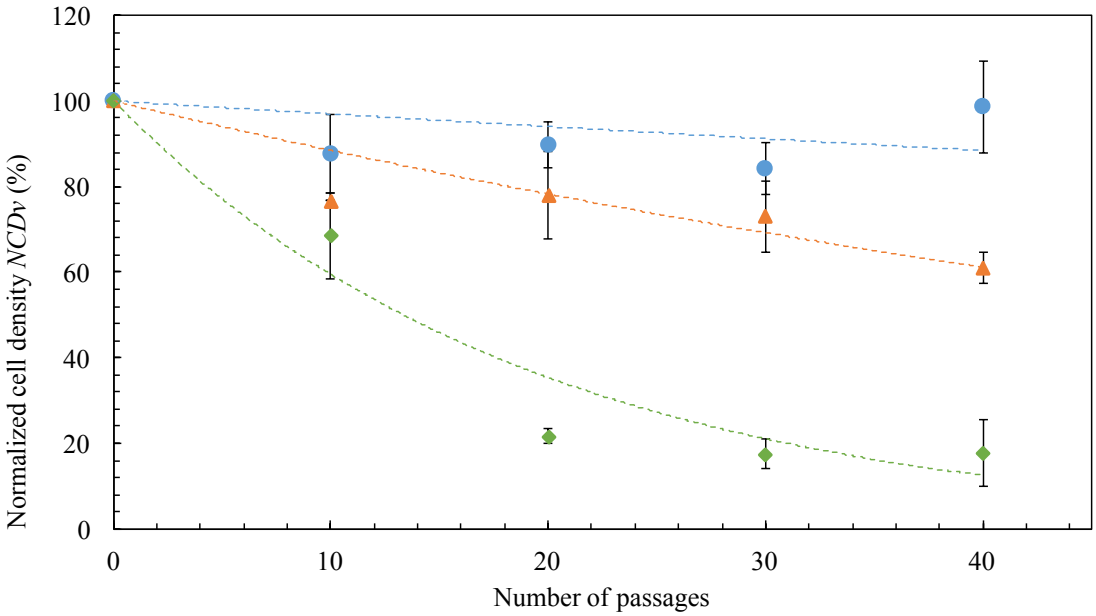

Figure 3.8: *Normalized cell density of viable cells per passage of the cell suspension through the capillary: (blue circles) flow rate* $0.045\,\mathrm{ml}\cdot\mathrm{sec}^{-1}$*; (orange triangles) flow rate* $0.18\,\mathrm{ml}\cdot\mathrm{sec}^{-1}$*; (green diamonds) flow rate* $0.36\,\mathrm{ml}\cdot\mathrm{sec}^{-1}$*; (dashed lines) exponential fit showing the general trend of the experimental data for each dataset. Each datapoint represents the mean of triplicate experiments, error bars indicate standard deviation from the mean (Zou, 2016).*

R^2 of 0.79) was determined, and for $0.36\,\mathrm{ml}\cdot\mathrm{sec}^{-1}$, a cell death rate of $7.62 \pm 2.16 \cdot 10^7\,\mathrm{h}^{-1}$ (with 95% confidence and an R^2 of 0.87), which are several orders of magnitude higher than the death rates measured in the previous experiments with the narrow-gap rheometer. The linear least-square fit of the experimental data that allowed for the determination of the death rates is presented in figures 3.9, and 3.10. It is clear that additional data would be required to obtain a better linear fit for the death rates, however this wouldn't be expected to significantly change the order of magnitude of the death rate, which was the main interest for comparing with other hydrodynamic setups.

3.2.3. Intracellular protein release

We used the Bradford assay, as discussed in section 2.1.3, to measure intracellular protein release at the end of each experiment, i.e. after 40 passages of the cell suspension through the capillary. We considered a maximum release of intracellular protein to be after 40 passages for a volumetric flow rate of $0.36\,\mathrm{ml}\,\mathrm{sec}^{-1}$, denoted as $100\,\%$, and the other measurements were re-calculated based on that value. The Bradford measurements were

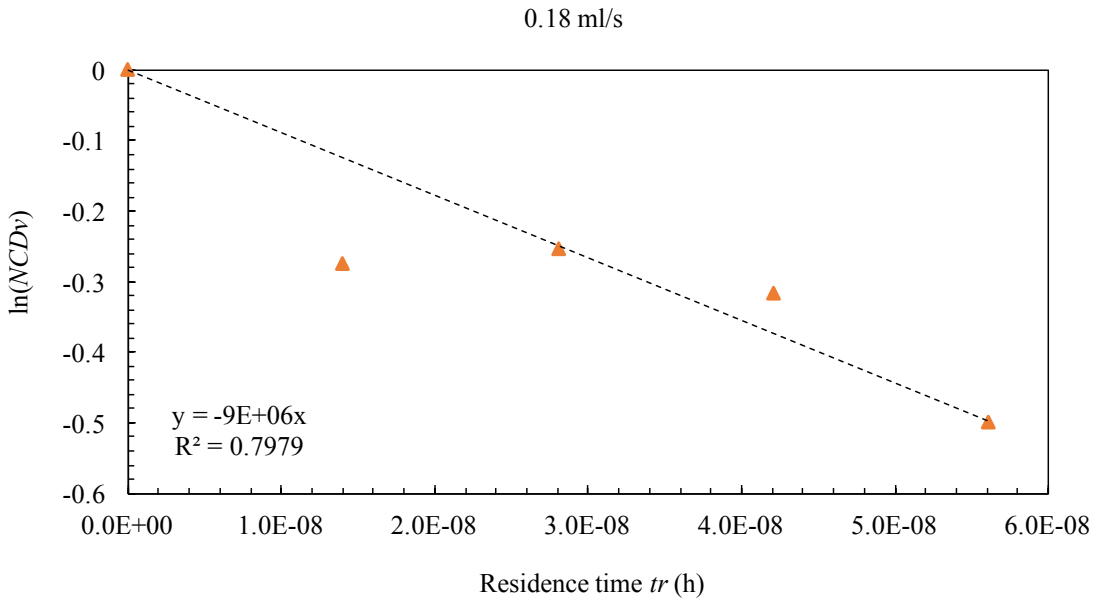

Figure 3.9: *Change in normalized cell density of the cell suspension for increasing residence time in the capillary, at a volumetric flow rate of* $0.18\,\mathrm{ml\,sec^{-1}}$*: (dashed line) best least-squares linear fit of the experimental data. The slope of the dotted line gives the death rate of the cells at* $0.18\,\mathrm{ml\,sec^{-1}}$*. Each datapoint represents the mean of triplicate experiments.*

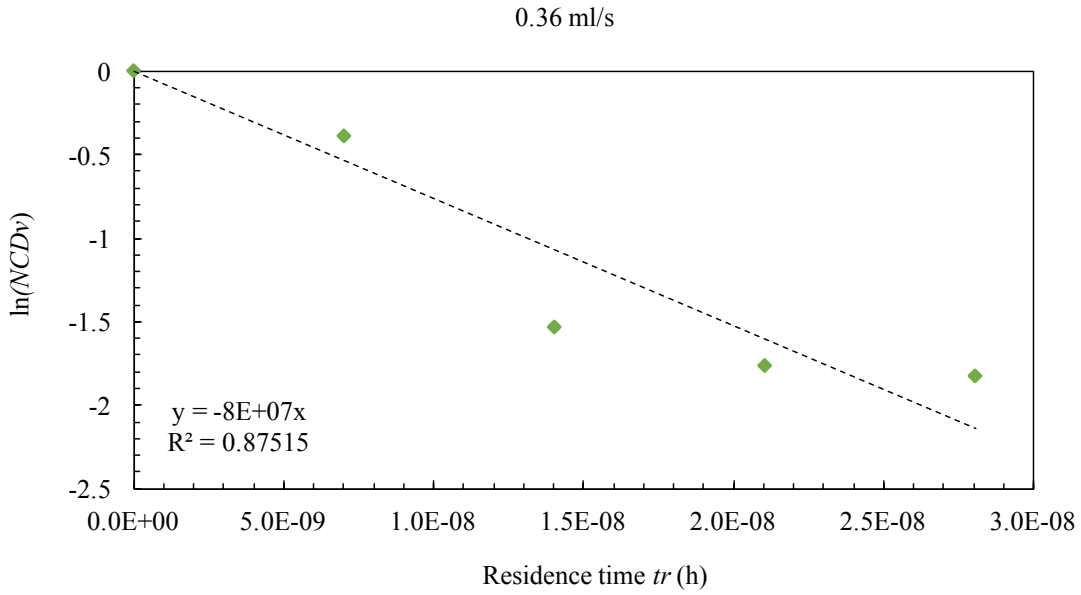

Figure 3.10: *Change in normalized cell density of the cell suspension for increasing residence time in the capillary, at a volumetric flow rate of* $0.36\,\mathrm{ml\,sec^{-1}}$*: (dashed line) best least-squares linear fit of the experimental data. The slope of the line gives the death rate of the cells at* $0.36\,\mathrm{ml\,sec^{-1}}$*. Each datapoint represents the mean of triplicate experiments.*

then plotted next to the measured decrease in viable cell density (i.e. $100 - NCD_v$), and the results are shown in figure 3.11. For a flow rate $0.045\,\mathrm{ml} \cdot \mathrm{sec}^{-1}$, there was an increase in abrsorbance Δa of about $20\,\%$ at the peak of $595\,\mathrm{nm}$, while there was no detectable decrease in cell viability, as measured by FDA fluorescence. This means that some intracellular protein release must have taken place, and indicates that the Bradford assay might be more accurate at determining small differences in the cell suspension regarding cell rupture due to hydrodynamic stress. Another possibility, would be that the cell membrane ruptured without the cell being completely disintegrated, and some intracellular proteins were released in the medium without the cell dying. This could be due to the cell membrane healing process, which is considered universal for all cell types (Sonnemann and Bement, 2011), which suggests that the cell membrane can be rebuilt by intracellular mechanisms if the cell is not completely disintegrated by the stressing. However, there are, to the author's knowledge, not sufficient data available regarding this phenomenon as experienced by microalgae cells, so this possibility is mostly speculation. It would still be more reasonable to assume that a few cells ruptured, without it being detectable by the fluorescence microscopy method.

For a flow rate $0.18\,\mathrm{ml} \cdot \mathrm{sec}^{-1}$, there was a 37% increase in absorbance, and a corresponding 39% decrease in viable cell density. The two phenomena seem to correlate well with each other, as an increase in absorbance in the Bradford test appears to lead to a similar decrease in the viable cell density. This indicates that cell viability loss through rupture of the cell membrane occurred in these experiments, leading to the release of intracellular proteins. Additionally, this suggests that the two types of measurements might be interchangeable in the case of measuring viability loss due to hydrodynamic stress for *D. salina* cells. This would be reasonable to expect, as intracellular protein content has been shown to correlate well with cell count for some microalgae species (Spiden et al., 2013). To the author's knowledge, this has not been previously shown for *D. salina*. Finally, it was expected that the critical hydrodynamic stress leading to the rupture of the cell membrane would occur at volumetric flow rates between $0.045\,\mathrm{ml} \cdot \mathrm{sec}^{-1}$ (no indication of a decrease in viable cell NCD; weak indication of intracellular protein release) and $0.18\,\mathrm{ml} \cdot \mathrm{sec}^{-1}$ (clear indication of a decrease in viable cell NCD and of intracellular protein release).

3.2.4. Cell proliferation ability

A classic question in experiments about hydrodynamic stressing of the cells, is whether the viable cells have lost their ability to proliferate after experiencing damaging levels of

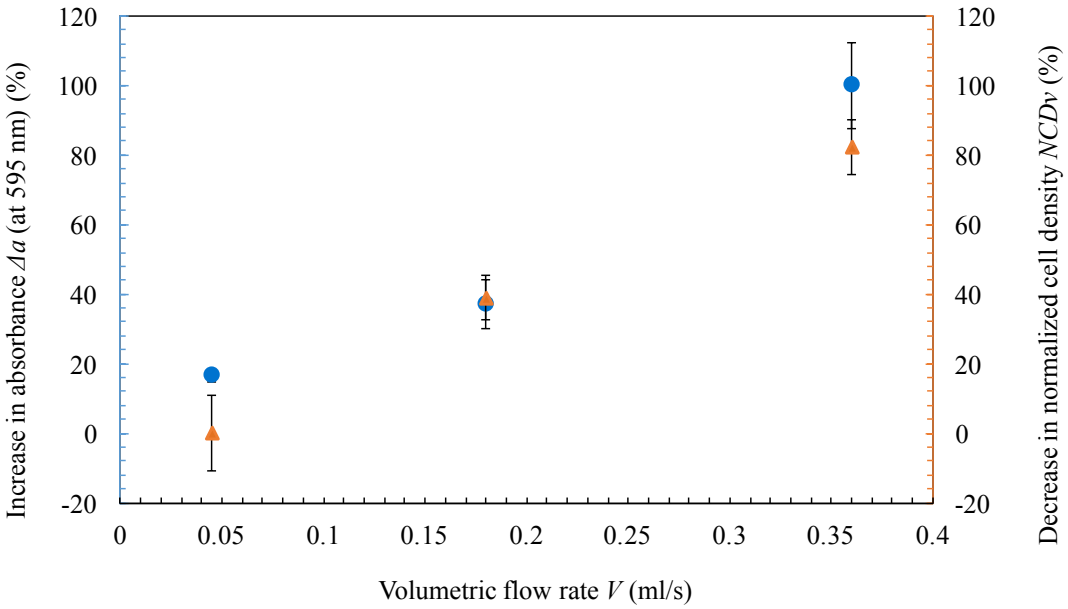

Figure 3.11: *Cumulative effect of* 40 *passages through the capillary on the cells for increasing flow rate: (blue circles) normalized absorbance at* $595\,\mathrm{nm}$ *using the Bradford assay; (orange triangles) decrease in viable cell density. Each datapoint represents the mean of triplicate experiments, error bars indicate standard deviation from the mean (Zou, 2016).*

hydrodynamic stress, as was e.g. the case for carrot cells in the experiments of Dunlop et al. (1994). To test this, samples from each experiment were taken after 40 passages through the capillary, placed it in fresh growth medium, and measured the corresponding population growth rates. The results are presented in figure 3.12. The measured average population growth rates k_e were between $2.9 - 3.6 \cdot 10^{-3}\,\mathrm{h}^{-1}$, with the difference in the averages being within the standard deviation of the measurements. There seemed to be an improvement in the case of $0.045\,\mathrm{ml} \cdot \mathrm{sec}^{-1}$, where the cell population growth rate was about 25% higher on average, but with such high standard deviation in that case, it wouldn't be advisable to draw any strong conclusions.

These results suggest that the cell's reproductive ability remained unaffected by the hydrodynamic damage they experienced at different flow rates. An alternative possibility, is that a fraction of cells never experienced any significant intensities of hydrodynamic stress, and therefore it was these cells that generated the measured growth rates. However, after 40 repetitions of the experiment for each flow rate, and especially for the case of $0.36\,\mathrm{ml} \cdot \mathrm{sec}^{-1}$, where the arising hydrodynamic stresses in the bulk of the flow are expected to be significantly higher than the critical shear stress for *D. salina*, the possibility that some cells were

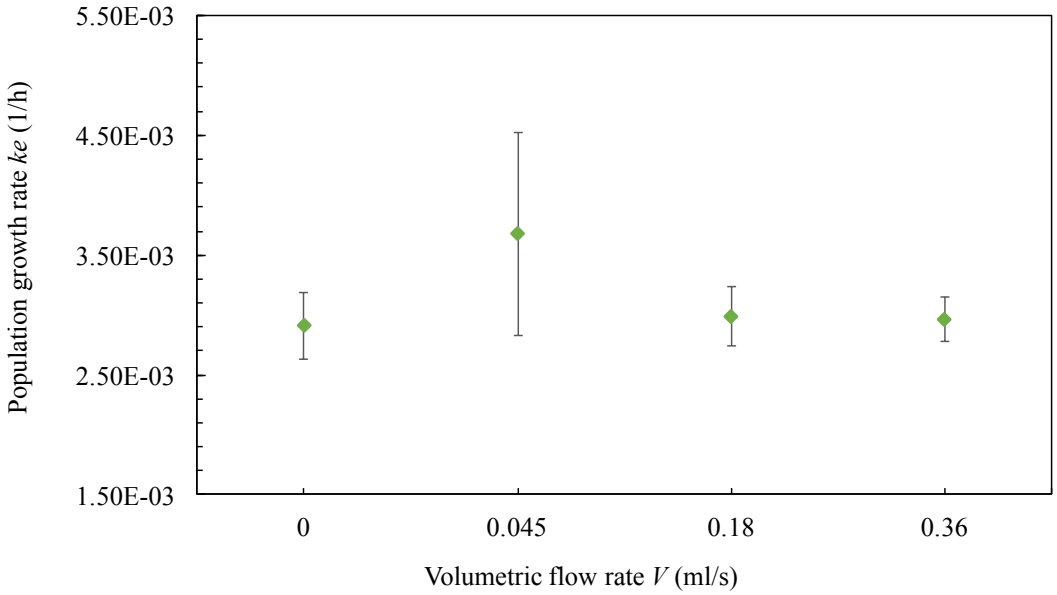

Figure 3.12: *Growth rates of D. salina populations that survived 40 passages through the capillary at different volumetric flow rates, compared with the untreated sample. Each datapoint represents the mean of triplicate experiments, error bars indicate standard deviation from the mean (Zou, 2016).*

completely unaffected is considered to be unlikely.

3.2.5. Critical hydrodynamic stress and energy dissipation

If the cell death in the syringe-capillary system is caused by hydrodynamic stress in the form of shear stress inside the capillary, the model regarding the geometry of the capillary that was described in section 2.3.10, should be able to predict cell death in this system with accuracy. As already described, to determine the critical shear stress, it was first necessary to obtain the death rate per passage in the capillary. We did so following the same method as for the death rates calculated in section 3.2.2, but having the number of passages in the x axis instead of the shearing duration. The resulting death rates k_{dp} were 0.0124/passage for a volumetric flow rate of $0.18\,\mathrm{ml}\cdot\mathrm{sec}^{-1}$, and 0.0535/passage for a volumetric flow rate $0.36\,\mathrm{ml}\cdot\mathrm{sec}^{-1}$, while it made no sense to calculate a death rate in the case of $0.045\,\mathrm{ml}\cdot\mathrm{sec}^{-1}$, since no consistent reduction in the viable cell density was measured. Using these death rates, a critical shear stress τ_{crit} of $223\,\mathrm{Pa}$ was calculated for the case of $0.18\,\mathrm{ml}\cdot\mathrm{sec}^{-1}$, and $439\,\mathrm{Pa}$ for the case of $0.36\,\mathrm{ml}\cdot\mathrm{sec}^{-1}$. In case cell death was really a result of shear stress as it arises inside the capillary, the value for the critical hydrodynamic stress would have been expected to be similar for both cases of $0.18\,\mathrm{ml}\cdot\mathrm{sec}^{-1}$ and $0.36\,\mathrm{ml}\cdot\mathrm{sec}^{-1}$, as the model

assumes a difference in the area of affected cells, while the critical hydrodynamic stress remains the same. This indicates that the passage through the capillary was not the primary cause of cell death in the syringe-capillary system. Additionally, these critical hydrodynamic stresses are one order of magnitude higher than the critical hydrodynamic stresses measured in the narrow-gap rheometer experiments, and therefore cell death would have been expected at much lower hydrodynamic stresses. This further suggests that the passage through the capillary was not the primary cause of cell death for *D. salina* in this system. This is supported by findings from the literature, where CFD simulations of similar syringe-capillary setups indicated that the cells would flow towards the center of the capillary and away from the capillary wall, thus experiencing lower intensities than the wall shear stress (Vickroy et al., 2007; Down et al., 2011). A CFD simulation of the setup would therefore be very useful in more accurately determining the levels of hydrodynamic stress that the cells actually experience in the syringe-capillary setup.

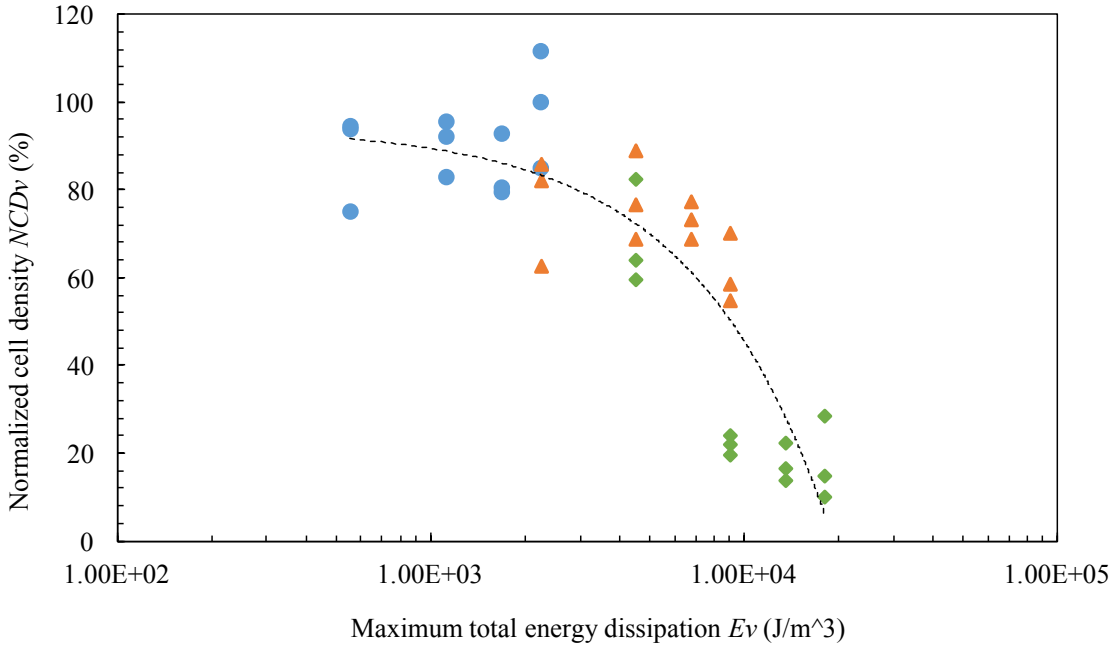

Figure 3.13: *Normalized cell density as a function of the maximum total energy dissipation near the capillary wall: (blue circles) flow rate* $0.045\,\mathrm{ml}\cdot\mathrm{sec}^{-1}$*; (orange triangles) flow rate* $0.18\,\mathrm{ml}\cdot\mathrm{sec}^{-1}$*; (green diamonds) flow rate* $0.36\,\mathrm{ml}\cdot\mathrm{sec}^{-1}$*; (dashed line) linear fit showing the general trend of the experimental data. Each datapoint represents a single measurement.*

Energy dissipation rates ϵ_V and total energy dissipation E_V were determined in the syringe-capillary system based on the maximum energy dissipation near the capillary wall, as

discussed in section 2.3.7. The range of energy dissipation rates was $2.79 \cdot 10^6 - 1.78 \cdot 10^8\,\mathrm{W \cdot m^{-3}}$, while for total energy dissipation, it was $55.4 - 1.77 \cdot 10^4\,\mathrm{J \cdot m^{-3}}$, based on the maximum hydrodynamic stress the cells could experience inside the capillary, which was near the capillary wall. These values are not important on their own, they serve more as an indication of the order of magnitude of energy dissipation that arose in the system, in order to compare it with other hydrodynamic setups. The value of total energy dissipation is plotted against the viable cell density for all the measurements in the syringe-capillary system in figure 3.13, in order to give a general sense of the relationship between the two. It is evident that the higher the maximum total ED the cells could have experienced, the lower the resulting viable cell density.

In the previous experiments mentioned in section 3.1, a range of maximum energy dissipation rates was determined that would lead to cell damage in the narrow-gap rheometer system. The measured EDR was $2.19 \cdot 10^4 - 7.23 \cdot 10^6\,\mathrm{W \cdot m^{-3}}$, for a total energy dissipation of $2.19 \cdot 10^7 - 7.23 \cdot 10^9\,\mathrm{J \cdot m^{-3}}$. It is clear that the maximum energy dissipation rates that arose in the syringe-capillary system were two orders of magnitude higher than they were in the narrow gap rheometer system, while the total energy dissipation experienced by the cells was at least five orders of magnitude lower. This happens because, while the energy dissipation rates are substantially high, the duration that the cells experienced damage due to energy dissipation is extremely short (in the scale of $\mu\,\mathrm{sec}$).

3.3. Rotor-stator stirring experiments

3.3.1. Cell morphology

In the rotor-stator stirring experiments, the FDA staining method was once more used to assess cell viability, and viable and dead cells were once more matched with their respective morphological characteristics. It was expected that it would be easy to distinguish between viable and dead cells using morphology only, given the background from the narrow gap rheometer experiments (presented in section 3.1.3), and the experiments using syringe-capillary setup (presented in section 3.2.1). The results matched the expectations, as the cells were clearly distinguishable between viable and dead from morphology only, and the images generated from this experiment matched the images presented in figure 3.7. Having witnessed *D. salina* cells in three hydrodynamic setups with vastly different hydrodynamic conditions, and having obtained such consistent results, it can be concluded that cell morphology alone

can serve as an indicator of cell viability loss for *D. salina*, in cases where the loss of cell viability is a result of rupturing of the cell membrane.

3.3.2. Cell viability loss

The measured normalized cell density NCD_v is presented in figure 3.14. Generally, the trend of the data is clear, higher stirring speed and longer duration of stirring led to less viable cells in the cell suspension. For a constant stirring speed of 3000 rpm, the viable cell density in the cell suspension decreased with time, reaching 41% after 4 h of being stirred by the rotor-stator. For a constant stirring speed of 5000 rpm, the viable cell density in the cell suspension decreased more rapidly with time, leading to an NCD_v of about 10%, after 4 h. After $2.5 - 3$ h at 5000 rpm, it was assumed that the limits of the accuracy of the method using fluorescence microscopy have been reached, as there were nearly no viable cells visible in the microscope pictures.

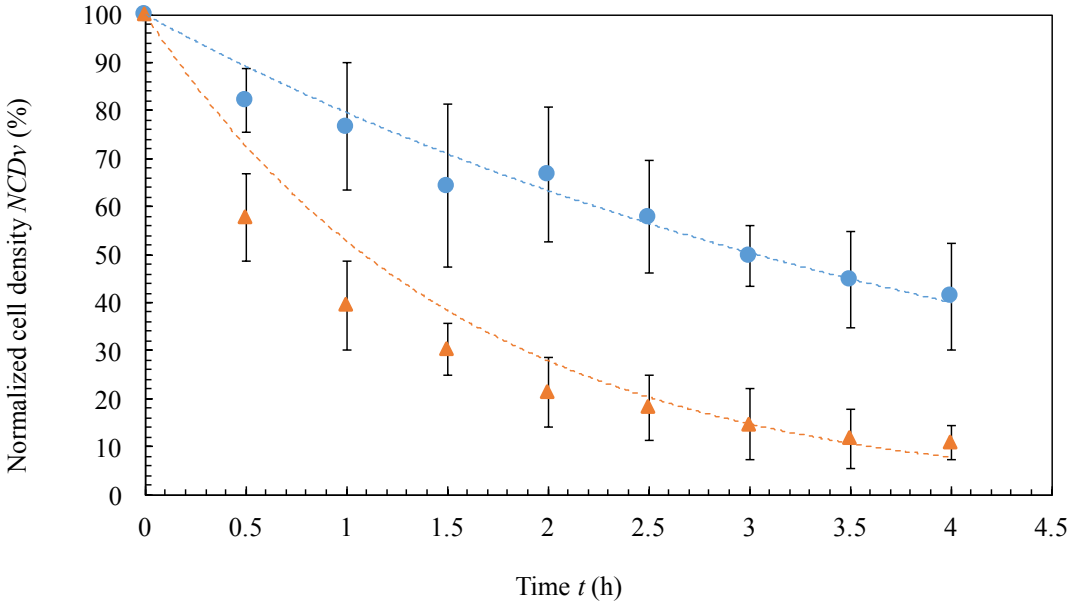

Figure 3.14: *Normalized cell density as a function of stirring time by the rotor-stator: (blue circles)* 3000 *rpm; (orange triangles)* 5000 *rpm; (dashed lines) exponential fit showing the general trend of the experimental data for each dataset. Each datapoint represents the mean of triplicate experiments, error bars indicate standard deviation from the mean.*

We have also determined cell death rates, using a linear least-square fit to the experimental data for viable cell density. The cell death rate k_d for a constant stirring speed of 3000 rpm was found to be $0.23 \pm 0.02\,\mathrm{h}^{-1}$ (with 95% confidence and an R^2 of 0.96), while for the higher

stirring speed 5000 rpm, it was found to be $0.66 \pm 0.08\,\mathrm{h}^{-1}$ (with 95% confidence and an R^2 of 0.91), both fits showing good correlation with the experimental data. The linear least-square fit that led to the determination of the death rates for each stirring speed is presented in figures 3.15 and 3.16. The death rates measured in the rotor-stator system are the lowest in all three systems, similar to the death rates that caused cell damage in the narrow-gap rheometer, and significantly lower than the death rates measured in the syringe-capillary system.

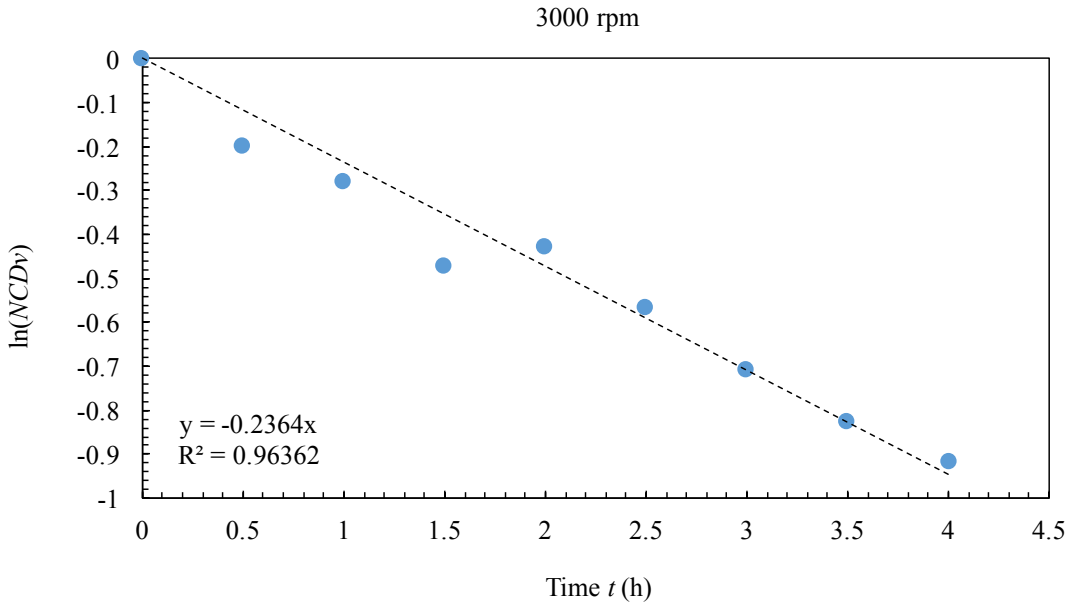

Figure 3.15: *Change in normalized cell density of the cell suspension at* 3000 *rpm stirring speed, as a function of stirring time by the rotor-stator: (dashed line) best least-squares linear fit of the experimental data. The slope of the line gives the death rate of the cells at* 3000 *rpm. Each datapoint represents the mean of triplicate experiments.*

3.3.3. Intracellular protein release

The measurements of the Bradford assay regarding intracellular protein release during the experiments are presented in figure 3.17. For a constant stirring speed of 3000 rpm, there was a steady increase of the released intracellular protein in the cell suspension up to the total duration of the experiment as indicated by the increase in absorbance Δa at $595\,\mathrm{nm}$. For a stirring speed of 5000 rpm, the amount of released protein reaches a plateau of maximum absorbance at about $2.5 - 3\,\mathrm{h}$, which coincides with the point where the viable cell density of the samples has reached below 20%, i.e. when there were nearly no viable cells in the microscope pictures. To put it more simply, it appears that when there were no more cells to rupture, there was also no more intracellular protein to be released. This supports the idea

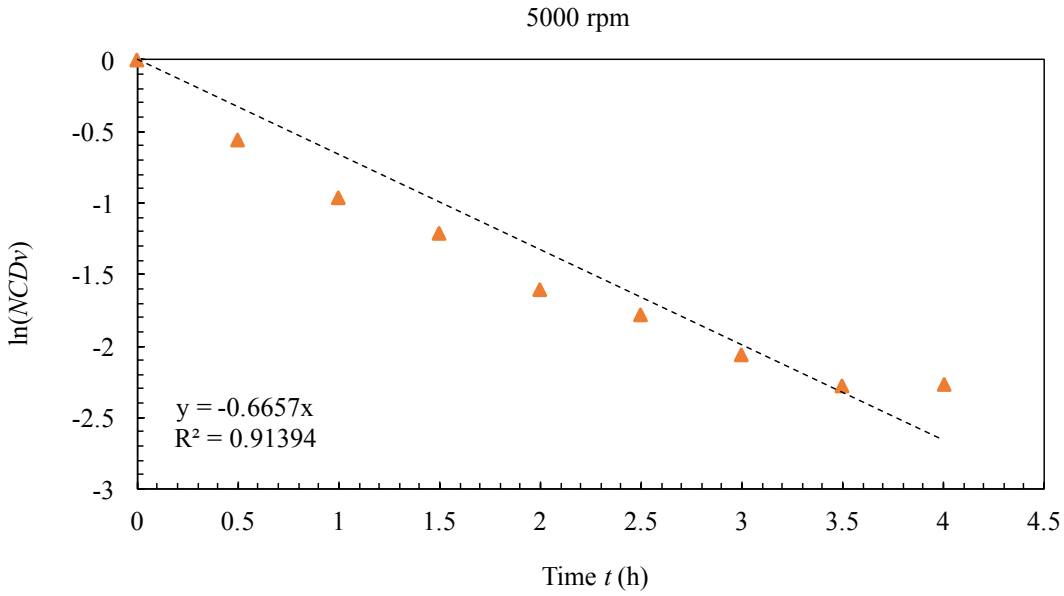

Figure 3.16: *Change in viable cell concentration in the suspension at* 5000 *rpm stirring speed, as a function of stirring time by the rotor-stator: (dashed line) best least-squares linear fit of the experimental data. The slope of the line gives the death rate of the cells at* 5000 *rpm. Each datapoint represents the mean of triplicate experiments.*

that the decrease in viable cell count correlates with the increase in released intracellular protein in the cell suspension, as they both relate to the phenomenon of cell rupture.

Given all the indications from the previous experiments, it seemed reasonable to directly test if the Bradford assay is a good predictor of cell rupture for *D. salina*. To test this, both measurements needed to be scaled, so that the maximum available value for one measurement would correspond to the maximum of the other, and the same would be necessary for the minimum. This is reasonable for describing this phenomenon, as there is a maximum possible value of intracellular protein release, which corresponds to all cells being ruptured in a given sample. The values for the viable cell density are scaled between $0\,\%$ and $100\,\%$. Therefore, in order to have the same scaling for the intracellular protein release, the intracellular protein release data need to be divided by the maximum value measured in the experiments. The maximum relative change in absorbance that was obtained for the Bradford measurement was clearly at about $3\,\mathrm{h}$ at $5000\,\mathrm{rpm}$, therefore the Bradford measurement data was re-scaled using the final measured value after $4\,\mathrm{h}$ as 100%.

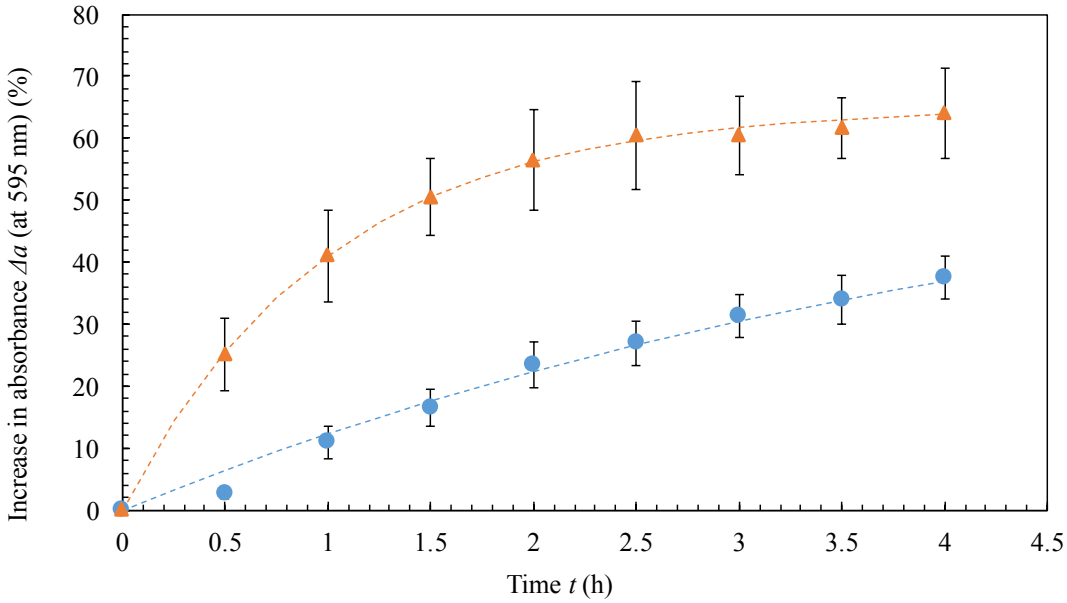

Figure 3.17: *Increase in absorbance at* $595\,\mathrm{nm}$ *as a function of stirring time by the rotor-stator: (blue circles)* 3000 *rpm; (orange triangles)* 5000 *rpm; (dashed lines) exponential fit showing the general trend of the experimental data for each dataset. Each datapoint represents the mean of triplicate experiments, error bars indicate standard deviation from the mean.*

Thus, the correlation graph was generated, presented in figure 3.18, including the linear least-square fit of the data, where the slope and correlation coefficient R^2 determine the goodness of fit (the closer to 1 the better, for both values). The linear regression line fitted to all the data, with a fixed point at $(0,0)$, had a slope of 1.021 and an R^2 of 0.95, which indicates a strong correlation between the predicted and the realized cell death. These results strongly suggest that the phenomena of intracellular protein release and cell viability loss correlate well with each other, and, that the two types of measurements are in fact interchangeable. Once more, it is worth mentioning that this would be reasonable to expect, given that intracellular protein content has been shown to correlate well with cell count for some microalgae species (Spiden et al., 2013). We consider this finding to be important, because the Bradford assay costs significantly less time and resources to be performed than fluorescence microscopy, which would make it ideal for determining cell viability loss in off-line measurements during any upstream process regarding *D. salina* cells.

3.3.4. Energy dissipation

To determine the energy dissipation in the rotor-stator system data provided from the manufacturer was used regarding the energy output of the stirrer for a $200\,\mathrm{ml}$ suspension of

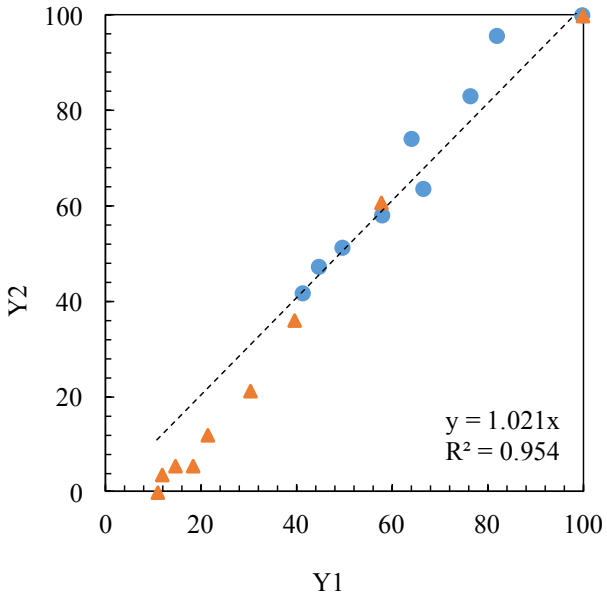

Figure 3.18: *Correlation between actual normalized cell viability (Y1) and predicted normalized cell viability based on the Bradford assay (Y2): (blue circles)* 3000 *rpm; (orange squares)* 5000 *rpm; (dashed line) best linear fit of all the data. Each datapoint represents the mean of triplicate experiments.*

water, which should be very near the energy required for the cell suspension. For a stirring speed of 3000 rpm, the measured energy input on the stirrer was about 14 W, while for a stirring speed of 5000 rpm it was about 26 W. Given these values, volume-average energy dissipation rates ϵ_V of $7 \cdot 10^4$ W $\cdot$ m^{-3}, and $1.3 \cdot 10^5$ W $\cdot$ m^{-3}, were determined for 3000 and 5000 rpm respectively. The range of volume-average total energy dissipation arising E_V in the rotor-stator experiments was between $1.2 \cdot 10^8$ J $\cdot$ m^{-3} and $2.9 \cdot 10^9$ J $\cdot$ m^{-3}. These values serve as an indication of the order of magnitude of energy dissipation that arose in this system, in order to compare it with other hydrodynamic setups. The volume-average total energy dissipation is plotted against the NCD_v of cells for all the measurements in figure 3.19, in order to provide a sense of the relationship between the two. It becomes clear that the higher the volume-average total energy dissipation in the cell suspension, the lower the resulting viable cell density.

Additionally, the Kolmogorov length scale of turbulence θ was calculated for the conditions of this experiment, based on equation 1.3, and the average energy dissipation rates of the two stirring speeds. A Kolmogorov length scale of 12 µm was determined for 3000 rpm, and 10 µm for 5000 rpm. It is worth noting that the length scale is very similar to the average cell size for

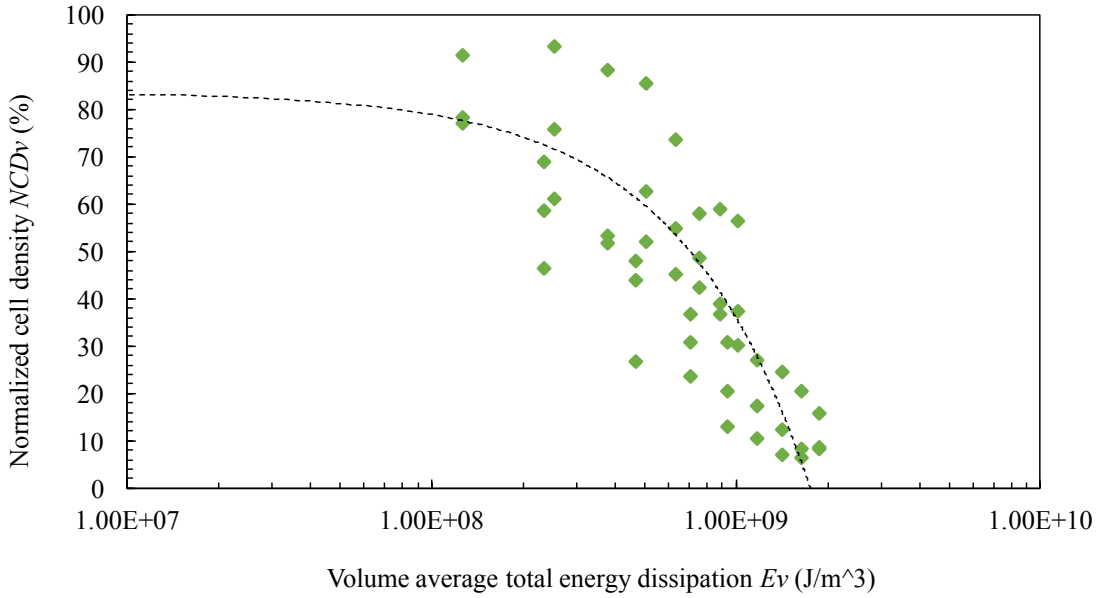

Figure 3.19: *Normalized cell density as a function of volume average total energy dissipation in the rotor-stator: (dots) experimental data; (dashed line) linear fit showing the general trend of the experimental data. Each datapoint represents a single measurement.*

D. salina cells, which have a documented average cell length of 14 µm, and an average cell width of about 11 µm (Richmond and Hu, 2013), and were of similar size in our experiments (as shown in figure 2.3).

In the previous experiments, presented in sections 3.1 and 3.2, the ranges of energy dissipation rates and total energy dissipation that arose in each system were also determined. The values determined in these systems are based on analytical equations about the maximum energy dissipation that the cells could experience in flow. Unfortunately, there are no such equations for this system, so only the volume average values were available. One way to compare between the three systems would be to use CFD simulations to determine the volume-average energy dissipation rates in the other two systems. Another way, that could be more accurate, would be to use CFD simulations of all three systems in combination with particle tracking, to obtain the real history of energy dissipation rates that the cells experienced during flow, and compare these, as performed by e.g. Liu et al. (2016) for *C. tinctorius* cells in a stirred tank reactor.

3.4. Population balance modeling of cell rupture under hydrodynamic stress

The present work on population balance modeling of microalgae lysis under hydrodynamic stress was published as conference proceedings in the special issue of Chemie Ingenieur Technik (Kokkinos et al., 2014).

A study case was prepared in order to demonstrate the capabilities of the population balance model designed in this work. In this study case, a population of cells growing over time unaffected by hydrodynamic stress was compared with another population of cells that grew under constant hydrodynamic stress. Given these conditions, the results of the model were observed with regard to cell population heterogeneity, which is the central subject of population balance models, and the cell population growth rate, which is mostly interesting regarding experimental and industrial applications. The values of the parameters used in the model are not to be taken literally, they were selected only for the purpose of showcasing the model's capabilities, since all the necessary parameter values for a single cell type could not be obtained, either through experiments or from existing scientific publications.

3.4.1. Cell population heterogeneity

Initially, at a simulated time of $0\,\mathrm{h}$, both populations are identical, and each forms a two-dimensional normal distribution. As the cells grow, and proliferate after reaching a certain size x, the distribution extends more in the axis representing cell radius, while no similar extension appears in the distribution of cell membrane's Young's modulus E_Y. This happens because, in the considerations of the model, the cell membrane's Young's modulus doesn't change over time and the daughter cells inherit the cell membrane's Young's modulus of the mother cell. For the population of cells affected by hydrodynamic stress, there is an additional change in the distribution. That is, cells will die out based on the critical capillary number Ca_{crit}, which translates in cells of larger radius or lower cell membrane's Young's modulus to have a higher probability of dying. Also, since some cells die out in the population affected by shear stress, while in the other this does not happen, there is a growing difference over time regarding their number density.

After a simulated time of $10\,\mathrm{h}$, there is a dramatic difference in the two-dimensional distributions of the two populations, as presented in figure 3.20. The population of unstressed cells has grown perfectly symmetrical with regard to the cell membrane's Young's modulus (figure

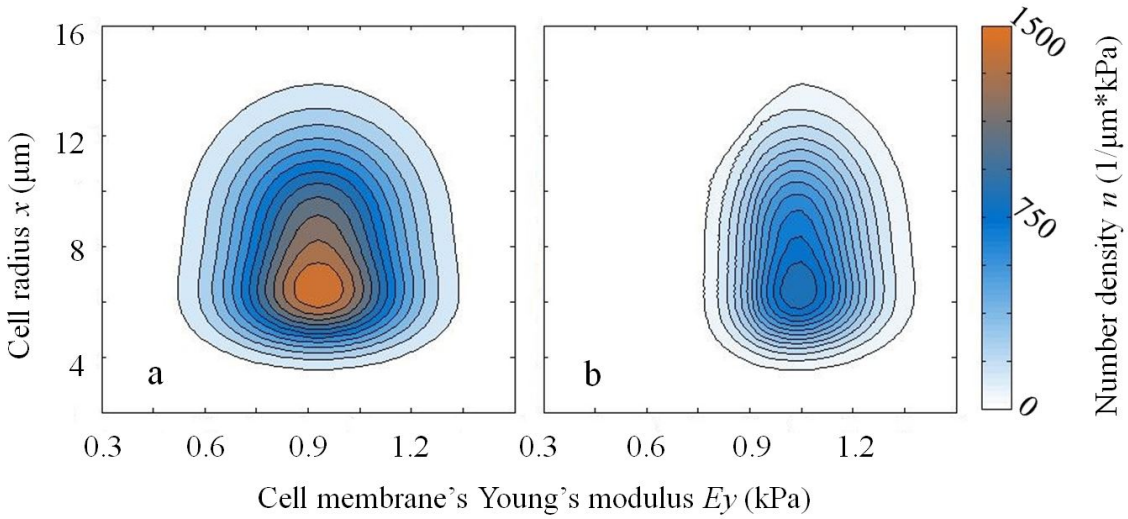

Figure 3.20: *Simulation of a two-dimensional distribution of cells after* 10 h *of growth: (a) unstressed cells; (b) shear stress equal to* 200 Pa*. Coloring indicates the number density of cells, as presented in the color bar (Kokkinos et al., 2014).*

3.20 a), and has a significantly higher number density than the population under constant hydrodynamic stress, which has also become asymmetrical due to the effect of the critical capillary number. More specifically, the critical capillary number leads to the instantaneous death of cells that correspond to the top left area of the two-dimensional diagram in figure 3.20 b, which decreases the population number density. Additionally, some of the larger cells die out without having a chance to proliferate, which also decreases the growth rate of the population number density, which is why the results of the two populations are so dramatically different. Increasing the intensity of constant hydrodynamic stress affecting the cells would further increase those differences, up to the point where the whole population of cells would die out, instead of just having a lower growth rate.

3.4.2. Cell population growth rate

Based on the same model parameters, it was attempted to observe the result of increasing hydrodynamic stress on the viable cell density of the population. The double integral of the distributions presented in the previous section at a specific point of simulation time, represents the viable cell density of each population (since the model doesn't in any way count the dead cells). Therefore, comparing that value at time t, with the initial value, the NCD_v of a population at a given time is obtained, which is the measure that receives the highest attention regarding cell death under hydrodynamic stress, as discussed in previous sections.

The resulting NCD_v (%) is presented in figure 3.21, for different values of hydrodynamic stress affecting the population. As expected, cell populations growing under higher intensities of hydrodynamic stress had a decreased population growth rate and thus a decrease in the resulting NCD_v. There is an intensity of hydrodynamic stress at which the population barely survives after $10\,\mathrm{h}$ of simulated time (at about $\tau = 250\,\mathrm{Pa}$), and for higher intensities the viable cell density decreases, or even the entire population dies out.

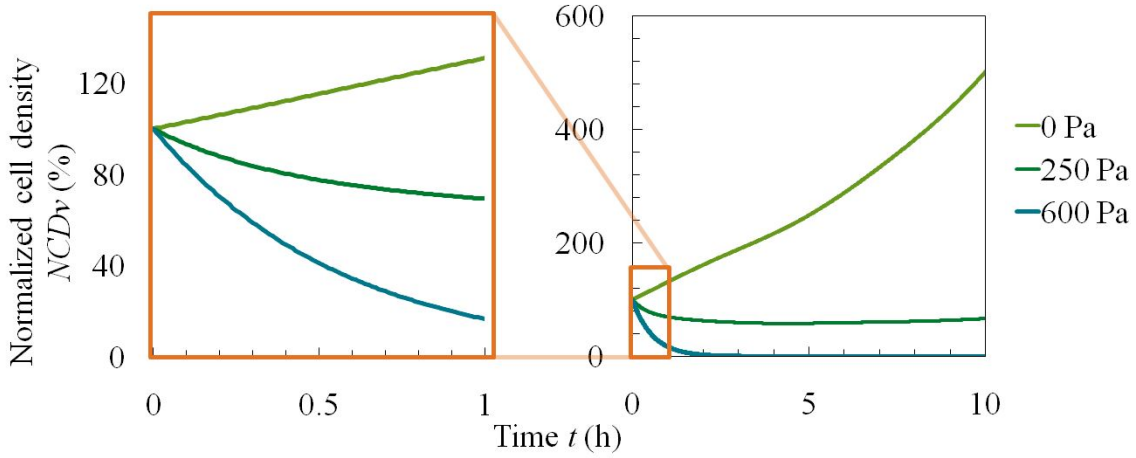

Figure 3.21: *Simulation of the temporal evolution of the viable cell density in a culture affected by constant shear stress. The orange box shows a zoomed region from the graph on the right (Kokkinos et al., 2014).*

Chapter 4

Discussion

Witnessing cell behavior in flow

A novel rheo-optic setup, capable of increasing the understanding of the hydrodynamic behavior of cells in simple shear flow, was used in this thesis. This setup, i.e. the narrow gap rheometer, is unique because it can obtain very high shear stresses by reducing the gap width of the parallel plates configuration with an accuracy of $1\,\mu\mathrm{m}$, which reaches shear rates far higher than commercially available rheometers, without the use of chemical thickeners. It has also been used for measuring other cells under high shear conditions, such as determining average viscoelastic cell properties of cell monolayers (Dakhil et al., 2016), and measuring the adhesion limit of fibronectin for fibroblasts (Dakhil et al., 2018).

The cells were observed forming chains following the flow direction, a finding which has also been recorded for polystyrene sphere suspensions, using a parallel plate setup as was the case in the narrow-gap rheometer experiments (Pasquino et al., 2010). According to the authors of the particular study, the spheres would form chains that would always align in the direction of flow regardless of their size, as long as a high enough shear rate was reached, but the chains would form only near the edge of the parallel plates, while near the center of the plates the spheres would remain randomly distributed. In this case, the objective of the camera was placed near the edge of the geometry, as the main interest was focused on the behavior of cells under high shear stress conditions. For low shear rates, all visible cells seemed randomly distributed and moving in the direction of flow, while for high shear rates, most cells seemed to form chains, which matches the expectations from the experiments of Pasquino et al. (2010), even though motile cells were used instead of spheres. Pasquino et al. (2010) also witnessed some particle migration towards the edge of the parallel plates,

which they confirmed by comparing the amount of spheres near the edge at the beginning of the experiment and the end. No such migration was noticed in the experiments, but to properly notice this phenomenon one should use a wider zoom angle, thus getting a better overview of how the cell population behaves, instead of trying to observe individual cells like in the experiments, where a $20x$ magnification was used, which is too high for this purpose. Additionally, the formation of large cell clusters was witnessed, which implied that the cells adhered to one another at some point during the experiment. In the rest of the experiments, witnessing such a cluster was a rare occurrence.

An additional comment worth mentioning is that it was not possible to witness cell rupture in flow, which comprised an initial goal while structuring the initial backbone of the proposed scientific work. The narrow-gap rheometer was considered ideal for these types of measurements, because it could generate high enough hydrodynamic stress to cause cell rupture for *D. salina* cells. It is reasonable to suggest that the setup used could be further improved by using a camera with a higher frame rate, which would conceivably allow for witnessing rupturing of a cell in shear flow and capture it on video. To the author's knowledge, this attempt has not been performed for microalgae cells during the duration of this thesis. In a similar attempt, a Master thesis in the Chair of Process Systems Engineering of the Technical university of Munich used microfluidic channels that allowed witnessing *D. salina* and *H. pluvialis* cells in simple shear and extensional flow (Mueller, 2016). Co-supervision of the experimental part of the thesis, along with the biological cells required for the experiments were provided by the current author. Tumbling and rotation was observed for both cell species placed in flow, with visible deformation when flowing near a narrowing of the microchannel, especially for cells flowing near the edges of the geometry. However, this effect was not consistent for all cells, and no bursting of cells could be observed in flow for either cell species.

There are some limited findings in the current literature, one of which was performed in microcapsules, which are similar to cells in terms of experimental design and choice of equipment. The authors of this study managed to capture the rupturing of the membrane of microcapsules at shear rates of about $42.5\,\mathrm{sec}^{-1}$ (Unverfehrt et al., 2015). There was also a study on human erythrocytes, which used fluorescent dye to better witness the leaking of the intracellular material due to the rupturing of the cell membrane through an intense shear flow generated by a cavitation bubble (Li et al., 2013). This idea could further improve the experimental design of this thesis, as long as the fluorescence dye used is compatible with *D.*

salina cells.

Mechanical and biological reactions of cells

Cell morphology can be influenced by hydrodynamic stress, and especially shear stress, a phenomenon witnessed in a wide range of cell types, from human osteoblasts (Horikawa et al., 2000; Altmann et al., 2014), to several microalgae species (Mitsuhashi et al., 1994; Michels et al., 2016). Given that morphology can determine the overall behavior of the cell in flow, including the hydrodynamic stresses that it experiences, it was deemed relevant to determine any noticeable morphological changes occurring in the experiments as a result of the hydrodynamic stress of *D. salina*. A common finding recorded in all the experiments was that cells experiencing damaging levels hydrodynamic stress had straightforward differences, as opposed to the unaffected cells. The latter were symmetrical, round or ellipsoidal in shape, and usually had visible flagellas (the flagellas being difficult to detect in the images since they are completely transparent). On the other hand, damaged cells had no visible flagellas, presented a "flatness" in their appearance, and were asymmetrical, with visible imperfections in the roundness of their membrane.

No other substantial morphological differences were observed, as was e.g. the case when *D. salina* cells were placed under UV-B radiation, where the cells appeared 20% larger in length and width after treatment (Masi and Melis, 1997). In this case, there was no indication that the cell size changed substantially, or could any other differences be detected, as e.g. increased carotenoid production which might also happen in *D. salina* cells in cases of stress. Regarding the loss of flagellas in the narrow-gap rheometer measurements at shear stresses of $20\,\mathrm{Pa}$ or higher, no relevant studies were found in the literature apart from a study of the dinoflagellate *C. cohnii* (Hu et al., 2008). The findings of this particular study showed that the studied organism could withstand levels of energy dissipation rates up to $5.8 \cdot 10^7\,\mathrm{Wm}^{-3}$ without loss of viability, but suffering a sub-lethal loss of flagellas even at lower energy dissipation levels. Given this, it becomes reasonable to assume that the loss of flagellas can serve as an indicator of damage due to hydrodynamic stress, but not as an indicator of cell viability loss.

Cell viability usually comprises the main focus of experiments on cells under the influence of high hydrodynamic stress. As methods of assessment, both cell morphology and the FDA fluorescence dye were used. The latter approach is significantly more popular as a

method of viability assessment and has been used extensively for *Dunaliella* strains (Hejazi et al., 2003; Barbosa et al., 2004), and other microalgae species, e.g. *Chlorella* sp., *C. muelleri*, and *T. suecica*, and (Franklin et al., 2001; Michels et al., 2010, 2016). The main reason for its popularity is that it has been shown that only fully viable cells are detected by this method (Altman et al., 1993), which makes it more accurate than other standard methods, as e.g. trypan blue assessment, where even apoptotic cells can be measured as false positives. Our experiments have shown that cell morphology was an equally good method of viability assessment for *D. salina*, when viability loss was due to hydrodynamic stress conditions. Cells retaining the original spherical or ellipsoidal form were found viable, as determined by their FDA-fluorescence, while cells that visibly deviated by the imperfections on their membrane were found non-viable, as determined by their FDA-fluorescence, in a way consistently identifiable in the microscope pictures. To the author's knowledge, this has not been previously shown for *D. salina* cells, and this notion is not necessarily generalizeable for other microalgae species, as e.g. for *C. muelleri* in the experiments of Michels et al. (2010), where no changes in morphology were identifiable and only through FDA fluorescence could cell viability be determined. This finding is useful for experimental design, as it only requires a microscope and comprises a cost-effective laboratory approach, compared to the fluorescence equipment required for FDA measurements. Furthermore, this approach enables the assessment of certain initial measurements, as a first step and before the implementation of fluorescence measurements. Additionally, loss of cell viability due to hydrodynamic stress was observed in both laminar and turbulent conditions, thus making the usefulness of the morphological assessment of viability applicable in both ends of the hydrodynamic spectrum of turbulence. In the literature regarding microalgae cells, there were only available mentions of morphology being used as a method for cell viability assessment in the case of microalgae *O. malhamensis* (Yang and Wang, 1992).

Intracellular protein release is commonly measured through the Bradford assay and is considered a standard for a long time now (Middelberg, 1995). The Bradford assay has also been used for several microalgae species in the experiments of Bronnenmeier and Maerkl (1982), where they tested time constraints for the measurement, and increasing pressure and hydrodynamic stress levels. Also, Spiden et al. (2013) has used Bradford and cell counts to determine whether cell rupture through high pressure homogenization (HPH) occurred for microalgae species *Nannochloropsis* sp., *Chlorella* sp., and *T. suecica*, without using a direct measurement of cell viability to compare to, they simply counted the visible cells in

the microscope pictures (which should be enough for HPH, as it completely disintegrates cells). The findings of the above mentioned study have shown that the Bradford assay can be successfully used to determine intracellular protein release for microalgae species, and that intracellular protein content can correlate with cell count (good correlation for *T. suecica*, worse for *Nannochloropsis* sp. and *Chlorella* sp.). It appears reasonable to expect better correlation of the intracellular protein release with viable cell count, in the case where cell viability loss only depends on mechanical cell rupture. After the relevant experiments were completed, it could be deduced that the Bradford test seems a better predictor of cell viability loss, compared to fluorescence microscopy. It had consistently smaller standard deviations than the fluorescence microscopy measurements, and it would measure differences when the fluorescence microscopy measurement could not (e.g. the case for capillary flow at volumetric flow rate of $0.045\,\mathrm{ml}\cdot\mathrm{sec}^{-1}$). Both methods can correlate with each other extremely well as long as the maximum intracellular protein release a given sample can have is known. In other words, both measurements can be used interchangeably for the particular systems tested, given the indications from the experiments. This knowledge can be extended and applied for similar systems such as stirred tank reactors, having the added advantage that the knowledge of both facts is obtainable by using only one measurement. In addition to that, the Bradford assay takes much less time than a microscope measurement, about $5-8$ min vs 15 min or more, which would then save time from in-line measurements. Since it determines the cell death rate, the Bradford assay could also be used to obtain information applicable to models of cell proliferation in reactors, such as population balance models, where a term for cell death might be relevant regarding the process (Ramkrishna and Singh, 2014). In literature, it is considered reasonable to assume that the FDA viability could be correlated to intracellular protein content, and thus to protein content measured by the Bradford assay (Stoddart, 2011). However, to the author's knowledge, the Bradford assay has not been previously used and proven to work for the indirect assessment of cell viability for any microalgae species, or *D. salina* cells in particular, which increases the scientific value of this contribution.

Cell proliferation ability, after the cells have been subject to hydrodynamic stress, has been put to question in a classic study by Dunlop et al. (1994), where carrot cells had shown decreased cell proliferation ability even at sub-lethal levels of hydrodynamic stress. These findings suggested that one might test if cells are viable by e.g. FDA fluorescence, and one might still not be certain that the cells remain useful for biotechnological applications such as cultivation. In the experiments in the syringe-capillary system, the proliferation

ability of D. salina cells was investigated, after the cells have been subjected to levels of hydrodynamic stress that led up to nearly all cells being shown dead in the microscope pictures after treatment. The cells exhibited similar growth rates in all cases and compared with the untreated sample, with a note bearing in mind that the cells treated with the least amount of hydrodynamic stress (i.e. for the case of flow rates $0.045\,\mathrm{ml\,sec^{-1}}$ and a maximum shear stress in the capillary of $56\,\mathrm{Pa}$) showed an increased proliferation rate. Nevertheless, for that particular indication the average values for all measurements were found within standard deviation range. This might be worth further investigation, as there have been indications in the literature that sub-lethal levels of hydrodynamic stress might assist microalgae growth (Wang and Lan, 2018). Such was the case in the experiments of Hosaka et al. (1995) with *Chlorella* sp., and Sobczuk et al. (2006) for *P tricornutum* and *P. cruentum*, where hydrodynamic stress enhanced the growth rates of the microalgae populations. The standard deviation of the population growth rates measured in all cases was relatively high compared to the average, ranging from 7% to 23% of the average value, which is higher than other publications, as e.g. was the case for *S. obliquus* cells grown in different pH and temperature conditions, with standard deviations of 1% to 10% of the average (Guedes et al., 2011). In our case, the high standard deviations can be mainly attributed to the measurements we took during the first days of incubation in the fresh medium, where the cells appearing in the counting chamber were too few to allow a more accurate estimation of the cell concentration.

Comparing different hydrodynamic setups and cell species

In general, the problem with comparing different hydrodynamic setups is that the knowledge gained from one setup is not necessarily relevant in another. The reasons behind this phenomenon include biological factors, as e.g. the cells not being from the same culture even if they were from the same species, or small deviations in the growth medium that different experimenters used, that might lead to dramatic differences in the behavior of cells. On top of that, there are differences in the hydrodynamic stress arising in each type of equipment, as e.g. if the flow is laminar or turbulent, or differences in the duration that the cells experienced critical levels of hydrodynamic stress. We wanted to design the experiments in such a way that would facilitate such a comparison. The cells were always cultivated in the same way, and experienced hydrodynamic stress in conditions mimicking their natural state, i.e. freely suspended cells, at room temperature, without any chemical thickeners in the cell medium. We also used three different hydrodynamic setups, witnessing in all cases the full spectrum

of population viability for *D. salina* cells, from the entire population of cells being fully viable and swimming constantly in the microscope pictures with the use of their flagellas, to having nearly exclusively ruptured cells and cell debris visible in the microscope pictures.

However, as already discussed in section 3.3.4, there was no available access to data from CFD simulations, that would offer us the information of what the cells actually experienced in flow. This would be achieved by lagrangian particle tracking, where multiple simulated particles are assumed to flow freely inside a simulation of the hydrodynamic setup, and then based on that simulation, predictions can be made about the levels of hydrodynamic stress that would cause cell rupture, and what percentage of cells would be affected at a given time. Such simulations have gained increased popularity over the years, and even though they are being constantly improved and re-assessed for accuracy (Greifzu et al., 2016), they have already provided some impressive results, as e.g. in the work of Down et al. (2011) for red-blood cells passing through a syringe-capillary system, or the work of Liu et al. (2016) for plant cells *C. tinctorius* flowing in a stirred-tank bioreactor.

Even by simply knowing the order of magnitude of hydrodynamic stress that could have affected the cells, successful comparisons can be made. For such comparisons between setups and cell species, the critical hydrodynamic stress is usually preferred as a measure, which is defined as the level of hydrodynamic stress below which no significant decrease in cell viability or cell population growth rate is detected (Wang and Lan, 2018). Among microalgae species, the highest sensitivity to hydrodynamic stress was measured for *P. reticulatum* (Garcia-Camacho et al., 2007), and *L. polyerdum* (Juhl et al., 2000), at critical shear stresses in the order of $10^{-4}\,\mathrm{Pa}$ and $10^{-3}\,\mathrm{Pa}$ respectively. *A. flos-aquae* cells were of similar sensitivity, as they disintegrated completely in a stirred-tank reactor reaching a maximum hydrodynamic stress of $0.45\,\mathrm{Pa}$ (Leupold et al., 2012). In the experiments of Michels et al. (2016) on various microalgae species, they used a rheometer with concentric cylinder geometry to inflict hydrodynamic stress upon the cells (in the form of shear stress), up to a maximum level of $88\,\mathrm{Pa}$. They found levels of shear stress of about $1.3\,\mathrm{Pa}$ would greatly reduce the levels of viability for *C. muelleri* cells, levels of about $1-10\,\mathrm{Pa}$ would reduce the viability of *I. galbana* and *S. costatum* cells, while, remarkably, even at $88\,\mathrm{Pa}$, the highest level of shear stress tried in these experiments, the viability of *T. suecica* cells remained unaffected. In the experiments with the narrow-gap rheometer, it was found that *D. salina* cell viability would reduce at levels of about $15-20\,\mathrm{Pa}$, which suggests it is more resistant to

shear stress than three out of four of the cell populations tried in the experiments of Michels et al. (2016). In the syringe-capillary setup, cell viability loss was witnessed at levels of wall shear stress similar to those expected for mammalian and insect cells (Tanzeglock et al., 2009; McQueen et al., 1987; Zhang et al., 1993; Ma et al., 2002) in studies using devices that generate capillary flow, while it wasn't possible to find any similar studies with microalgae cells.

The experiments with the rotor-stator setup are harder to compare using hydrodynamic stress directly, as there are no available data for the hydrodynamic stresses arising near the rotor-stator stirrer as there are for other, more standardized stirrers. Also, the type of hydrodynamic stress in this setup is turbulent, which is expected to differ in the damage it can cause to the cells (Dunlop et al., 1994), when compared to the other two setups where the cells flowed in laminar conditions. In an attempt to obtain data of *D. salina* cells subjected to hydrodynamic stress generated by a more standardized stirrer, we used an anchor-type stirrer in the experiments for a Master thesis in the Chair of Process Systems Engineering of the Technical University of Munich (Syngelaki, 2014). Supervision of the thesis, along with the biological cells required for the experiments were provided by the current author, in collaboration with Prof. Dr. Andreas Boudouvis and Dr. Mihalis Kavousanakis of the National Technical University of Athens. A $450\,\mathrm{ml}$ cell suspension was stirred at $400 - 500\,\mathrm{rpm}$ on for a total duration of $4\,\mathrm{d}$, and compared with an untreated sample placed next to the stirred sample to make sure they received the same lighting conditions. We measured cell viability and intracellular protein release, as in the rest of the experiments, but could find no conclusive evidence that cell viability loss occurred for the experimental parameters tested, as both the viable cell density and the intracellular protein release were of similar levels for the treated and the untreated sample. However, it remains possible that cell death occurred, but at rates much lower than the growth rate of the cell population, in which case it would be undetectable in the viable cell density measurements. A way to assess that possibility would be to have two reactors at different stirring speeds (e.g. 250 and 500rpm), with the populations of cells growing side by side for the duration of $4\,\mathrm{d}$, and compare the effective growth rates of the two populations. If there was a difference in the effective growth rates, it would be possible to connect this difference to cell death due to hydrodynamic stress, as was the case in the experiments of Contreras et al. (1998) on *P. tricornutum* cells. Another factor that could have affected a measurement on such a long timescale would be the death of cells due to natural deterioration (aging). If the death rate due to aging was considerably high, any smaller death

rates due to hydrodynamic stress would have been undetectable in this experimental setup. Regarding microalgae cells, this death rate due to aging is usually considered negligible when compared with the population growth rate (Kim et al., 2002; Silva et al., 2016), unless serious substrate starvation occurs (Jiang et al., 2012). In a case where it was estimated using cultivation data for microalgae *Desmodesmus sp.* (Eze et al., 2018), the death rate due to aging was found to be two orders of magnitude lower than the estimated population growth rate. Therefore, we would expect that the death rates due to aging of would have been irrelevant for the experiments of (Syngelaki, 2014), despite the long timescale.

Apart from hydrodynamic stress, there exist other ways for comparing different hydrodynamic setups, that have been extensively used in the literature. One commonly used way is comparing cell death rates, a comparison mostly used by biologists and biotechnologists, as it offers an immediate estimate of how lethal a setup is for a microorganism, or how better some microorganisms fare in the same conditions when compared to others, i.e. which microorganisms are stronger and which are weaker against hydrodynamic stress. Also, they provide a quick way to estimate whether a microorganism would be able to grow in a hydrodynamic setup, when knowing both the death rates of similar microorganisms in that setup and the growth rate of that microorganism in similar setups. Ordering the hydrodynamic setups used by how deadly they were for *D. salina* cells, starting with the least deadly, the rotor-stator setup comes first, resulting in death rates up to $0.66\,\mathrm{h}^{-1}$, the the narrow-gap rheometer with death rates up to $10\,\mathrm{h}^{-1}$, and, significantly deadlier than the other two, was the syringe-capillary system with death rates up to $8 \cdot 10^{7}\,\mathrm{h}^{-1}$.

We can compare these with the death rates measured by Barbosa et al. (2004) for *D. salina* and *D. tertiolecta*, where they cultivated the cells in bubble-column reactors, which are widely used for microalgae (Hamed, 2016). In such bioreactors, bubbles can cause cell death due to hydrodynamic stress in multiple ways: where the bubbles form, while the bubbles flow through the medium, or, as most research suggest, when the bubbles burst at the surface releasing energy Meier et al. (1999). The death rates in their experiments were up to $1.62\,\mathrm{h}^{-1}$ for *D. salina*, and up to $1.05\,\mathrm{h}^{-1}$ for *D. tertiolecta*, which was deemed more resilient as a *Dunaliella* species. This shows that the death rates measured in the rotor-stator and the narrow-gap rheometer measurements can occur even in normal cultivation conditions for *D. salina*. For other species, cell death in reactors can reach even higher death rates, as e.g. up to $10^{4}\,\mathrm{h}^{-1}$ for mouse hybridoma cells in a bubble-column reactor (Orton, 1992), or $8 \cdot 10^{3}\,\mathrm{h}^{-1}$ for *C.*

tinctorius in a stirred tank reactor Liu et al. (2016). For the exceptionally higher cell death rates in the syringe-capillary setup, it is possible to compare with other cell types in similar conditions, as e.g.the study of Vickroy et al. (2007) on CHO (Chinese Hamster Ovary) cells, where they measured cell death rates up to $10^5\,\mathrm{h}^{-1}$, for flow rates through the capillary up to $0.5\,\mathrm{ml}\cdot\mathrm{sec}^{-1}$. This suggests that the measured death rates in the syringe-capillary system are reasonable, especially if it is taken into account the fact that *D. salina* cells are considered particularly vulnerable to hydrodynamic stress, because they lack a cell wall and are only protected by a plasma membrane Barbosa et al. (2003).

Another way for comparing different hydrodynamic setups is by comparing energy dissipation rates, which is a way mostly used by engineers, not only because they facilitate a comparison between different hydrodynamic conditions, but also because they allow for a quick estimation of the costs and efficiency of a setup. We measured cell viability loss at maximum energy dissipation rates of $10^5 - 10^6\,\mathrm{W}\cdot\mathrm{m}^{-3}$ in the narrow gap rheometer, $10^7 - 10^8\,\mathrm{W}\cdot\mathrm{m}^{-3}$ in the syringe-capillary system, and volume average energy dissipation rates of $10^4 - 10^5\,\mathrm{W}\cdot\mathrm{m}^{-3}$ for the rotor-stator setup. The maximum energy dissipation rate of the rotor-stator setup should be higher than the volume average, and it is reasonable to expect it to be up to two orders of magnitude higher, given available experimental data on other types of stirrers (Hu et al., 2011). It is important to notice that the two setups that had energy dissipation rates of a similar order of magnitude also exhibited cell death rates of a similar order of magnitude, while the setup with significantly higher energy dissipation rates also had significantly higher cell death rates. This suggests that energy dissipation rate might work as a predictor regarding cell viability loss of *D. salina* cells in different hydrodynamic setups. However, in order to properly investigate this, it is necessary to determine the actual levels of energy dissipation that the cells experienced in flow (through CFD, particle tracking, etc.), as already discussed in section 3.3.4.

Regarding other microalgae species, there were several species that experienced cell death at energy dissipation rates of about $10^1 - 10^3\,\mathrm{W}\cdot\mathrm{m}^{-3}$, such as *C. muelleri*, *I. galbana*, and *S. constatum* (Michels et al., 2016), which are energy dissipation rates much lower than the ones investigated in the current thesis. An extreme case in this direction was microalgae *P. retuculatum*, which was found to experience cell damage and death at EDR of about $10^{-3}\,\mathrm{W}\cdot\mathrm{m}^{-3}$ (Garcia-Camacho et al., 2007). On the other hand, microalgae *T. suecica* was found to be resistant to energy dissipation rates up to $10^5\,\mathrm{W}\cdot\mathrm{m}^{-3}$, with the cells showing no

signs of damage or viability loss (Michels et al., 2016).

The energy dissipation rates arising in all three setups can be further put into perspective using data from the literature (Hu et al., 2011). The maximum energy dissipation rates in the narrow-gap rheometer are similar to the maximum energy dissipation rates of $10\,\mathrm{L}$ reactor with a stirring speed of 700 rpm (Zhou and Kresta, 1996), or the energy release caused by the rupture of a $6.32\,\mathrm{mm}$ bubble (Garcia-Briones et al., 1994). The maximum energy dissipation rates in the syringe-capillary setup are similar to the maximum energy dissipation rates of a standard membrane filtration system and other syringe-capillary setups (Vickroy et al., 2007), or the energy release caused by the rupture of a $1.7\,\mathrm{mm}$ bubble (Garcia-Briones et al., 1994). Finally, the volume average energy dissipation rates in the rotor-stator setup are four orders of magnitude higher than the typical energy dissipation rates in animal cell cultures (where animal cells are considered particularly susceptible to hydrodynamic stress) (Varley and Birth, 1999), and one order of magnitude higher than the volume average energy dissipation rate of an impeller in a $22000\,\mathrm{L}$ reactor operating at 140 rpm (Wernersson and Tragardh, 1999).

Finally, in turbulent conditions, the Kolmogorov length scale of turbulence θ is commonly used as a way to assess whether cells could have been damaged by the eddies in the turbulent field (Cherry and Papoutsakis, 1986), and can also provide a reference to the turbulent conditions arising in different systems. McQueen et al. (1987) placed a mouse myeloma cell suspension in turbulent flow in a capillary tube, with the cells being of about $10\,\mu\mathrm{m}$ in size, and found that detectable cell damage and lysis occurred when the Kolmogorov length scale was smaller than the average size, at about $3.5\,\mu\mathrm{m}$. Croughan et al. (1989) experimented with FS-4 cells attached to microcarriers, subjected to increased levels of agitation using spinner vessels. The authors found a reduction in the relative specific growth rate of the cells at a θ of about $130\,\mu\mathrm{m}$, which was smaller to the average microcarrier size of about $185\,\mu\mathrm{m}$. At conditions of even smaller θ, further decreases in the specific growth rate were measured. Contreras et al. (1998) investigated the growth of *P. tricornutum* cells suspended in an airlift photobiorector, and found a decrease in the specific growth rate of the cells at a Kolmogorov length scale of $45\,\mu\mathrm{m}$ or lower, which was similar to the *P. tricornutum* cell size, with an average length of about $35\,\mu\mathrm{m}$, and an average width of about $3\,\mu\mathrm{m}$. In the rotor-stator experiments presented in the current thesis, it was calculated that θ was about $10-12\,\mu\mathrm{m}$, which is similar to the average *D. salina* cell size of about $14\,\mu\mathrm{m}$ length and $11\,\mu\mathrm{m}$ width. This suggests, given the expectations from the literature, that the turbulent eddies

could have caused cell damage and death in the experimental conditions investigated using the rotor-stator setup.

Population balance modeling of cell rupture under hydrodynamic stress

To the author's knowledge, this is the first population balance model dealing exclusively with cell rupture, so it isn't possible to compare directly with the findings of another model. The results will instead be compared with the expectations provided by experimental data from the literature. First, regarding the heterogeneity of the population of cells, two measures of differentiation were discussed, cell radius and cell membrane's Young's modulus. While there were no experiments in the scientific literature, where the distribution of the cell membrane's Young's modulus was measured before and after the cells experiencing hydrodynamic stress, this was not the case for cell size. Acosta-Martinez et al. (2010) used a syringe-capillary system to inflict high levels of hydrodynamic stress on two human cell lines, OnyCap23 and P4E6, and measured, among other parameters, the average cell size. In the case of OnyCap23 cells, the average cell size increased when comparing with the untreated sample, while in the case of P4E6 the average cell size sharply decreased, which they attributed to possible loss of material attached to the cells or break-up of weak cell aggregates. However, when taking the model into account, an alternative explanation can be offered for the case of P4E6 cells, since the model predicts that larger cells would be more likely to die out, as they would have an increased value of capillary number. Therefore the average cell size of the population would be expected to decrease after treatment, which matches the experimental result. For the case of OnyCap23 cells, the opposite happened from what the model would have expected. However, many of the model assumptions remain unchecked, as e.g. the assumption that the cell size and cell membrane's Young's modulus are uncorrelated, which is true for some cell types, e.g. *S. cerevisiae* (Stenson et al., 2011), and *A. thaliana* cells (Radotic et al., 2012). If it was the case that larger OnyCap23 cells are also more resistant, i.e. they have a much higher membrane's Young's modulus, then it might well be that the cells with the highest capillary number are the smallest for that population, and they would die out leading to an increase of average cell size after treatment. The advantage of the experiments by Acosta-Martinez et al. (2010) was that the hydrodynamic stressing of the cells was rapid, and therefore there was no time for their biological reactions to kick in, as that could also greatly affect the size distribution. This was the case in the experiments of Edwards et al. (1989) where they used a cone-and-plate viscometer to inflict hydrodynamic damage on *E*

coli cells. They found that the cells not only appeared larger after $18\,\mathrm{h}$ hours of shearing, but also formed chains 6-8 cells long which were not present in the untreated sample. Both cases demonstrate that the reactions of cells are complex and very specific to cell type, which is why, even with the correct modeling of the mechanics, the rest of the model will need to be tailored to the microorganism that is under investigation.

Regarding the cell population growth rate, the model expectations fit the trend of the data presented in many publications for very different cell types, from murine hybridomas (Born et al., 1992), to dinoflagellates (Juhl et al., 2000), to several microalgae species (Michels et al., 2016). Additionally, there are cases where there's a trade-off between better mixing in the reactor and too high levels of hydrodynamic stress that might damage the cells, as was the case in the experiments of Sobczuk et al. (2006) on *P. Tricornutum* and *P. cruentum* cells, or those of Garcia-Ochoa et al. (2015) on *R. erythropolis* cells. With a proper addition to the growth rate term to incorporate the improvement of growth rates due to better mixing, the results of these experiments should also be replicable. An additional improvement for the model would be to also incorporate the temporal evolution of the cell membrane's Young's modulus, in cases where this might be applicable Radotic et al. (2012)

Generally, it is reasonable to assume that modeling of cell death by hydrodynamic stress would be especially relevant for microalgae, as many microalgae are considered susceptible to hydrodynamic stress (Wang and Lan, 2018), especially in cases where they lack a rigid cell wall (Barbosa et al., 2003). In the past few years, there has been increasing interest in using population balance modelling on microalgae cells (Altimari et al., 2013; Bertucco et al., 2015; Pahija et al., 2017). This increases the scientific relevance of the model presented here, as population balance models can be combined with each other (e.g. using a more accurate growth term from one model, and a more accurate death term from another), to create a model that offers improved capabilities of prediction.

Conclusions

With the present work, additional insight was provided, regarding the cell death of *D. salina* due to hydrodynamic stress. We obtained measures of hydrodynamic sensitivity, such as cell death rates, required both in upstream and downstream processing of the cells. The tested methodology is applicable to a wide variety of microorganisms and conditions, from observing different types cells under high hydrodynamic stress without the use of thickeners,

to predicting cell viability loss through intracellular protein release in the cell suspension. Additionally, the limitations of comparing different hydrodynamic systems were studied, and cell rupture was modelled in a way that can be applied for all tested combinations.

The study of shear sensitivity of cells is far from over. Not only because of the countless new biological cells of scientific and commercial relevance that are introduced every year, some with very unique characteristics (e.g. microalgae producing calcite crystals (Jakob et al., 2016), or cyanobacteria producing ethanol (Silva and Bertucco, 2016)), but also because of the lack of accurate description of the underlying mechanisms, both biologically (e.g. mechanostasis) and regarding hydrodynamics (e.g. modeling turbulent flow).

Bibliography

Abureesh, I. and Kargi, F. (1991). Biological Responses of Hybridoma Cells to Hydrodynamic Shear in an Agitated Bioreactor. *Enzyme and Microbial Technology*, 13(11):913–919.

Acosta-Martinez, J., Papantoniou, I., Lawrence, K., Ward, S., and Hoare, M. (2010). Ultra Scale-Down Stress Analysis of the Bioprocessing of Whole Human Cells as a Basis for Cancer Vaccines. *Biotechnology and Bioengineering*, 107:953–963.

Altimari, P., Pagnanelli, F., and Toro, L. (2013). Application of Structured Population Balance Model for the Numerical Simulation of a Continuous Photobioreactor. In Pierucci, S and Klemes, JJ, editor, *ICHEAP-11: 11th International Conference on Chemical and Process Engineering, PTS 1-4*, volume 32 of *Chemical Engineering Transactions*, pages 1027–1032. 11th International Conference on Chemical and Process Engineering (ICheaP), Milan, Italy, June 02-05, 2013.

Altman, S., Randers, L., and Rao, G. (1993). Comparison of Trypan Blue-Dye Exclusion and Fluorometric Assays for Mammalian-Cell Viability Determinations. *Biotechnology Progress*, 9:671–674.

Altmann, B., Loechner, A., Swain, M., Kohal, R., Giselbrecht, S., Gottwald, E., Steinberg, T., and Tomakidi, P. (2014). Differences in morphogenesis of 3D cultured primary human osteoblasts under static and microfluidic growth conditions. *Biomaterials*, 35(10):3208–3219.

Apel, J., Paul, R., Klaus, S., Siess, T., and Reul, H. (2001). Assessment of hemolysis related quantities in a microaxial blood pump by computational fluid dynamics. *Artificial Organs*, 25(5):341–347.

Assuncao, P., Molina, R., Caujape-Castells, J., Wolf, M., Buchheim, M., de la Jara, A., Duarte, L., Freijanes, K., and Mendoza, H. (2013). Phylogenetic analysis of its2 sequences suggests the taxonomic re-structuring of dunaliella viridis (chlorophyceae, dunaliellales). *Phycological Research*, 61:81–88.

Baas-Becking, L. (1931). Salt effects on swarmers of dunaliella viridis teod. *J Gen Physiol*, 14:765–779.

Barbosa, M., Albrecht, M., and Wijffels, R. (2003). Hydrodynamic stress and lethal events in sparged microalgae cultures. *Biotechnology and Bioengineering*, 83:112–120.

Barbosa, M., Hadiyanto, and Wijffels, R. (2004). Overcoming shear stress of microalgae cultures in sparged photobioreactors. *Biotechnology and bioengineering*, 85:78–85.

Barsanti, L. and Gualtieri, P., editors (2014). *Algae: Anatomy, Biochemistry, and Biotechnology, 2nd Edition*. RC Press-Taylor & Francis Group.

Barthés-Biesel, D. (1998). Mechanics of encapsulated droplets. In Rehage, H and Peschel, G, editor, *Structure, Dynamics and Properties of Disperse Colloidal Systems*, volume 111 of *Progress in Colloid and Polymer Science*, pages 58–64. Steinkopf Darmstadt. 38th General Meeting of the German-Colloid-Society, Univ Essen, Essen, Germany, Sep 29 - Oct 02, 1997.

Behera, S., Singh, R., Arora, R., Sharma, N., Shukla, M., and Kumar, S. (2015). Scope of Algae as Third Generation Biofuels. *Frontiers in Bioengineering and Biotechnology*, 2:90.

Ben-Amotz, A. (1995). New mode of Dunaliella biotechnology: two-phase growth for β-carotene production. *Journal of Applied Phycology*, 7(1):65–68.

Ben-Amotz, A. and Avron, M. (1989). *Algal and Cyanobacterial Biotechnology*, chapter The biotechnology of mass culturing of Dunaliella for products of commercial interest, pages 90–114. Longman Scientific and Technical Press.

Bertucco, A., Sforza, E., Fiorenzato, V., and Strumendo, M. (2015). Population balance modeling of a microalgal culture in photobioreactors: Comparison between experiments and simulations. *AIChE Journal*, 61(9):2702–2710.

Bird, R., Stewart, W., and Lightfoor, E. (2002). *Transport Phenomena*. John Wiley & Sons, 2nd edition.

Bitog, J., Lee, I., Lee, C., Kim, K., Hwang, H., Hong, S., Seo, I., Kwon, K., and Mostafa, E. (2011). Application of computational fluid dynamics for modeling and designing photobioreactors for microalgae production: A review. *Computers and Electronics in Agriculture*, 76:131–147.

Blaser, S. (2000). Break-up of flocs in contraction and swirling flows. *Colloids and Surfaces A: Physicochemical and Engineering Aspects*, 166(1-3):215–223.

Bluestein, M. and Mockros, L. (1969). Hemolytic effects of energy dissipation in flowing blood. *Medical and biological engineering*, 7(1):1–16.

Born, C., Al-Rubeai, M., and Thomas, C. R. (1992). Estimation of Disruption of Animal Cells by Laminar Shear Stress. *Biotechnology and Bioengineering*, 40:1004 – 1010.

Borowitzka, L. (1981). The Microflora. Adaptations to Life in Extremely Saline Lakes. *Hydrobiologia*, 81-2:33–46.

Borowitzka, L. and Borowitzka, M. (1989). *Biotechnology of Vitamins, Pigments and Growth Factors*, chapter β-Carotene (Provitamin A) Production with Algae, pages 15–26. Springer Netherlands.

Borowitzka, L., Borowitzka, M., and Moulton, T. (1984). The mass-culture of Dunaliella-salina for fine chemicals - from laboratory to pilot-PL. *Hydrobiologia*, 116:115–121.

Borowitzka, M. (1999). Commercial production of microalgae: ponds, tanks, tubes and fermenters. *Journal of Biotechnology*, 70:313–321.

Borowitzka, M. and Borowitzka, L. (1987). Limits to growth and carotenogenesis in laboratory and large-scale outdoor cultures of Dunaliella salina. In Stadler, T., Mollion, J., Verdus, M., Karamanos, Y., Morvan, H., and Christiaen, D., editors, *Algal biotechnology*, pages 371–381. Elsevier Applied Science. Proceedings of the 4th International Meeting of the SAA, held in Villeneuve d'Ascq, France, 15-17 September 1987.

Bradford, M. (1976). Rapid and Sensitive Method for Quantitation of Microgram Quantities of Protein Utilizing Principle of Protein-Dye Binding. *Analytical Biochemistry*, 72:248–254.

Brindley, A., Lopez, G., Acien, F., Fernindez Sevilla, J., Garcia Sanchez, J., and Molina Grima, E. (2004). Influence of power supply in the feasibility of Phaeodactylum tricornutum cultures. *Biotechnology and Bioengineering*, 87(6):723–733.

Brock, T. (1975). Salinity and the ecology of dunaliella from great salt lake. *J Gen Microbiol*, 89(285-292).

Bronnenmeier, R. and Maerkl, H. (1982). Hydrodynamic stress capacity of microorganisms. *Biotechnology and Bioengineering*, 24(3):553–578.

Brooks, D. (1984). The biorheology of tumor cells. *Biorheology*, 21(1-2):85–91.

Brown, A. (1990). *Microbial water stress physiology: principles and perspectives*. Chichester: John Wiley & Sons.

Brown, F., Sussman, I., Avron, M., and Degani, H. (1982). NMR studies of glycerol permeability in lipid vesicles, erythrocytes and the alga Dunaliella. *Biochimica et Biophysica Acta (BBA) - Biomembranes*, 690(2):165 – 173.

Chan, D., Van Dyke, W., Bahls, M., Connell, S., Critser, P., Kelleher, J., Kramer, M. a., Pearce, S., Sharma, S., and Neu, C. (2011). Mechanostasis in apoptosis and medicine. *Progress in biophysics and molecular biology*, 106(3):517–24.

Cherry, R. (1993). Animal cells in turbulent fluids - Details of the physical stimulus and the biological response. *Biotechnology Advances*, 11:279 – 299.

Cherry, R. and Papoutsakis, E. (1986). Hydrodynamic effects on cells in agitated tissue culture reactors. *Bioprocess Engineering*, 1(1):29–41.

Chew, K., Yap, J., Show, P., Suan, N., Juan, J., Ling, T., Lee, D., and Chang, J. (2017). Microalgae biorefinery: High value products perspectives. *Bioresource Technology*, 229:53–62.

Chisti, Y. (2001). Hydrodynamic damage to animal cells. *Critical reviews in biotechnology*, 21(2):67–110.

Clausen, J. and Aidun, C. (2010). Capsule dynamics and rheology in shear flow: Particle pressure and normal stress. *Physics of Fluids*, 22(12).

Collins, J. and Richmond, M. (1962). Rate of Growth of Bacillus cereus Between Divisions. *Journal of General Microbiology*, 28:15–33.

Contreras, A., Garcia, F., Molina, E., and Merchuk, J. (1998). Interaction between CO2-mass transfer, light availability, and hydrodynamic stress in the growth of Phaeodactylurn tricornutum in a concentric tube airlift photobioreactor. *Biotechnology and Bioengineering*, 60:317–325.

Croughan, M., Sayre, E., and Wang, D. (1989). Viscous reduction of turbulent damage in animal cell culture. *Biotechnology and Bioengineering*, 33(7):862–872.

Dakhil, H., Do, H., Hübner, H., and Wierschem, A. (2018). Measuring the adhesion limit of fibronectin for fibroblasts with a narrow-gap rotational rheometer. *Bioprocess and Biosystems Engineering*, 41(3):353–358.

Dakhil, H., Gilbert, D., Malhotra, D., Limmer, A., Engelhardt, H., Amtmann, A., Hansmann, J., Hübner, H., Buchholz, R., Friedrich, O., and Wierschem, A. (2016). Measuring average rheological quantities of cell monolayers in the linear viscoelastic regime. *Rheologica Acta*, 55(7):527–536.

Dakhil, H. and Wierschem, A. (2014). Measuring Low Viscosities and High Shear Rates With A Rotational Rheometer In A Thin-Gap Parallel-Disk Configuration. *Applied Rheology*, 24(6):10–15.

Del Campo, J., Garcia-Gonzalez, M., and Guerrero, M. (2007). Outdoor cultivation of microalgae for carotenoid production: current state and perspectives. *Applied Microbiology and Biotechnology*, 74:1163–1174.

Dormido, R., Sanchez, J., Duro, N., Dormido-Canto, S., Guinaldo, M., and Dormido, S. (2014). An Interactive Tool for Outdoor Computer Controlled Cultivation of Microalgae in a Tubular Photobioreactor System. *Sensors*, 14:4466–4483.

dos Santos, C., Dionisio, R., Cerqueira, H., Sousa-Aguiar, E., Mori, M., and d Avila, M. (2007). Three-dimensional gas-liquid CFD simulations in cylindrical bubble columns. *International Journal of chemical reactor engineering*, 5(1).

Down, L., Papavassiliou, D., and O'Rear, E. (2011). Significance of extensional stresses to red blood cell lysis in a shearing flow. *Annals of biomedical engineering*, 39:1632–1642.

Dunlop, E., Namdev, P., and Rosenberg, M. (1994). Effect of fluid shear forces on plant cell suspensions. *Chemical Engineering Science*, 49:2263–2276.

Durand, P., Rashidi, A., and Michod, R. (2011). How an Organism Dies Affects the Fitness of Its Neighbors. *American Naturalist*, 177(2):224–232.

Edwards, N., Beeton, S., Bull, A. T., and Merchuk, J. C. (1989). A novel device for the assessment of shear effects on suspended microbial cultures. *Applied Microbiology and Biotechnology*, 30(2):190–195.

Ekambara, K., Dhotre, M., and Joshi, J. (2005). CFD simulations of bubble column reactors: 1D, 2D and 3D approach. *Chemical Engineering Science*, 60(23):6733–6746.

Elias, R., Kellerby, S., and Decker, E. (2008). Antioxidant Activity of Proteins and Peptides. *Critical Reviews in Food Science and Nutrition*, 48(5):430–441.

Elowitz, M., Levine, A., Siggia, E., and Swain, P. (2002). Stochastic gene expression in a single cell. *Science*, 297:1183–1186.

Eze, V., Velasquez-Orta, S., Hernandez-Garcia, A., Monje-Ramirez, I., and Orta-Ledesma, M. (2018). Kinetic modelling of microalgae cultivation for wastewater treatment and carbon dioxide sequestration. *Algal Research*, 32:131–141.

Fernandes, R., Nierychlo, M., Lundin, L., Pedersen, A., Puentes Tellez, P., Dutta, A., Carlquist, M., Bolic, A., Schäpper, D., Brunetti, A., Helmark, S., Heins, A., Jensen, A., Nopens, I., Rottwitt, K., Szita, N., van Elsas, J., Nielsen, P., Martinussen, J., Sø rensen, S., Lantz, A. E., and Gernaey, K. (2011). Experimental methods and modeling techniques for description of cell population heterogeneity. *Biotechnology Advances*, 29:575–599.

Fisher, M., Gokhman, I., Pick, U., and Zamir, A. (1996). A Salt-resistant Plasma Membrane Carbonic Anhydrase Is Induced by Salt in Dunaliella salina. *Journal of Biological Chemistry*, 271:17718–17723.

Fisher, M., Gokhman, I., Pick, U., and Zamir, A. (1997). A Structurally Novel Transferrin-like Protein Accumulates in the Plasma Membrane of the Unicellular Green Alga Dunaliella salina Grown in High Salinities. *Journal of Biological Chemistry*, 272:1565–1570.

Franklin, N. M., Adams, M. S., Stauber, J. L., and Lim, R. P. (2001). Development of an Improved Rapid Enzyme Inhibition Bioassay with Marine and Freshwater Microalgae Using Flow Cytometry. *Archives of Environmental Contamination and Toxicology*, 40(4):469–480.

Gallardo Rodriguez, J., Sanchez Miron, A., Garcia Camacho, F., Ceron Garcia, M., Belarbi, E., Chisti, Y., and Molina Grima, E. (2009). Causes of Shear Sensitivity of the Toxic Dinoflagellate Protoceratium reticulatum. *Biotechnology Progress*, 25(3):792–800.

Garcia-Briones, M., Brodkey, R., and Chalmers, J. (1994). Computer-Simulations of the Rupture of a Gas Bubble at a Gas-Liquid Interface and its Implications in Animal-Cell Damage. *Chemical Engineering Science*, 49:2301–2320.

Garcia-Camacho, F., Gallardo Rodriguez, J., Sanchez Miron, A., Ceron Garcia, M., Belarbi, E., and Grima, E. (2007). Determination of shear stress thresholds in toxic dinoflagellates cultured in shaken flasks - Implications in bioprocess engineering. *Process Biochemistry*, 42:1506–1515.

Garcia-Chavarria, M. and Lara-Flores, M. (2013). The use of carotenoid in aquaculture. *Research Journal of Fisheries and Hydrobiology*, 8:38–49.

García-González, M., Moreno, J., Manzano, J., Florencio, F., and Guerrero, M. (2005). Production of Dunaliella salina biomass rich in 9-cis-beta-carotene and lutein in a closed tubular photobioreactor. *Journal of biotechnology*, 115(1):81–90.

Garcia-Ochoa, F., Escobar, S., and Gomez, E. (2015). Specific oxygen uptake rate as indicator of cell response of Rhodococcus erythropolis cultures to shear effects. *Chemical Engineering Science*, 122:491–499.

Garcia-Ochoa, F., Gomez, E., Alcon, A., and Santos, V. (2013). The effect of hydrodynamic stress on the growth of Xanthomonas campestris cultures in a stirred and sparged tank bioreactor. *Bioprocess and Biosystems Engineering*, 36:911–925.

Ge, B., Qin, S., Han, L., Lin, F., and Ren, Y. (2006). Antioxidant properties of recombinant allophycocyanin expressed in Escherichia coli. *Journal of Photochemistry and Photobiology B: Biology*, 84(3):175–180.

Gilbert, F., Galgani, F., and Cadiou, Y. (1992). Rapid assessment of metabolic activity in marine microalgae: application in ecotoxicological tests and evaluation of water quality. *Marine Biology*, 112(2):199–205.

Gimmler, H. and Hartung, W. (1988). Low Permeability of the Plasma Membrane of Dunaliella parva for Solutes. *Journal of Plant Physiology*, 133(2):165–172.

Grace, H. (1982). Dispersion Phenomena In High-Viscosity Immiscible Fluid Systems And Application Of Static Mixers As Dispersion Device In Such Systems. *Chemical Engineering Communications*, 14(3-6):225–277.

Greifzu, F., Kratzsch, C., Forgber, T., Lindner, F., and Schwarze, R. (2016). Assessment of particle-tracking models for dispersed particle-laden flows implemented in OpenFOAM and ANSYS FLUENT. *Engineering Applications of Computational Fluid Mechanics*, 10(1):30–43.

Gudin, C. and Chaumont, D. (1991). Cell Fragility - The Key Problem of Microalgae Mass-Production in Closed Photobioreactors. *Bioresource Technology*, 38:145–151.

Guedes, A., Amaro, H., Pereira, R., and Malcata, F. (2011). Effects of temperature and ph on growth and antioxidant content of the microalga scenedesmus obliquus. *Biotechnology Progress*, 27(5):1218–1224.

Guelcher, S. and Kanel, J. (1999). Method for dewatering microalgae with a bubble column.

Guenerken, E., D'Hondt, E., Eppink, M., Garcia-Gonzalez, L., Elst, K., and Wijffels, R. (2015). Cell disruption for microalgae biorefineries. *Biotechnology Advances*, 33:243–260.

Guerin, M., Huntley, M., and Olaizola, M. (2003). Haematococcus astaxanthin: applications for human health and nutrition. *Trends in Biotechnology*, 21(5):210–216.

Hamburger, C. (1905). Zur kenntnis der dunaliella salina und einer amoebe aus salinenwasser von cagliari. *Arch f Protistenkd*, 6(111-131).

Hamed, I. (2016). The evolution and versatility of microalgal biotechnology: A review. *Comprehensive Reviews in Food Science and Food Safety*, 15(6):1104–1123.

Hamel, G. (1931). Chlorophycees des cotes francaises. *Extr Rev Algol*, 4(4-6).

Hejazi, M., Andrysiewicz, E., Tramper, J., and Wijffels, R. (2003). Effect of mixing rate on beta-carotene production and extraction by Dunaliella salina in two-phase bioreactors. *Biotechnology and Bioengineering*, 84:591–596.

Hejazi, M., Barzegari, A., Hosseinzadeh Gharajeh, N., and Hejazi, M. (2010). Introduction of a novel 18S rDNA gene arrangement along with distinct ITS region in the saline water microalga Dunaliella. *Saline Systems*, 6:4.

Hernandez-Onate, M. and Herrera-Estrella, A. (2015). Damage response involves mechanisms conserved across plants, animals and fungi. *Current Genetics*, 61:359–372.

Hinze, J. (1975). *Turbulence*. Mc-Graw-Hill, New York.

Horikawa, A., Okada, K., Sato, K., and Sato, M. (2000). Morphological changes in osteoblastic cells (MC3T3-E1) due to fluid shear stress: Cellular damage by prolonged application of fluid shear stress. *Tohoku Journal of Experimental Medicine*, 191(3):127–137.

Hosaka, K., Hioki, T., and Furuune, H. (1995). Augmentation of Microalgae Growth due to Hydrodynamic Activation. *Energy Conversion and Management*, 36:725–728.

Hosikian, A., Lim, S., Halim, R., and Danquah, M. (2010). Chlorophyll Extraction from Microalgae: A Review on the Process Engineering Aspects. *International Journal of Chemical Engineering*, pages 1–11.

Hsieh, M. and Nguyen, H. (2005). Molecular mechanism of apoptosis induced by mechanical forces. In Jeon, KW, editor, *International Review of Cytology - A Survey of Cell Biology*, volume 245, pages 45–90. Elsevier.

Hu, W., Berdugo, C., and Chalmers, J. (2011). The potential of hydrodynamic damage to animal cells of industrial relevance: current understanding. *Cytotechnology*, 63:445–460.

Hu, W., Gladue, R., Hansen, J., Wojnar, C., and Chalmers, J. (2008). The Sensitivity of the Dinoflagellate Crypthecodinium cohnii to Transient Hydrodynamic Forces and Cell-Bubble Interactions. *Biotechnology Progress*, 23(6):1355–1362.

Hutmacher, D. and Singh, H. (2008). Computational fluid dynamics for improved bioreactor design and 3D culture. *Trends in biotechnology*, 26(4):166–172.

Jahnke, L. (1999). Massive carotenoid accumulation in Dunaliella bardawil induced by ultraviolet-A radiation. *Journal of Photochemistry and Photobiology B: Biology*, 48(1):68–74.

Jakob, I., Chairopoulou, M., Vucak, M., Posten, C., and Teipel, U. (2016). Biogenic calcite particles from microalgae - Coccoliths as a potential raw material. *Engineering in Life Sciences*, 17(6):605–612.

Jaouen, P., Vandanjon, L., and Quemeneur, F. (1999). The shear stress of microalgal cell suspensions (Tetraselmis suecica) in tangential flow filtration systems: the role of pumps. *Bioresource Technology*, 68:149–154.

Jiang, Q., Zhao, L., Dai, J., and Wu, Q. (2012). Analysis of autophagy genes in microalgae: Chlorella as a potential model to study mechanism of autophagy. *PLOS ONE*, 7(7):1–16.

Jochem, F. (1999). Dark survival strategies in marine phytoplankton assessed by cytometric measurement of metabolic activity with fluorescein diacetate. *Marine Biology*, 135:721–728.

Joebses, I., Martens, D., and Tramper, J. (1991). Lethal events during gas sparging in animal cell culture. *Biotechnology and Bioengineering*, 5(37):484–490.

Johnson, M., Johnson, E., Macelroy, R., Speer, H., and Bruff, B. (1968). Effects of Salts on Halophilic Alga Dunaliella Viridis. *Journal of Bacteriology*, 95:1461–1468.

Joshi, J., Elias, C., and Patole, M. (1996). Role of hydrodynamic shear in the cultivation of animal, plant and microbial cells. *The Chemical Engineering Journal*, 62:121–141.

Juhl, A., Velasquez, V., and Latz, M. (2000). Effect of growth conditions on flow-induced inhibition of population growth of a red-tide dinoflagellate. *American Society of Limnology and Oceanography*, 45:905–915.

Katz, A. and Avron, M. (1985). Determination of intracellular osmotic vol- ume and sodium concentration in Dunaliella. *Plant Physiology*, 78:817–820.

Kim, N., Suh, I., Hur, B., and Lee, C. (2002). Simple monodimensional model for linear growth rate of photosynthetic microorganisms in flat-plate photobioreactors. *Journal of Microbiology and Biotechnology*, 12(6):962–971.

Kleinegris, D., Janssen, M., Brandenburg, W., and Wijffels, R. (2011). Continuous production of carotenoids from Dunaliella salina. *Enzyme and Microbial Technology*, 48:253–259.

Kleinegris, D., van Es, M., Janssen, M., Brandenburg, W., and Wijffels, R. (2010). Carotenoid fluorescence in Dunaliella salina. *Journal of applied phycology*, 22(5):645–649.

Kokkinos, D., Braun, A., and Briesen, H. (2014). Modelling the impact of shear stress on microalgae populations. In *Chemie Ingenieur Technik*, volume 86-9, page 1394. Proceedings of the ProcessNet Conference, held in Aachen, Germany, 30/9 - 2/10/2014.

Kokkinos, D., Dakhil, H., Wierschem, A., Briesen, H., and Braun, A. (2016). Deformation and rupture of Dunaliella salina at high shear rates without the use of thickeners. *Biorheology*, 53(1):1–11.

Kresta, S. (1998). Turbulence in stirred tanks: anisotropic, approximate, and applied. *The Canadian Journal of Chemical Engineering*, 76(3):563–576.

Krinsky, N. (1989). Antioxidant functions of carotenoids. *Free Radical Biology and Medicine*, 7(6):617–635.

Kunas, K. and Papoutsakis, E. (1990). Damage mechanisms of suspended animal cells in agitated bioreactors with and without bubble entrainment. *Biotechnology and bioengineering*, 36(5):476–483.

Kutalik, Z., Razaz, M., Elfwing, A., Ballagi, A., and Baranyi, J. (2005). Stochastic modelling of individual cell growth using flow chamber microscopy images. *International journal of food microbiology*, 105(2):177–190.

Lac, E. and Parry, A. (2017). Non-Newtonian end-effects in standard oilfield rheometers. *Journal of Rheology*, 61(4):833–843.

Lam, M. and Lee, K. (2012). Microalgae biofuels: A critical review of issues, problems and the way forward. *Biotechnology Advances*, 30(3):673–690.

Lange, H., Taillandier, P., and Riba, J. (2001). Effect of high shear stress on microbial viability. *Journal of Chemical Technology & Biotechnology*, 76(5):501–505.

Lee, S. Y., Cho, J. M., Chang, Y. K., and Oh, Y.-K. (2017). Cell disruption and lipid extraction for microalgal biorefineries: A review. *Bioresource Technology*.

Lehto, K., Lehto, H., and Kanervo, E. (2006). Suitability of different photosynthetic organisms for an extraterrestrial biological life support system. *Research in Microbiology*, 157:69–76.

Lerche, W. (1937). Untersuchungen ueber entwicklung und fortpflan zung in der gattung dunaliella. *Arch f Protistenkd*, 88:236–268.

Leupold, M., Hindersin, S., Gust, G., Kerner, M., and Hanelt, D. (2012). Influence of mixing and shear stress on Chlorella vulgaris, Scenedesmus obliquus, and Chlamydomonas reinhardtii. *Journal of Applied Phycology*, 25(2):485–495.

Levesque, M. and Nerem, R. (1985). The Elongation and Orientation of Cultured Endothelial Cells in Response to Shear Stress. *Journal of Biomechanical Engineering*, 107(4).

Li, F., Chan, C., and Ohl, C. (2013). Yield Strength of Human Erythrocyte Membranes to Impulsive Stretching. *Biophysical Journal*, 105(4):872–879.

Li, F., Hashimura, Y., Pendleton, R., Harms, J., Collins, E., and Lee, B. (2006). A Systematic Approach for Scale-Down Model Development and Characterization of Commercial Cell Culture Processes. *Biotechnology Progress*, 22(3):696–703.

Liska, A., Shevchenko, A., Pick, U., and Katz, A. (2004). Enhanced Photosynthesis and Redox Energy Production Contribute to Salinity Tolerance in Dunaliella as Revealed by Homology-Based Proteomics. *Plant Physiology*, 136:2806–2817.

Liu, Y., Wang, Z., Xia, J., Haringa, C., Liu, Y., Chu, J., Zhuang, Y., and Zhang, S. (2016). Application of Euler Lagrange CFD for quantitative evaluating the effect of shear force on Carthamus tinctorius L. cell in a stirred tank bioreactor. *Biochemical Engineering Journal*, 114:209–217.

Loeblich, L. (1969). Aplanospores of dunaliella salina (chlorophyta). *J Protozool*, pages 22–23.

Lordan, S., Ross, R., and Stanton, C. (2011). Marine Bioactives as Functional Food Ingredients: Potential to Reduce the Incidence of Chronic Diseases. *Marine Drugs*, 9(6):1056–1100.

Ma, N., Chalmers, J., Aunins, J., Zhou, W., and Xie, L. (2004). Quantitative studies of cell-bubble interactions and cell damage at different pluronic F-68 and cell concentrations. *Biotechnology Progress*, 20(4):1183–1191.

Ma, N., Koelling, K., and Chalmers, J. (2002). Fabrication and use of a transient contractional flow device to quantify the sensitivity of mammalian and insect cells to hydrodynamic forces. *Biotechnology and bioengineering*, 80(4):428–437.

Malkin, A. and Isayev, A. (2006). *Rheology: Concepts, Methods and Applications*. ChemTec Publishing, 1st edition.

Mantzaris, N., Liou, J., Daoutidis, P., and Srienc, F. (1999). Numerical solution of a mass structured cell population balance model in an environment of changing substrate concentration. *Journal of Biotechnology*, 71:157–174.

Marchesini, F., Naccache, M., Abdu, A., Alicke, A., and De Souza Mendes, P. (2015). Rheological characterization of yield-stress materials: Flow pattern and apparent wall slip. *Applied Rheology*, 25(5):53883.

Marre, E. and Servettaz, A. (1959). Sul meccanismo di adattemento a condizioni osmotiche estreme in dunaliella salina. ii. rapporto fra concentrazioni del mezzo esterno e composizione del succo cellulare. *Atti Accad Naz Lincei Cl Sci Fis Mat Nat Rend Ser*, 26:272–278.

Masi, A. and Melis, A. (1997). Morphological and molecular changes in the unicellular green alga Dunaliella salina grown under supplemental UV-B radiation: cell characteristics and Photosystem II damage and repair properties. *Biochimica et Biophysica Acta (BBA) - Bioenergetics*, 1321(2):183–193.

Massyuk, N. (1973). *Morphology, Taxonomy, Ecology and Geographic Distribution of the Genus Dunaliella Teod. and Prospects for its Potential Utilization*. Naukova Dumka. (written in Russian).

McQueen, A., Meilhoc, E., and Bailey, J. (1987). Flow Effects on the Viability and Lysis of Suspended Mammalian-Cells. *Biotechnology Letters*, 9(12):831–836.

Meier, S., Hatton, T., and Wang, D. (1999). Cell death from bursting bubbles: Role of cell attachment to rising bubbles in sparged reactors. *Biotechnology and Bioengineering*, 62(4):468–478.

Merchuk, J. and Wu, X. (2003). Modeling of photobioreactors: application to bubble column simulation. *Journal of Applied Phycology*, 15(2-3):163–169.

Michels, M., van der Goot, A., Norsker, N., and Wijffels, R. (2010). Effects of shear stress on the microalgae Chaetoceros muelleri. *Bioprocess and Biosystems Engineering*, 33:921–927.

Michels, M., van der Goot, A., Vermuë, M., and Wijffels, R. (2016). Cultivation of shear stress sensitive and tolerant microalgal species in a tubular photobioreactor equipped with a centrifugal pump. *Journal of Applied Phycology*, 28(1):53–62.

Middelberg, A. (1995). Process-scale disruption of microorganisms. *Biotechnology advances*, 13(3):491–551.

Milledge, J. (2011). Commercial application of microalgae other than as biofuels: a brief review. *Reviews in Environmental Science and Bio/Technology*, 10(1):31–41.

Miron, A., Garciia, M., Gomez, A., Camacho, F., Grima, E., and Chisti, Y. (2003). Shear stress tolerance and biochemical characterization of Phaeodactylum tricornutum in quasi steady-state continuous culture in outdoor photobioreactors. *Biochemical Engineering Journal*, 16:287–297.

Mitsuhashi, S., Fujimoto, M., Muramatsu, H., and Tanishita, K. (1994). Effect of Simple Shear Flow on Photosynthesis Rate and Morphology of Micro Algae. *Acta Astronautica*, 33:179–187.

Moreno-Garrido, I. and Canavate, J. (2001). Assessing chemical compounds for controlling predator ciliates in outdoor mass cultures of the green algae dunaliella salina. *Aquacultural Engineering*, 24(2):107–114.

Mueller, A. (2016). Hydrodynamics of Microalgae in Rectangular Microchannels. Master Thesis, Technical University of Munich.

Mutanda, T. (2013). *Biotechnological Applications of Microalgae: Biodiesel and Value-added Products*, chapter Introduction, pages 1–4. CRC Press.

Oh, S., Nienow, A., Al-Rubeai, M., and Emery, A. (1989). The effects of agitation intensity with and without continuous sparging on the growth and antibody production of hybridoma cells. *Journal of Biotechnology*, 12(1):45–61.

Olmos-Soto, J., Ochoa, L., Paniagua-Michel, J., and Contreras, R. (2009). DNA fingerprinting differentiation between β-carotene hyperproducer strains of Dunaliella from around the world. *Saline Systems*, 5(1):5.

Olmos-Soto, J., Paniagua, J., and Contreras, R. (2000). Molecular identification of Dunaliella sp. utilizing the 18S rDNA gene. *Letters in applied microbiology*, 30:80–84.

Olmos-Soto, J., Paniagua-Michel, J., Contreras, R., and Ochoa, L. (2012). *Microbial Carotenoids from Bacteria and Microalgae: Methods and Protocols*, chapter DNA Fingerprinting Intron-Sizing Method to Accomplish a Specific, Rapid, and Sensitive Identification of Carotenogenic Dunaliella Species, pages 269–281. Humana Press.

Oren, A. (2005). A hundred years of dunaliella research: 1905005. *Saline Systems*, 1(2):1–2.

Oren, A., Gurevich, P., Anati, D., Barkan, E., and Luz, B. (1995). A bloom of dunaliella parva in the dead sea in 1992: biological and bio-geochemical aspects. *Hydrobiologia*, 297(173-185).

Orton, D. (1992). *Quantitative and mechanistic effects of bubble aeration on animal cells in culture*. PhD thesis, Massachusetts Institute of Technology, Cambridge, MA.

Pahija, E., Liang, Y., and Hui, C. (2017). Determination of Microalgae Growth in Different Temperature Condition Using a Population Balance Equation . *Chemical Engineering Transactions*, 61:721–726.

Papaioannou, A. (2002). *Fluid Mechanics*, volume 2, chapter Secondary energy losses, pages 238–251. Koralli Publications, 2nd edition. (written in Greek).

Pasquino, R., Snijkers, F., Grizzuti, N., and Vermant, J. (2010). The effect of particle size and migration on the formation of flow-induced structures in viscoelastic suspensions. *Rheologica Acta*, 49:993–1001.

Perner, I., Posten, C., and Broneske, J. (2003). CFD optimization of a plate photobioreactor used for cultivation of microalgae. *Engineering in life sciences*, 3(7):287–291.

Polle, J., Tran, D., and Ben-Amotz, A. (2009). *The Alga Dunaliella. Biodiversity, Physiology, Genomics and Biotechnology.*, chapter History, distribution, and habitats of algae of the genus Dunaliella Teodoresco (Chlorophyceae), pages 1–13. Enfield, NH: Science Publishers.

Post, F., Borowitzka, L., Borowitzka, M., Mackay, B., and Moulton, T. (1983). The protozoa of a Western Australian hypersaline lagoon. *Hydrobiologia*, 105(1):95–113.

Pramparo, L., Pruvost, J., Stüber, F., Font, J., Fortuny, A., Fabregat, A., Legentilhomme, P., Legrand, J., and Bengoa, C. (2008). Mixing and hydrodynamics investigation using CFD in a square-sectioned torus reactor in batch and continuous regimes. *Chemical Engineering Journal*, 137(2):386–395.

Preisig, H. (1992). *Dunaliella: Physiology, Biochemistry and Biotechnology.*, chapter Morphology and taxonomy, pages 1–15. CRC Press.

Press, W., Teukolsky, S., Vetterling, W., and Flannery, B. (1992). *Numerical Recipes in Fortran. The Art of Scientific Computing.* Cambridge University Press.

Priyadarshani, I. and Rath, B. (2012). Commercial and industrial applications of microalgae - A Review. *Journal of Algal Biomass Utilization*, 3:89–100.

Quitt, D. (2015). Shear sensitivity of Dunaliella salina in different growth phases. Bachelor Thesis, Technical University of Munich. Written in German.

Radotic, K., Roduit, C., Simonovi, J., Hornitschek, P., Fankhauser, C., Steinbach, G., Dietler, G., and Kasas, S. (2012). Atomic Force Microscopy Stiffness Tomography on Living Arabidopsis thaliana Cells Reveals the Mechanical Properties of Surface and Deep Cell-Wall Layers during Growth. *Biophysical Journal*, 103:386–394.

Rajesh, K., Rohit, M., and Venkata Mohan, S. (2017). Chapter 7 - microalgae-based carotenoids production. In Rastogi, R., Madamwar, D., and Pandey, A., editors, *Algal Green Chemistry*, pages 139–147. Elsevier.

Ramkrishna, D. and Singh, M. (2014). Population Balance Modeling: Current Status and Future Prospects. In Prausnitz, JM and Doherty, MF and Segalman, RA, editor, *Annual Review of Chemical and Biomolecular Engineering*, volume 5, pages 123–146. Annual Reviews.

Ranade, V. and Tayalia, Y. (2001). Modelling of fluid dynamics and mixing in shallow bubble column reactors: influence of sparger design. *Chemical Engineering Science*, 56(4):1667–1675.

Rasmussen, R. and Morrissey, M. (2007). Marine Biotechnology for Production of Food Ingredients. In *Advances in Food and Nutrition Research*, volume 52, pages 237–292. Academic Press.

Richmond, A. and Hu, Q., editors (2013). *Handbook of Microalgal Culture: Applied Phycology and Biotechnology, Second Edition*. John Wiley & Sons, Ltd.

Ross, D., Joneckis, C., Ordonez, J., Sisk, A., Wu, R., Hamburger, A., and Nora, R. (1989). Estimation of cell survival by flow cytometric quantification of fluorescein diacetate/propidium iodide viable cell number. *Cancer Research*, 49(14):3776–3782.

Sager, N. (2014). Recognizing and splitting attached objects in microscope pictures. Bachelor Thesis, Technical University of Munich. Written in German.

Sammy, N. (1987). Method for harvesting algae.

Sastre, R. (2012). *Microalgal Biotechnology: Integration and Economy*, chapter Products from microalgae: An overview, pages 13–44. De Gruyter.

Shadden, S. and Arzani, A. (2015). Lagrangian Postprocessing of Computational Hemodynamics. *Annals of biomedical engineering*, 43(1):41–58.

Silva, C. and Bertucco, A. (2016). Bioethanol from microalgae and cyanobacteria: A review and technological outlook. *Process Biochemistry*, 51(11):1833–1842.

Silva, C., Gris, B., and Bertucco, A. (2016). Simulation of microalgae growth in a continuous photobioreactor with sedimentation and partial biomass recycling. *Brazilian Journal of Chemical Engineering*, 33(4):773–781.

Silva, H., Cortinas, T., and Ertola, R. (1987). Effect of Hydrodynamic Stress on Dunaliella Growth. *Journal of Chemical Technology and Biotechnology*, 40(1):41–49.

Sobczuk, M., Grima, C. M., and Chisti, Y. (2006). Effects of agitation on the microalgae Phaeodactylum tricornutum and Porphyridium cruentum. *Bioprocess and biosystems engineering*, 28:243–250.

Sonnemann, K. and Bement, W. (2011). Wound Repair: Toward Understanding and Integration of Single-Cell and Multicellular Wound Responses. In *Annual Review of Cell and Developmental Biology*, volume 27, pages 237–263. Annual Reviews.

Sonntag, R. and Russel, W. (1987). Structure and breakup of flocs subjected to fluid stresses. *Journal of Colloid and Interface Science*, 115(2):378–389.

Spiden, E., Yap, B., Hill, D., Kentish, S., Scales, P., and Martin, G. (2013). Quantitative evaluation of the ease of rupture of industrially promising microalgae by high pressure homogenization. *Bioresource Technology*, 140(0):165–171.

Stahl, W. and Sies, H. (2003). Antioxidant activity of carotenoids. *Molecular Aspects of Medicine*, 24(6):345–351.

Stathopoulos, N. and Hellums, J. (1985). Shear stress effects on human embryonic kidney cells in Vitro. *Biotechnology and Bioengineering*, 27(7):1021–1026.

Stenson, J., Hartley, P., Wang, C., and Thomas, C. (2011). Determining the mechanical properties of yeast cell walls. *Biotechnology progress*, 27(2):505–512.

Stoddart, M., editor (2011). *Mammalian Cell Viability: Methods and Protocols*, chapter Chapter 13: Fluorescein Diacetate for Determination of Cell Viability in 3D Fibroblast-Collagen-GAG Constructs, pages 115–126. Humana Press, Springer.

Strikwerda, J. (1989). *Finite Difference Schemes and Partial Differential Equations*. Chapman and Hall.

Sukenik, A. and Shelef, G. (1984). Algal autoflocculation: verification and proposed mechanism. *Biotechnology and Bioengineering*, 26:142–147.

Sutera, S., Nowak, M., Joist, J., Zeffren, D., and Bauman, J. (1988). A programmable, computer-controlled cone-plate viscometer for the application of pulsatile shear stress to platelet suspensions. *Biorheology*, 25(3):449–59.

Suzuki, T., Matsuo, T., Ohtaguchi, K., and Koide, K. (1995). Gas-Sparged bioreactors for CO2 fixation by Dunaliella tertiolecta. *Journal of Chemical Technology & Biotechnology*, 62(4):351–358.

Syngelaki, M. (2014). Development of the size distribution of the Microalgae Dunaliella salina under constant shear stress. Master Thesis, Technical University of Munich.

Szafran, R. and Kmiec, A. (2004). Application of CFD modelling technique in engineering calculations of three-phase flow hydrodynamics in a jet-loop reactor. *International Journal of Chemical Reactor Engineering*, 2(1).

Tanzeglock, T., Soos, M., Stephanopoulos, G., and Morbidelli, M. (2009). Induction of Mammalian Cell Death by Simple Shear and Extensional Flows. *Biotechnology and Bioengineering*, 104(2):360–370.

Teodoresco, E. (1906). Observations morphologiques et biologiques sur le genre dunaliella. *Rev Gen Bot*, 18(353-371).

Tseng, C. (2001). Algal biotechnology industries and research activities in China. *Journal of Applied Phycology*, 13(4):375–380.

Unverfehrt, A., Koleva, I., and Rehage, H. (2015). Deformation, orientation and bursting of microcapsules in simple shear flow: Wrinkling processes, tumbling and swinging motions. *Journal of Physics: Conference Series*, 602(1):012002.

Vandanjon, L., Rossignol, N., Jaouen, P., Robert, J. M., and Quemeneur, F. (1999). Effects of shear on two microalgae species. Contribution of pumps and valves in tangential flow filtration systems. *Biotechnology and Bioengineering*, 63(1):1–9.

Varley, J. and Birth, J. (1999). Reactor design for large scale suspension animal cell culture. *Cytotechnology*, 29(3):177–205.

Vickroy, B., Lorenz, K., and Kelly, W. (2007). Modeling shear damage to suspended CHO cells during cross-flow filtration. *Biotechnology Progress*, 23(1):194–199.

Wang, C. and Lan, C. (2018). Effects of shear stress on microalgae - A review. *Biotechnology Advances*, 36(4):986–1002.

Ward, O. and Singh, A. (2005). Omega-3/6 fatty acids: Alternative sources of production. *Process Biochemistry*, 40:3627–3652.

Wegmann, K., Ben-Amotz, A., and Avron, M. (1980). Effect of Temperature on Glycerol Retention in the Halotolerant Algae Dunaliella and Asteromonas. *Plant Physiology*, 66(6):1196–1197.

Wernersson, E. and Tragardh, C. (1999). Scale-up of Rushton turbine-agitated tanks. *Chemical Engineering Science*, 54:4245–4256.

Williams, P. and Laurens, L. (2010). Microalgae as biodiesel & biomass feedstocks: Review & analysis of the biochemistry, energetics & economics. *Energy & Environmental Science*, 3(5):554–590.

Yang, J. and Wang, N. (1992). Cell Inactivation in the Presence of Sparging and Mechanical Agitation. *Biotechnology and Bioengineering*, 40:806–816.

Zamani, H., Moradshahi, A., and Karbalaei-Heidari, H. (2011). Characterization of a new Dunaliella salina strain MSI-1 based on nuclear rDNA ITS sequences and its physiological response to changes in composition of growth media. *Hydrobiologia*, 658(1):67–75.

Zhang, Z., Al-Rubeai, M., and Thomas, C. (1993). Estimation of disruption of animal cells by turbulent capillary flow. *Biotechnology and bioengineering*, 42(8):987–993.

Zhou, G. and Kresta, S. (1996). Distribution of energy between convective and turbulent flow for three frequently used impellers. *Chemical Engineering Research & Design*, 74:379–389.

Zhu, Y. and Jiang, J. (2008). Continuous cultivation of Dunaliella salina in photobioreactor for the production of β-carotene. *European Food Research and Technology*, 227(3):953–959.

Zou, J. (2016). Investigation of the shear sensitivity of D. salina through Capillary measurements. Master Thesis, Technical University of Munich. Written in German.

Appendix A

Essential parts of the code used for the cell counts, including descriptive comments for each part of the code, taken from the Bachelor work of Sager (2014), where A is the directly uploaded image to MATLAB (version R2015a):

```
[...]

% Splitting image in the three color channels
redChannel = A(:, :, 1);
greenChannel = A(:, :, 2);
blueChannel = A(:, :, 3);

 % Thresholding and binarization
Equation = eval(get(handles.colorThr_edit, 'String')); % User input:
greenChannel - redChannel
level = graythresh(Equation);
BW = im2bw(Equation, level);
[~, threshold] = edge(BW, 'canny');
fudgeFactor = .5;
BW = edge(BW,'canny', threshold * fudgeFactor);

[...]

% Morphological editing of the objects
seD = strel('diamond',3);
BWnobord = imclearborder(BW, 4);
BWcl = imclose(BWnobord,seD);
BWfill = imfill(BWcl, 'holes');
BWop = imopen(BWfill,seD);

% Removing small objects
sizesmallobj = str2double(get(handles.bwarea_edit, 'String'));
BWop = bwareaopen(BWop, sizesmallobj);

% Obtaining total object count and additional information, e.g. object area
[B,L] = bwboundaries(BWop,'noholes');
BWfill = bwfill(BWop,'holes');
stats = regionprops(BWfill, 'Area', 'MajorAxisLength');
totalAreas = [totalAreas; cat(1,stats.Area)];
totalMajorAxisLengths = [totalMajorAxisLengths;
cat(1,stats.MajorAxisLength)];

[...]

% Saving the total object count for the output
totalNumberOfObjects = totalNumberOfObjects + length(B);

[...]
```

Figure 4.1: *Sample MATLAB code snippet for counting microalgae cells in microscope images. For the rest of the code, please refer to (Sager, 2014).*

Appendix B

Derivation of equation 2.15 as suggested by Papaioannou (2002). The friction height for a cylindrical tube can be calculated by the Darcy-Weisbach equation:

$$h_f = f\frac{l}{d}\frac{v^2}{2g} \tag{4.1}$$

where v^2 is the mean fluid velocity in the tube. The friction height for a narrowing from a cylindrical tube to a smaller one is given by the equation:

$$h_m = k_m\frac{v_2^2}{2g} \tag{4.2}$$

where v_2 is the fluid velocity after the narrowing and k_m is an empirical factor depending on the relationship between the diameter of the tube before the narrowing d_1 and the diameter of the tube after the narrowing d_2, as described by the equation:

$$k_m = 0.42\left(1 - \frac{d_2}{d_1}\right)^2, \text{ for } d_2/d_1 \leq 0.76 \text{ and} \tag{4.3}$$

$$k_m = \left(1 - \left(\frac{d_2}{d_1}\right)^2\right)^2, \text{ for } d_2/d_1 > 0.76. \tag{4.4}$$

In the used system, the syringe consisted of the main syringe, the tip and the capillary connected to the tip, thus three different types of tube and two narrowings in between, amounting to a total friction height h_t:

$$h_t = h_{f_s} + h_{f_{st}} + h_{f_c} + h_{m_s} + h_{m_{st}} \tag{4.5}$$

where h_{f_s} is the friction height due to the length of the syringe, $h_{f_{st}}$ is the friction height due to the length of the syringe tip, h_{f_c} is the friction height due to the length of the capillary, h_{m_s} is the friction height due to the narrowing between the syringe and the syringe tip, and $h_{m_{st}}$ is the friction height due to the narrowing between the syringe tip and the capillary. The result of this equation is then substituted in equation 2.15, in order to calculate the total pressure drop in the syringe-capillary system.